Fracture Mechanics of High Performance Nylon Fibers

A Thesis
Presented to
The Academic Faculty

By

Rodney Dewayne Averett

In Partial Fulfillment
Of the Requirements for the Degree
Master of Science in Mechanical Engineering

Georgia Institute of Technology

May 1, 2004

Fracture Mechanics of High Performance Nylon Fibers

Approved by:

Dr. Mary L. Realff, Advisor (Co-chair)

Dr. Richard W. Neu (Co-chair)

Dr. Jianmin Qu

Date Approved: April 9, 2004

In memory of Grandma ("Grannie") and Buck

Dedicated to Jordan

ACKNOWLEDGEMENTS

First of all, I want to thank the Lord Almighty for giving me the ability to complete such an educational task and for giving me the strength and courage to go on day by day. This experience has shown me that through God, all things are possible.

Next, I would like to thank the National Textile Center for providing the funds to do this research. I would also like to thank my advisor, Dr. Mary Lynn Realff for giving guidance and providing me with the opportunity to work on this project. I also appreciate the long and arduous work of Dr. Stephen Michielsen, who believed that this research could be accomplished, despite what was unsuccessful in the past. In addition, I would like to thank my co-chair, Dr. Richard Neu for helping me with technical related questions, even when he was busy, and for convincing me that this fracture mechanics research would work. I would also like to thank Dr. Jianmin Qu for agreeing to serve on my committee and providing technical expertise as well.

In addition, I would also like to thank the love of my life, my wife Melody Averett, for supporting me throughout this arduous journey. More hard work and late nights are still to follow. But we will get through this! I would also like to thank my mom and dad, Jesse and Corene Averett for supporting me through all of my educational endeavors. You all have given me so much throughout my life, and I am sincerely grateful for that. Also, I want to thank Steve, Cheryl (Lynn), and Anthony (Tony) for being there when I needed them most. You guys have helped me a lot through the years.

TABLE OF CONTENTS

LIST OF FIGURES

LIST OF TABLES

ABSTRACT

A fracture mechanics protocol appropriate for small fibers (35μm dia.) is presented, which allows for the determination of the strength limitations of high performance nylon 6,6 fibers. Specifically, linear elastic fracture mechanics (LEFM) techniques are employed in addition to elastic-plastic fracture mechanics (EPFM) theories to achieve this.

We assume that a minute semi-elliptical flaw of an unknown size exists in the specimen, as a result of the detrimental effects of the manufacturing process (melt spinning). Next, we seek to propagate this flaw in a stable manner through an ancillary process such as high cycle or low cycle fatigue (load-unload). After propagation, uniaxial tensile experiments are performed on the fatigued samples, by which the crack growth eventually becomes catastrophic during the process. After performing scanning electron microscope (S.E.M.) techniques and reviewing fractography, we are able to determine the critical flaw size and ligament length that leads to unstable crack propagation. These results are substituted into the appropriate LEFM equations and are in close agreement with material properties for nylon 6,6. A discussion is provided that draws parallel to the topics discussed in the literature investigation and the experimental results of this study.

CHAPTER 1

INTRODUCTION

High modulus/high tenacity fibers are either produced by solution spinning of liquid crystalline polymers or by gel spinning. The current method of fabrication for these technologies produces fibers that are uneconomical, and in some instances the manufacturing processes are environmentally unfriendly. For the majority of industrial applications, a 50% increase in the modulus and tenacity of the conventional fibers would be adequate, if they retain some of their high toughness and can be produced at a price lower than the current high performance fibers. The modulus of fibers is controlled by the orientation distribution of the chain segments and the degree of crystallinity[35]. Since the fiber tenacity is determined by flaws, not morphology, an extensive investigation has been conducted on the failure analysis of polyamide fibers. The proposed investigation assumes that these imperfections lead to cracks and ultimately catastrophic failure. Because the cross-section of the fibers is microscopic (35μm diameter), only modestly successful research exists on the mode and analysis of failure in single nylon fibers. Most research dedicated to the determination of tensile failure in single nylon filaments has been based on Weibull statistics. In this theory, the fiber is viewed as a continuous array of interwoven links, and the flaws represent the "weakest links" of the domain[39]. The Weibull distribution function is given as:

$$F_i = 1 - \exp\left(\frac{\sigma}{\sigma_0}\right)^m$$

Here, F_i represents the probability of failure for a particular link in the fiber at a stress level σ. The scale factor is represented by σ_0 and m represents the flaw distribution shape

factor. Additionally, Kausch et al.[27] expressed the strength distribution of the fiber in a similar manner, evincing that increases in specimen length generates a decrease in the ultimate mechanical strength of the sample. The relationship is given as:

$$g(L,x) = Ln_0 f(x)\left[1 - \int_{-\infty}^{x} f(y)dy\right]^{Ln_0 - 1}$$

Here, n_0 represents the number of defects per unit length and $f(x)$ is the cumulative strength distribution function. For nylon 6 fibers, the effect of specimen length on the strength is depicted in Figure 1.1.

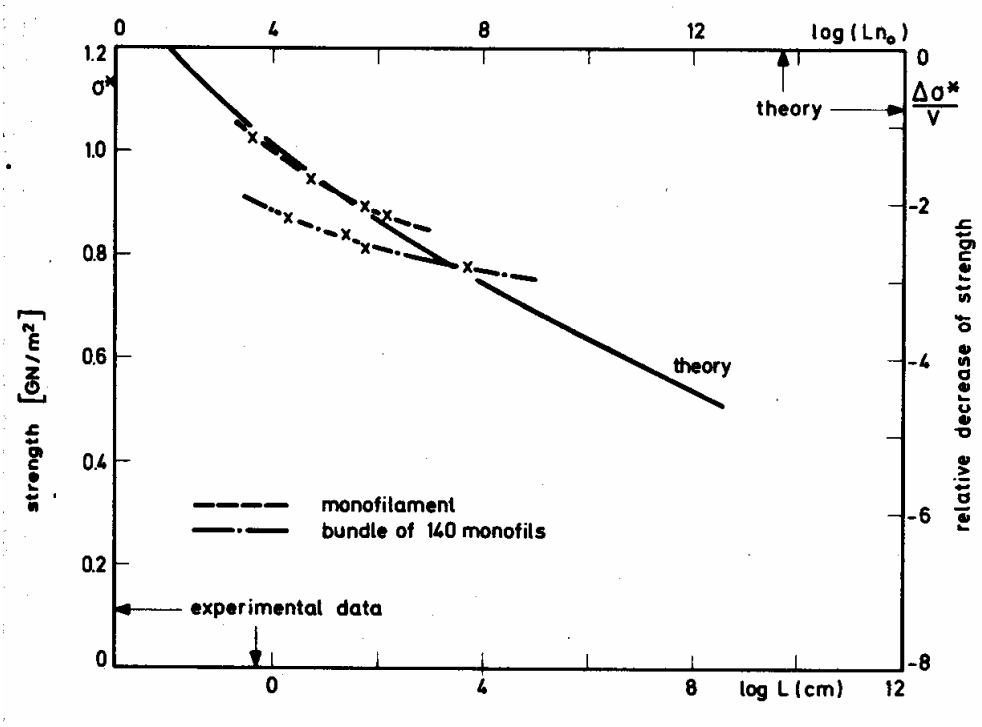

Figure 1.1. Theoretical and Experimental Data Displaying Effect of Specimen Length on Ultimate Tensile Strength in Nylon 6 Fibers[27]

These results are intuitive, nevertheless, given that an increase in specimen length increases the defect density of the sample and thus reduces the fracture strength.

These techniques for analyzing failure in nylon fibers are adequate for statistical failure studies, but have obvious inadequacies in the field of fracture mechanics. The main component omitted in the Weibull distribution function is the size, shape, and geometry of the flaws present in the sample. Furthermore, the Weibull parameter does not reveal how the flaws led to critical propagation, or at what value it actually occurred. The field of fracture mechanics encompasses maximum stress level, flaw size and geometry, and many other factors that Weibull statistics fail to quantify in materials.

Based on this information, the main objective of the research was to develop a fracture mechanics protocol appropriate for small fibers and apply it to determine the strength limitations of nylon 6,6 and other polyamide fibers[44]. In essence, the techniques devised in this study can be used to conduct fracture mechanics investigations on any fiber that possesses a microscopic cross-section. There are three phases in the development of this technique:

1) Devise a technique suitable for tensile and cyclic loading of small fibers
2) Fatigue individual fibers in an effort to increase the existing flaw (crack) size
3) Perform tensile tests on the fatigued samples of various crack lengths to obtain J_c (critical nonlinear energy release rate)

Manufacturers in the domain of fiber development will gain useful knowledge as to how individual fibers should be processed in order to obtain certain mechanical properties. For example, one such application for this research exists in the airliner industry. With an appropriate fracture mechanics protocol, airplane tires can be manufactured in a manner that will decrease the weight of the tires, and thus decrease the amount of fuel needed for operation, while keeping the failure strength of the tires

constant. This is directly proportional to cost savings for the airline industry as well as the manufacturers. Recently, nylon 6 and nylon 6,6 fibers have been used as tire cords for reinforcement. This obviates the need for conventional materials such as steel and polyester, which exhibit poor performance in cyclic tension experiments as compared to polyamide fibers. Thus a fracture mechanics assessment would greatly enhance the knowledge pertaining to limitations and shortcomings of polyamide fibers for researchers and manufacturers seeking better performance in composites.

CHAPTER 2

MOLECULAR ASPECTS OF NYLON FIBERS

2.1. Nylon Fibers: Chemical Structure

Nylon fibers are highly complex in structure and orientation, which makes it difficult to thoroughly prescribe a fracture mechanics protocol or constitutive model that explains their behavior. In particular, the polyamide nylon 6,6 is a useful industrial fiber that spans into many industries, to include composites and textiles. The bonds in nylon 6,6 are similar to those of other competing materials, such as metallics and ceramics, in which primary and secondary bonds provide the intensity to bind the atoms. The main contrast with polymeric materials, however, is that covalent bonds are the responsible primary bonds, dissimilar to metallic and ionic bonds in other materials. The chemical structure is composed of hydrogen, nitrogen, carbon, and oxygen atoms which form a repeating unit. A schematic of this is shown below in Figure 2.1.

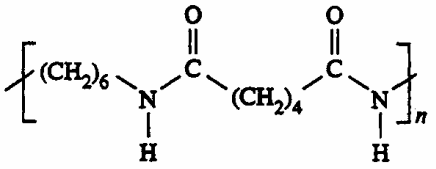

Figure 2.1. Chemical Structure of Nylon 6,6[60]

The structure of nylon 6 is very similar to that of nylon 6,6. Additionally, the behavior and morphological features of nylon 6 form a close resemblance to that of nylon 6,6. Notice the difference between the polyamides nylon 6,6 and nylon 6 from Figure 2.1 and Figure 2.2.

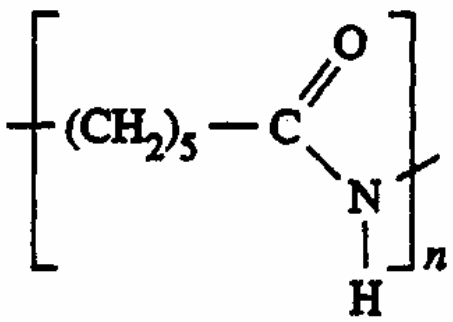

Figure 2.2. Chemical Structure of Nylon 6[60]

Crystallinity in nylon fibers affects the fatigue and fracture performance significantly. In fact, the global nature of this project presupposes that the crystallinity, morphology, and fracture behavior of nylon 6,6 fibers are all related through a complex and unknown algorithm. Previous investigations have shown that all polyamides are semicrystalline in nature, and therefore contain chain disentanglements among the atoms. Basically, the term "semicrystalline" is apposite for polyamides because the long chains are entangled in the melt and, upon cooling, the chains cannot disentangle sufficiently rapidly to crystallize[60]. Figure 2.3 provides a unit cell of nylon 6,6. In this figure, only two of the four chains are displayed. Also, one can see that a molecule of nylon 6,6 penetrates each corner of the unit cell, and hydrogen bonding needs are satisfied.

The structure of nylon 6,6 consists of two phases, in which there are crystalline and amorphous regions of the chemical structure. This semicrystalline nature is considered adverse in most circumstances, as it causes brittleness and premature fracture of the nylon fibers. This leads to reduced fatigue and fracture performance for a particular engineering application, which lowers the amount of useful energy that is

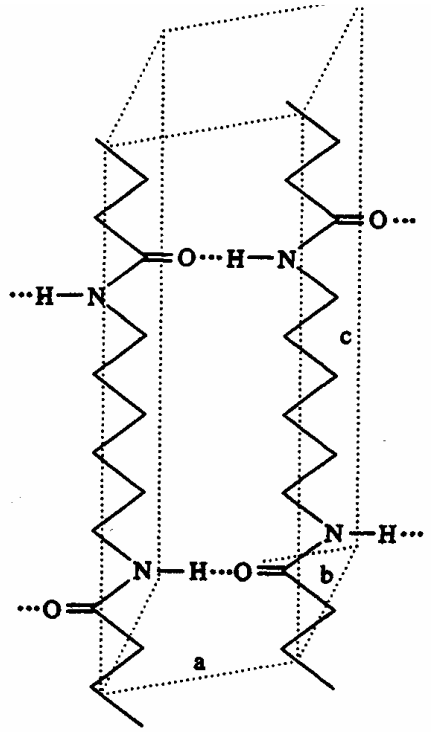

Figure 2.3. Unit Cell of Nylon 6,6[9]

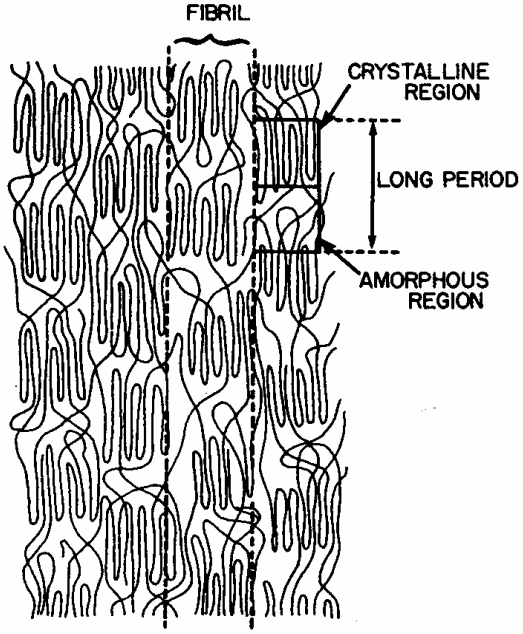

Figure 2.4. Molecular Arrangement of a Drawn Nylon 6 Fiber[22]

available to the specimen during the deformation process. Notice from Figure 2.4 the discontinuities produced by the amorphous regions and the ordered phases of the crystalline regions.

X-ray diffraction techniques are normally employed to determine a material's degree of crystallinity. This is done in an effort to determine the atomic spacing in a material, which is normally on the angstrom or nm length scale. Diffraction is based on the wavelength of the beam used to probe the given material, and is commonly known as Bragg's law:

$$n\lambda = 2(d \sin\theta)$$

In essence, this relationship evinces that diffraction occurs when the two emitted beams coincide, and are therefore in phase with one another. A pictorial representation of the X-ray diffraction technique is shown below in Figure 2.5.

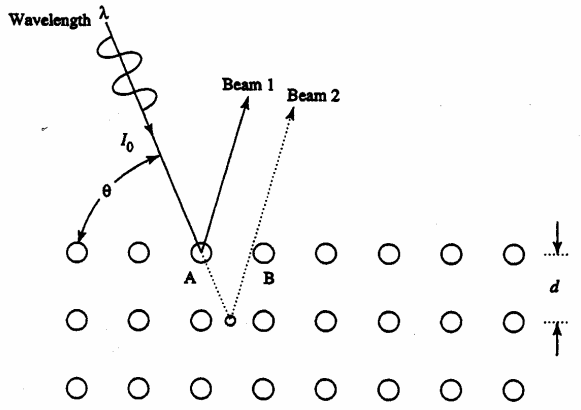

Figure 2.5. Schematic of X-ray Diffraction[60]

In accordance with the Argon theory of craze initiation, Zhurkov, Kuksenko, and Slutsker used small angle X-ray scattering techniques to detect submicroscopic cracks in

polymers[58,61]. To supplement these findings, Kausch later concluded that this submicroscopic formation is independent of chain scission[58,28].

In addition to these factors, the orientation factor and birefringence are of particular interest in the fracture behavior of nylon 6,6 fibers because they provide an assessment to the degree of molecular axial orientation[33]. Hermans et al.[20] have provided a thorough analysis of the orientation factor, *f*, and its effects on axial alignment. Ziabicki and Kedzierska[33.62,63] proved that the birefringence of the as-spun fibers increases at a monotonic rate with the reciprocal of fiber diameter. Also, Ishibashi[33,25] has provided an equation that describes how birefringence decreases with spinning temperature. This equation is described as:

$$\frac{d\Delta n}{dt} = A(\theta)\left(\frac{dV}{dx}\right) - \frac{\Delta n}{\tau(\theta)}$$

Here, $A(\theta)$ is an optical constant, $\tau(\theta)$ is the associated relaxation time, $d\Delta n/dt$ is the resultant speed of molecular orientation, and dV/dx is the velocity gradient along the spin line. A pictorial representation of the melt spinning apparatus used to develop this correlation is shown in Figure 2.6.

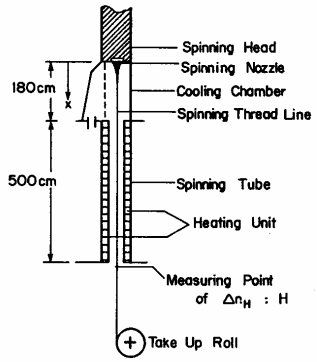

Figure 2.6. Melt-Spinning Apparatus with Heater Hood Installed 180 cm. Below the Spinneret[25]

Shigemitsu et al.[65] developed a theoretical framework for analyzing polarized fluorescence intensity in an anisotropic polymer and verified its direct application to molecular orientation measurements in nylon 6 fibers. They proved that the fluorescence technique can be used to measure the effects and structural changes to nylon 6 under the drawing process. Figure 2.4 in the previous pages depicts a fiber that has undergone the drawing process. Lim et al.[33] conducted an extensive investigation on nylon 6 and determined that because of the drawing process, the molecules orient themselves preferentially either parallel or approximately parallel to the fiber axis. Figure 2.4 also illustrates the randomness and unpredictability of the molecular arrangement in polyamides due to the drawing process. Also, in reference to the effects of drawing on molecular orientation and birefringence, Ito et al.[26] have shown that molecular weight affects these factors significantly. From a comparison of tensile modulus vs. draw ratio, the researchers revealed that the draw efficiency of nylon 6 was greatly affected by the draw technique, predrawn morphology, and molecular weight. They concluded that the draw efficiency increased with increasing molecular weight, with a tendency more prominent in the noncrystalline networks than crystalline networks. Murthy et al.[37] investigated the effects of annealing on the structural characteristics of nylon 6 fibers. This was done in conjunction with the drawing experiments in an effort to increase the crystallinity and crystalline volume. From experimental results, they deduced that annealing increases the crystallinity and crystalline perfection, and in addition increases the density of the fiber to a large extent. Figure 2.7 clearly demonstrates this effect. These consequences of the annealing process are due to the crystallization of the amorphous phase in the fiber, in contrast to the drawing process. This is one of a

plethora of studies that have been conducted on single nylon filaments with the aim of increasing the structural and mechanical properties. It was an early research effort and relatively unsophisticated method with the aim of increasing microstructural attributes in high-performance nylon fibers. Some sophisticated methods to enhance the microstructure and physical properties of nylon fibers include high-temperature zone-drawing (HTZD), in which the drawing process was performed in different temperature phases[52]. This method led to increased elastic modulus and fracture strength for the fibers. A later study by the same investigators applied high tension annealing (HTA) along with HTZD to obtain further increased crystallinity and mechanical properties[53]. Further augments in the elastic modulus and tensile strength were obtained, due to increases in the crystallinity and orientation factors. A summary of the improvements in tensile properties from HTZD and HTA treatments for nylon fibers are shown in Table 2.1. Suzuki et al.[54] also developed a continuous zone-drawing (CZD) technique for enhancement of microstructural and mechanical properties of nylon 6,6 fibers. For this method, the crystallinity increased from 25% to 37% and the orientation factor increased dramatically for the fibers tested. As with the other methods, increases

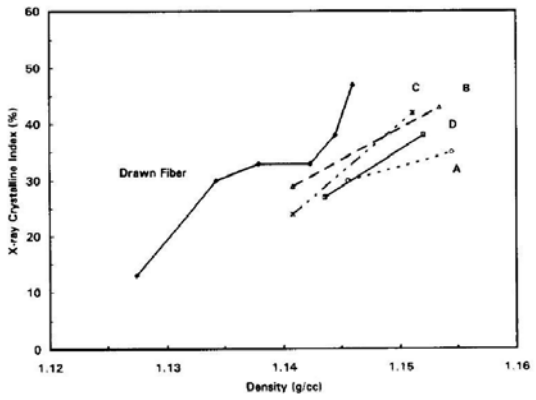

Figure 2.7. Crystallinity vs. Fiber Density for Nylon 6[37]

Table 2.1. Increase in Tensile Properties from HTZD and HTA Treatments[53]

Fibre	Young's modulus (GPa)	Tensile strength (GPa)	Elongation at break (%)
Original	1.1	0.18	385.6
HT-ZD1	4.7	0.54	34.5
HT-ZD2	6.4	0.75	12.9
HTA1	8.2	1.10	13.4
HTA2	9.5	1.18	12.6
HTA3	12.3	1.42	13.1

in the elastic modulus and fracture strength were obtained as well. Penning et al.[47] recently applied a network model approach to describe the deformation mechanisms in nylon 6 fibers under numerous spinning and drawing conditions. They found that the network draw ratio can be discovered by superposition of the true stress-strain curves and can be associated with fiber orientation using relationships for network deformation. In sum, these enrichment techniques can be used in alliance with the fracture mechanics protocol formulated in this research to fabricate a robust, high-performance nylon fiber.

2.2. Anisotropy in Nylon Fibers

Ward and Hadley[58] have summarized that the mechanical anisotropy of solid polymers is determined by the following factors:

1) the structure of the molecular chain and the crystal structure
2) the molecular orientation and morphology
3) thermally activated relaxation processes in crystalline and non-crystalline regions

Lim et al.[33] confirmed that the existence of an anisotropic phase in a polymer is critical to the formation of fibrils. They also discussed how an anisotropic material

possesses the intrinsic low entropy characteristic, which is reminiscent of fibrillar structures. These fibrillar structures have been examined by many researchers and have been proven to materialize from amorphous fluids. Cook and Gordon[4,66] determined the stress components at the crack tip in an anisotropic solid and confirmed that the crack propagates in the direction that displays the least material strength. Cherry and Harrison[4,67] proved that in quasi-static deformation the two crack paths have equal probabilities of occurring when:

$$\frac{1}{R_{II}}\left(\frac{d(u/X)}{dA}\right)_{II} = \frac{1}{R_{\perp}}\left(\frac{d(u/X)}{dA}\right)_{\perp}$$

Here, R is the resistance of the material to crack propagation, u is the energy released during the deformation process, and A is the crack surface area. This study was actually performed on composite materials, in which they considered alternative cases of cracking perpendicular to fibers or cracking parallel to fibers. This is analogous to the case of single fiber deformation, where anisotropy in the longitudinal or transverse direction governs the crack path. A typical crack propagation path of an oriented polymer, provided by Kausch[27], is provided in Figure 2.8.

Nylon 6,6 is characterized as a transversely isotropic polymer. The compliance equation for transverse isotropy is given as:

$$s_{\theta} = s_{11}\sin^4\theta + s_{33}\cos^4\theta + (2s_{13} + s_{44})\sin^2\theta\cos^2\theta$$

In essence, as molecular orientation in the fiber direction increases, Young's modulus ($1/s_{\theta}$, E) in the axial direction increases dramatically. The converse to this statement also holds true, in that Young's modulus measured in the transverse direction decreases as the molecular orientation increases along the fiber axis[60]. The tensile modulus, when measured perpendicular to the chain direction, is considerably lower because of the weak

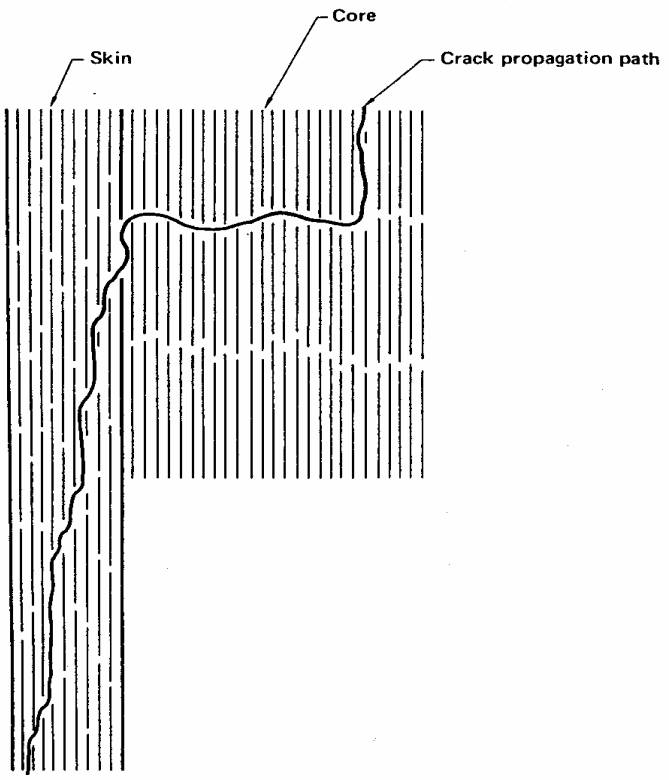

Figure 2.8. Crack Propagation Path in Typical Polymeric Fiber Skin[27]

secondary van der Waals' bonds between the chains. Hadley et al.[58,79] determined the five elastic constants for oriented filaments of nylon 6,6, where the orientation was determined in terms of draw ratio and optical birefringence. Further studies showed that X-ray diffraction measurements were also pertinent to the determination of mechanical anisotropy. Figure 2.9 shows extensional (E_3), transverse (E_1), and torsional moduli (G) vs. draw ratio for nylon 6,6 single filaments. The figure also depicts theoretical estimates of these moduli based on simple aggregate theory for comparison to the experimental data. Murthy et al.[37] examined the effects of drawing and annealing on anisotropy in nylon 6 fibers using X-ray diffraction and other methods. Concomitant with the results from Ward and Hadley[58], they confirmed that the distinct ramifications of the drawing

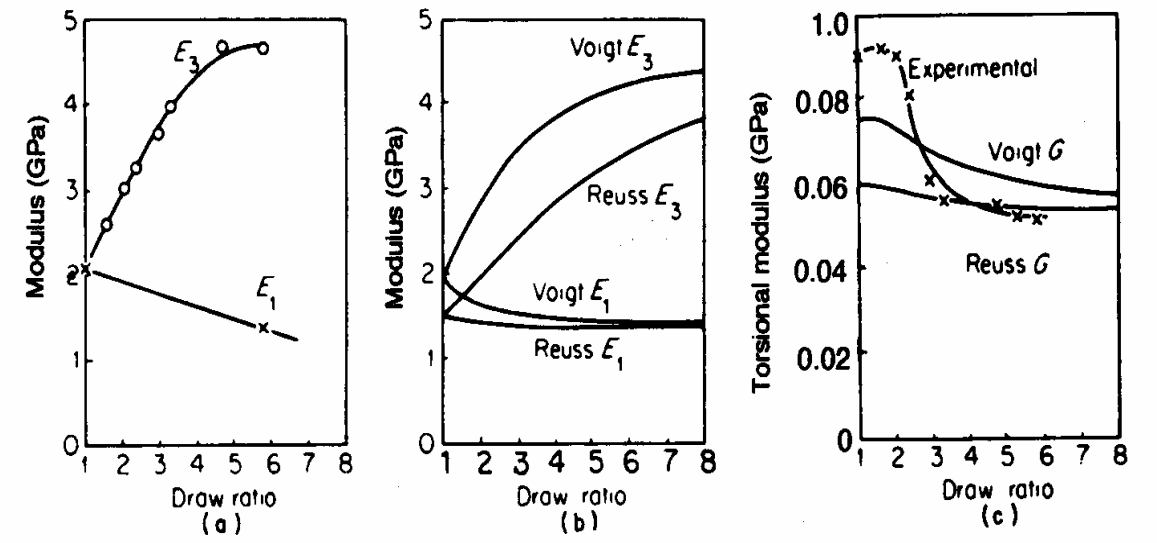

Figure 2.9. Nylon Filaments: Extensional (E_3), Transverse (E_1), and Torsional Moduli (G); Comparison Between Experimental Results and Simple Aggregate Theory for E_3 and E_1 ((a) and (b)) and for G (c)[58]

process are increases in crystallinity, crystalline perfection, and molecular orientation. In addition, they determined that the anisotropy in the amorphous region increases with increasing draw ratio of the sample. Both of these observations are shown in Figure 2.10, which displays the effect of draw ratio on orientation in the sample and amorphous anisotropy.

2.3. Nylon Fibers Used as Reinforcement Agents

Nylon has been employed as a reinforcing agent for several materials, in particular rubber composites. However, to demonstrate how nylon covers the gamut of engineering applications, a recent study has been done on nylon straps used in the development of cerclage fixation techniques[18]. With the employment of nylon 6,6 straps for this medical application, the purpose was to achieve temporary fracture fixation.

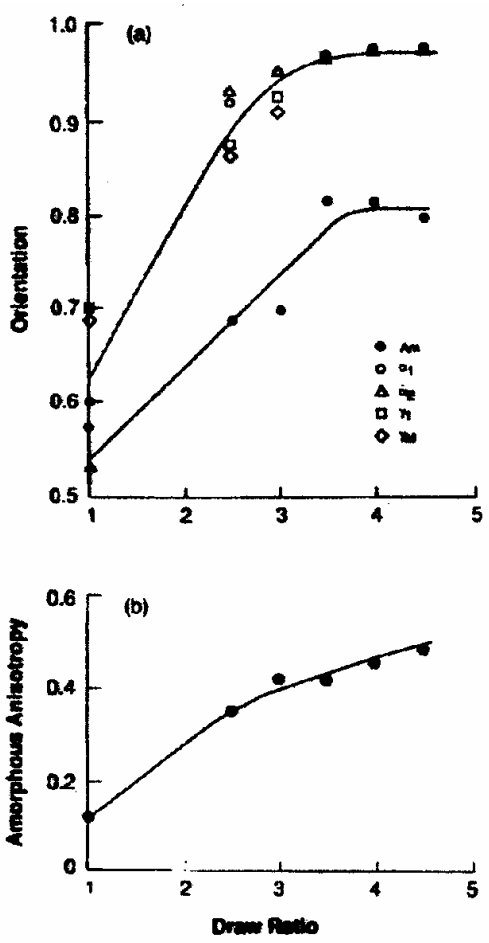

Figure 2.10. (a) Effect of Draw Ratio on Molecular Orientation for Nylon 6 (b) Effect of Draw Ratio on Amorphous Anisotropy[37]

Another useful application of nylon 6,6 and nylon 6 fibers is for tire reinforcement, which facilitates in absorbing the structural load caused by the interaction between the tires and the pavement. Aside from steel, nylon 6, nylon 6,6, and polyester are the most widely used tire reinforcement materials[38]. It is of interest to designers and researchers to ascertain how these materials respond under certain stress loads, and more significantly how they degrade over time. Researchers in the Indian heavy vehicle tire market have substantiated that tires composed of nylon cords exhibit superior endurance in comparison to those made of polyester cords[38,49]. They performed a series of degradation

experiments on nylon 6, nylon 6,6, and polyester cords using cyclic compression and cyclic tension loading onto the reinforced rubber composite at different strain levels and time intervals. The research served as corroboration for nylon 6,6 and nylon 6 fibers being employed as reinforcement agents in rubber composites. Polyester proved to exhibit poor fatigue resistance, while nylon 6,6 registered 80% fatigue strength retention and nylon 6 showed 62% retention[38,49]. Prevorsek et al.[38,48] have determined that under dynamic conditions, nylon 6,6 demonstrates a higher heat generation rate than nylon 6. This excessive thermal generation lowers the achievable stress level for nylon 6,6 fibers, which is adverse for tire reinforcement applications. Fujii[15] has performed an extensive computational analysis on motorcycle tire, in which the tire, nylon cord, air, and aluminum rim were modeled in the finite element experiments. Specifically, the research sought to determine if the results from a crash simulation correlated well with static and dynamic experiments. In the study, the nylon cords were modeled as layers of membrane elements reinforced in one direction for a particular layer. For the wheel, only the rim was modeled, and the rim joints and spokes served as constraint points. Figures 2.11 and 2.12 provide a representation of the tire structure and FEM model section, respectively. When the models were compared with and without nylon cords, the stiffness of the model in the absence of nylon in tension was much lower than that of the model with the presence of nylon. However, the compression models exhibited a much smaller difference in magnitude in stiffness for tires with and without nylon reinforcement.

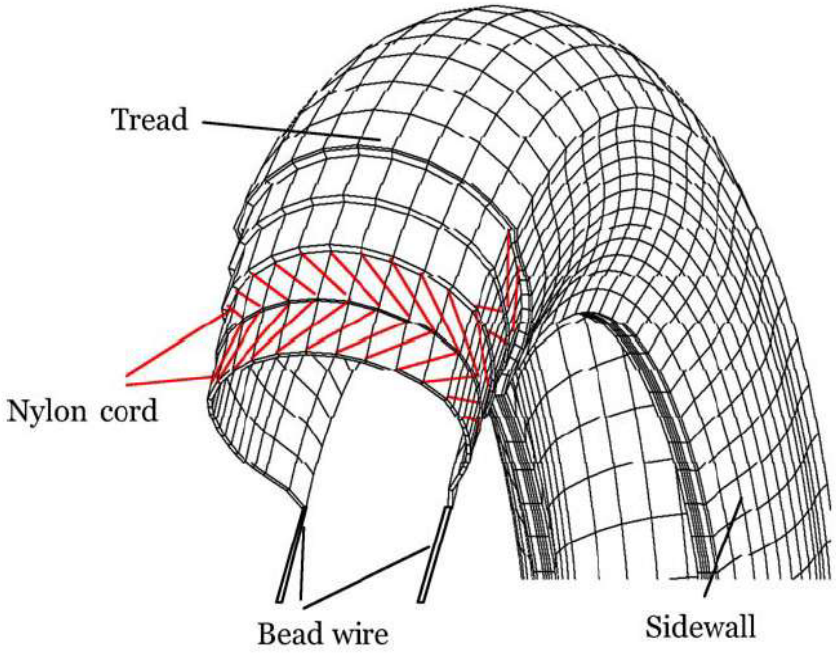

Figure 2.11. Tire Structure Used in FEM Study Showing Tread, Nylon Cord, Bead Wire, and Sidewall[15]

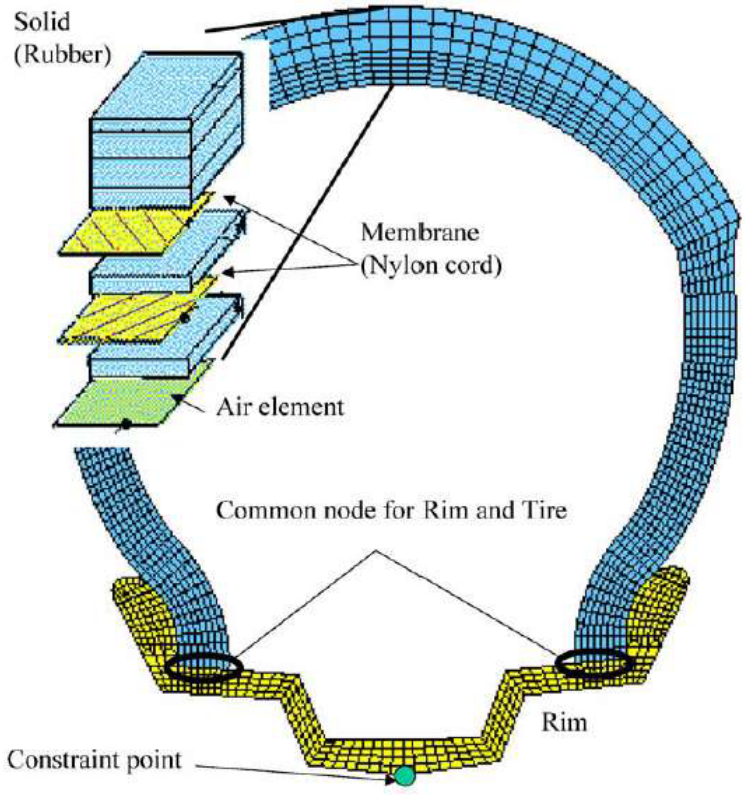

Figure 2.12. 2-D Section Cut of Tire Used in FEM Study[15]

CHAPTER 3

PLASTICITY CONSIDERATIONS IN NYLON FIBERS

3.1. Plasticity Theory: General Deformation and Yield Principles

Understanding yield and plasticity effects in polymers can also help to illuminate the fracture process in nylon 6,6, since these phenomena precede fracture and are responsible for much of the damage accumulation that is experienced by the material. One should first be conversant with elasticity theory, since it is a basic constituent of plasticity, and Timoshenko and Goodier[56] have developed a rigorous elasticity framework that is applicable to most engineering materials. Specifically, the classical theory of plasticity was developed to study the stress-strain relationship of plastically deformed metals. However, these laws are applicable to a wide range of materials, and can be utilized to quantify plasticity effects in nylon 6,6 and nylon 6 fibers. The initial experimental stress-strain response of the nylon 6,6 filaments considered for this study are linear-elastic, strain hardening with varying elastic moduli for different draw ratios. One can employ empirical relationships such as Ramberg-Osgood, linear-elastic strain hardening, or inverse hyperbolic tangent to reproduce experimental data. These empirical relationships are experiential in nature, however, and one should devise constitutive equations to determine the relationships of stress to strain/strain rate. Before discussing such rigorous mathematical models, rudimentary thermodynamic principles will be presented to establish the basis of plasticity theory. These two concepts, based on considerations by Khan and Huang[30], are presented as:

1) Plastic deformation involves dissipation effects in materials, which affirms that it as an irreversible process.

2) Because of the nature of irreversibility, plastic deformation is a path dependent process.

Krempl and Bordonaro[32] have validated path dependence for biaxial-torsional loading of nylon 6,6, in which they performed displacement-controlled experiments on 50% crystalline tubular specimens. They also determined that the time-dependent effects interact with plasticity effects for biaxial-torsional loading of nylon 6,6. For the classical theory of plasticity, plastic deformation is considered to be rate insensitive. However, the viscous component in the constitutive model for nylon fibers precludes this assumption, and rate sensitivity should be considered for this analysis. The constitutive laws for polyamides in general will include time dependent parameters, which serve as an auxiliary in quantifying the effects of creep, strain rate, and viscosity.

3.2. Criteria for Constitutive Models and Yield Criteria in Polymer Fibers

In regards to constitutive equations, there are specific criteria that are pertinent to the successful development of these models for plastically deformed materials[30]:

1) The initial yield point of the material must be determined. From this, an initial yield surface should be constructed and formulated as follows:

$$F\left(\underset{\approx}{\sigma}, \sigma_Y^0\right) = 0$$

Here, $\underset{\approx}{\sigma}$ is the second-order stress tensor and σ_Y^0 is the accompanying initial yield stress. This yield surface is constructed in six-dimensional stress space, in which the six dimensions correspond to the independent components of stress.

2) Subsequent yield surfaces must be determined. These surfaces in general will follow the relationship:

$$\sigma_Y = \sigma_Y(\alpha_i)$$

As shown from this equation, the subsequent yield surfaces are a function of the component α_i, where they represent the possible hardening parameters.

3) Constitutive equations should be developed in rate or increment form, due to path dependence and rate insensitivity.
4) Loading-unloading criteria must be established, which differentiates nonlinear elasticity theory from plasticity theory.

An accurate formulation of the yield surface in polymeric materials can be a formidable task, due to the ambiguous nature of the yield point from nonlinearity of the stress-strain curve. Because of the nonlinear behavior of nylon 6,6 fibers after subsequent loading, one should consider utilization of the endochronic theory[30] of plasticity for inelastic deformation analysis. This theory obviates the need for the determination of the yield surface of the material and is based on concepts of irreversibility in thermodynamic systems. Valanis[72,73] has proposed this theory and the general form of the equation is:

$$\overset{\approx}{S} = 2G\int_0^z \rho\left(z - z'\right)\frac{d\overset{\approx}{\varepsilon}^p}{dz'}dz'$$

Here, $\boldsymbol{S}$ is the second-order tensorial deviatoric stress component, $\boldsymbol{\varepsilon^p}$ is the second-order tensorial deviatoric strain component, G is the shear modulus, ρ is the material kernel function, and z is the intrinsic time value. This equation was later modified to determine the single component of stress for the uniaxial tension case in nylon 6,6 fibers and is provided as:

$$\sigma_{11} = \frac{3}{2}S_y^0\frac{d\varepsilon_{11}^p}{dz} + 3G\int_0^z \rho\left(z - z'\right)\frac{d\varepsilon_{11}^p}{dz'}dz'$$

Notice the resemblance of the uniaxial tension case to the general form of the endochronic theory, where in the uniaxial case $S_y^0 = 2G\rho_0$. An exhaustive proof of this theory is provided by Valanis[72,73] and one should refer to these references in more rigorous elastic-plastic analyses and constitutive model development of nylon 6,6 fibers.

Although developed as a measure to quantify the effects of plasticity in metals, these classical plasticity and constitutive model criteria can be used to determine the stress-strain response in polyamide fibers. One other important fundamental assumption about the deformation process is that it is isochoric, which implies that the sum of the components of the plastic principal strain tensor is zero. By using this assumption in combination with strain hardening effects from uniaxial loading, the Poisson's ratio for linear-elastic strain hardening materials can be determined. This equation is provided as[30]:

$$\nu^P = \frac{1}{2} - \left(\frac{1}{2} - \nu\right)\left(\frac{\sigma_Y^0 - E'\varepsilon_Y^0}{E\varepsilon_{xx}} + \frac{E'}{E}\right)$$

All of these assumptions and equations in elementary plasticity theory are not sufficient alone for understanding inelastic deformation in polyamide fibers. Several researchers have attempted to explicate the phenomenon of yielding in polymeric fibers, and little success has followed. Ahzi et al.[1] examined the large-scale deformation in a multitude of crystalline polymers and determined that the crystal lattice of nylon 6 is monoclinic in nature and deforms by crystallographic slip. They disregarded the amorphous phase and confirmed that there are only three distinct and independent slip systems for nylon 6 single crystals. It was also confirmed that the amorphous phase in semi-crystalline polymers provides additional straining, since the macromolecular texture

results in the idealized crystalline model occurred at a lower strain than the experimental results.

Northolt et al.[43] performed experiments on linear extended polymer fibers below the glass transition temperature and attempted to establish plasticity criteria. The parameters of interest were chain orientation distribution, average shear modulus between chains, and chain modulus. What was of significant importance in this research was the determination of a yield criterion based on the critical resolved shear stress. Based on the modified series model[43,40,41,42], the tensile modulus of the fiber is provided as:

$$\frac{1}{E} = \frac{1}{e_c} + \frac{\left\langle \sin^2 \phi_0 \right\rangle_E}{2g}$$

In this equation, E represents the tensile modulus, $<sin^2\phi_0>_E$ is the second moment of the domain orientation distribution, e_c is the chain modulus, and g is shear modulus between the chains. A schematic of the fiber exposed to normal stress, σ, under tensile loading is provided in Figure 3.1. Understanding how the normal stress is resolved into shear stress components in this diagram is vital to the understanding of yield and fracture in polyamide 6,6 fibers. From simple geometric relationships, one can determine scalar values of the normal and shear stresses acting on the domain with orientation angle ϕ. As stated earlier, the fundamental aspect is that Northolt et al.[43] proposed that the critical shear stress, τ_y, is responsible for the yielding mechanism in polymeric fibers. From Figure 3.1, one can deduce that the critical shear stress is given as:

$$\tau_Y = \sigma \sin\phi \cos\phi$$

Northolt et al.[43] have concluded that this shear stress engenders yielding through an immediate and permanent deformation mechanism. This theory is reminiscent of

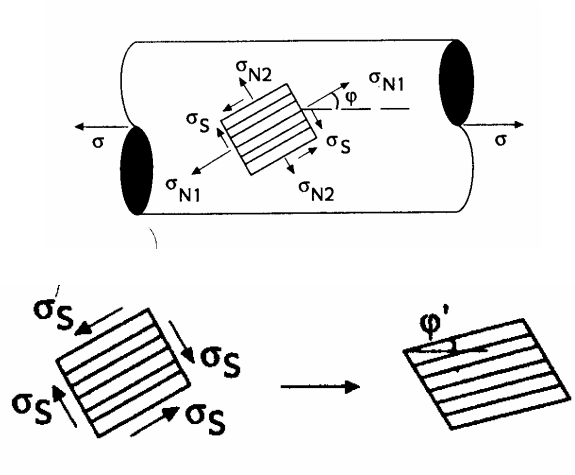

Figure 3.1. Normal and Shear Stresses Acting on Fiber Domain[43]

Schmid's law, which confirms that slip is initiated when the resolved shear stress reaches a critical value[43,10,59]. The findings contrast plasticity theory in metals, in which the plastic deformation of the sample is autonomous of the first invariant of the stress tensor. Thus the von Mises and Tresca yield criteria from classical plasticity theory are not apposite for studying yielding mechanisms in polyamide fibers. The Coulomb-Mohr yield criterion[58,11] would be an applicable criterion for studying yielding in polymeric fibers, since it expresses the critical shear stress as a function of the hydrostatic pressure. The magnitude of the shear stress is specified as:

$$\tau = C - \sigma_n \tan\phi$$

Here, C is the cohesive stress, σ_n is the normal stress, and ϕ is the angle of internal friction[30]. As shown, the Coulomb-Mohr criterion is based on tribological concepts and is dependent on the first invariant of the stress tensor. Kausch et al.[29] confirmed the appropriateness of this relationship for characterizing nylon 6,6 materials. They computed the $tan\phi$ value for nylon 6,6 at room temperature as 0.03. In two-dimensional

stress space, the yield surface for the Coulomb-Mohr criterion is viewed as an asymmetrical hexagon, in contrast to the Drucker-Prager[14] criterion which can also be employed for hydrostatic dependent materials[30]. The yield locus of the Drucker-Prager criterion is circular in geometry, and is merely a modification of the classical von Mises theory. Basically, the addition of the hydrostatic stress component to the von Mises criterion establishes the Drucker-Prager condition[30]. The yield surface of the Drucker-Prager criterion, based on the first invariant of the stress tensor and the second invariant of the deviatoric stress component, is given as:

$$F\left(J_1, J_2^{'}\right) = \sqrt{J_2^{'}} - \alpha J_1 - \kappa = 0$$

In this equation, J_1 is the first invariant of the stress tensor and $J_2^{'}$ is the second invariant of the deviatoric stress tensor. The constants α and κ are material constants, which should be determined from experimental results. The essential aspect here is the dependency on the hydrostatic pressure, which is a typical characteristic of nylon 6,6 fibers. Kausch et al.[29] ascertained the effects of pressure dependence on the elastic modulus for nylon 6,6 samples. Essentially, the elastic modulus is an obscure quantity for most polymers and its value is significantly altered with changes in hydrostatic pressure. They observed that the ratio of the elastic modulus at 50,000 psi to that at atmospheric conditions is 1.9 for nylon 6,6. Although the assumption of hydrostatic pressure dependence normally contradicts the isochoric assumption in typical materials, the volume changes are assumed to be infinitesimally small for the nylon 6,6 fibers in this research. Ward and Hadley[58] described this phenomenon for polymer systems that are sensitive to hydrostatic pressure and concluded that the isochoric assumption is still valid.

They concluded that the pressure changes increase the yield stress of the polymer material; however, the volume changes were found to be negligible.

3.3. Hysteresis in Polyamide Fibers

Understanding the repercussions of hysteresis is a vital component of plasticity effects in nylon fibers. The hysteresis phenomenon is experienced in many metals and polymers, and nylon 6,6 fibers have shown no exception to the rule. Hysteresis involves the effects of relaxation in materials, in which they traverse different paths for loading and reloading of the sample in tension or compression. Typically, this behavior is contingent upon the actual time the sample is allowed to recover following initial deformation. As a general rule in polyamide fibers, the more time an individual specimen is allowed to recuperate subsequent to plastic deformation, the closer it will resemble the original deformation path on the stress-strain curve. Many theorists have attempted to elucidate this tendency in polymer fibers, and have concluded that it is due to the rupture of bonds upon initial loading and the ensuing convalescence of these bonds after a substantial period of recovery. Particularly, Northolt et al.[43] performed studies on several polymer fibers and concluded that the two important factors in the recovery process are the flexibility of the chains and the intermolecular secondary bonds. They concluded that when the sample is unloaded to zero during a stress-strain experiment, the chains attempt to return to their initial configuration while the secondary bonds attempt to recover. A depiction of this phenomenon is shown in Figure 3.2. The sample tested in this experiment was a poly(ethylene terephthalate) (PET) fiber; however, the stress-strain response and behavior of this material are in close resemblance to that of nylon 6,6. The

main difference in the samples is the value of the initial yield point, which is an attribute that varies for different materials. Notice from Figure 3.2 that the sample experienced a large amount of hysteresis after one second of recovery, yet it almost traversed the original path on the stress-strain curve after 61,200 seconds. One can rationalize this behavior through concepts in molecular bonding of polymers, where the bonds sundered during the deformation process and regenerated upon ample recovery time.

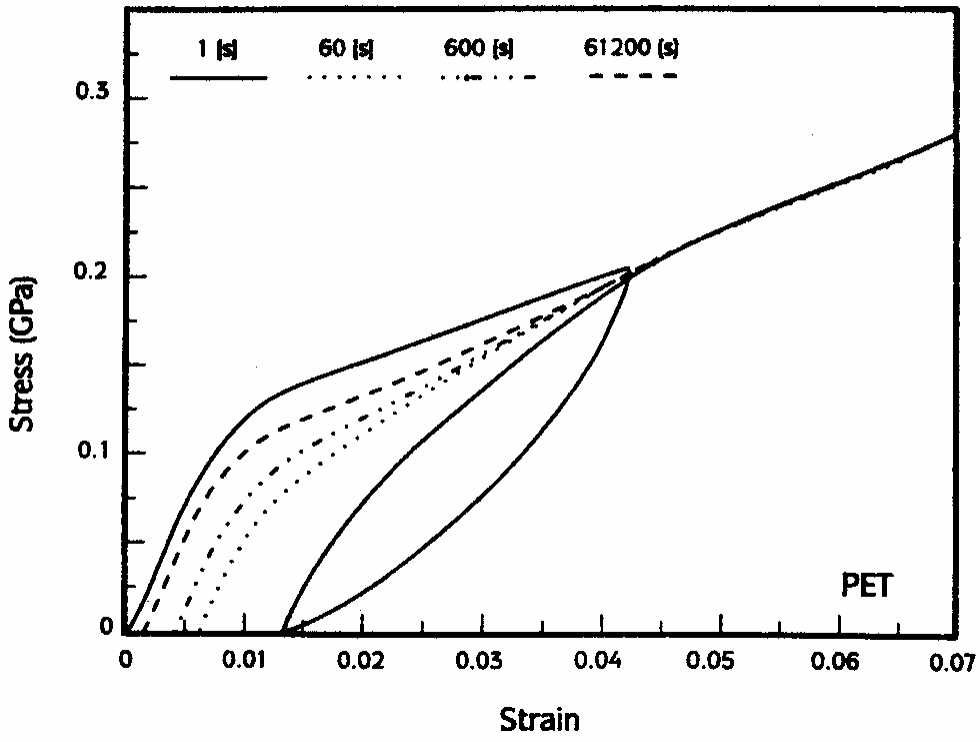

Figure 3.2. Recovery of Strain for Various Times[43]

CHAPTER 4

FRACTURE CONSIDERATIONS IN NYLON FIBERS

4.1. Fracture Models: Background of Theoretical vs. Actual Strength of a Specimen

The ambition of the field of fracture mechanics is to allow one to understand how flaws ultimately govern the behavior of materials. Moreover, fracture mechanics presupposes that either a congenital or manufactured flaw exists in the specimen, which under certain stress conditions will ultimately become critical and lead to final fracture. Research has shown that in the absence of these inhomogeneities, materials would exhibit strengths up to three orders of magnitude of the experimental strength. The theoretical cohesive stress of a material is derived by determining the amount of force required to separate individual atoms for a prescribed interatomic separation distance. Figure 4.1 provides a pictorial representation of this theory, in which one can see the potential energy and applied force versus interatomic separation distance. In this diagram, the applied force is assumed to be of a *sine* function, and the theoretical cohesive stress is calculated by determining the maximum force in tension and equating the stress value. Since the cohesive stress indicates the value at which atoms separate, it is an adequate measure of the theoretical strength limitation for a given material. Termonia and Smith[55] have developed a Monte-Carlo approach to assess the theoretical tensile behavior of polymeric fibers, in which they quantified the effects of inhomogeneities among atoms on ultimate tensile strength. A two dimensional representation of the nodal array used in this analysis is provided in Figure 4.2. The model was developed based on premises in kinetic theory, in which the activation energy of individual bonds is the decisive

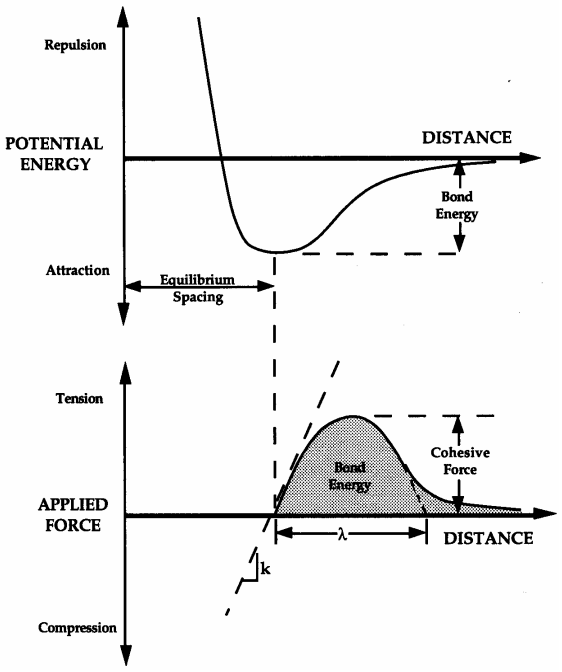

Figure 4.1. Potential Energy and Applied Force vs. Interatomic Separation Distance for Materials[2]

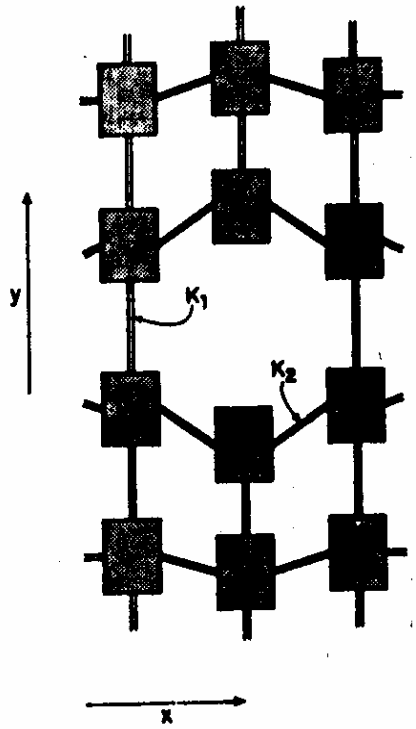

Figure 4.2. 2-D Model Used to Estimate Tensile Strength in Polymeric Fiber[55]

parameter for determining when failure will occur among the polymer chains. This degree of failure is expressed in the following form:

$$v_i = \tau \exp[\frac{\left(-U_i + \beta_i \sigma_i\right)}{kT}$$

In this expression, τ signifies the thermal vibration energy, β_I is the activation volume, σ_I is the local stress field, k is the Boltzmann constant, and T represents the absolute temperature in the experimental process. Other constraints used in this study were molecular weight, strain rate, and temperature, which used in conjunction with the effect of inhomogeneities assist in determining the ultimate strength of polymer fibers. The studies were conducted through usage of computer simulation techniques and closely correlated with experimental results for this polymeric fiber. Lim et al.[33] confirmed that the theoretical strength of a nylon fiber is based on the force between the carbon-carbon bonds and the molecular cross-sectional area. This relationship is expressed as:

$$\text{Theoretical strength (GPa)} = \frac{Bond}{} \frac{Strength}{MA\left(nm^2\right)} \frac{(dyne)\times 10^4}{}$$

For nylon 6,6 and nylon 6 fibers, the theoretical strength, as provided by Mark's breaking load for a carbon-carbon bond is 28.3 GPa[33,57]. An equation to estimate the total theoretical elastic energy stored in a sample with modulus E and length L is given as[27]:

$$W_k = \frac{qL\psi^2}{2E}$$

In this expression, q represents the cross-section of the material and ψ represents the rupture strength. Even though these inquiries represent viable options for establishing the theoretical inadequacies in polymer fibers, they are of little consequence to the fracture mechanics community, because no perfectly homogeneous material exists. They only

provide a basis for ascertaining the degree of variation between experimental and theoretical strength of solid materials.

In 1913, Inglis[24] presented a rigorous mathematical analysis to evaluate the stress concentrations in a material with an elliptical cavity. By allowing the ellipse to be idealized as additional configurations, he was also able to determine the stress components for cracked bodies with circular and sharp geometries. Later in 1920, Griffith[17] was able to articulate to the engineering community that surface defects are directly related to the process of rupture in solid materials. These concepts were established on principles of potential energy and external work required to create external surfaces in a material body. Griffith conducted theoretical and experimental investigations to establish a well-known rupture theory for brittle, elastic materials. In fact, the First Law of Thermodynamics is applicable to Griffith's rupture theory of solids, where an infinitesimal increase in crack area is given as[2]:

$$\frac{dE}{dA} = \frac{d\Pi}{dA} + \frac{dW_s}{dA} = 0$$

$$-\frac{d\Pi}{dA} = \frac{dW_s}{dA}$$

Here, Π represents the potential energy of the specimen and is equated as:

$$\Pi = \Pi_0 - \frac{\pi\sigma^2 a^2 B}{E}$$

W_s represents the work required in the creation of crack surfaces and is equated as:

$$W_s = 4aB\gamma_s$$

In these equations, σ represents the stress on the body, a is the crack length, B is the ligament length, E is the elastic modulus, and γ_s represents the surface energy of the material. For completeness, in the study of thermodynamic systems the infinitesimal

surface area quantities are replaced by infinitesimal time parameters and the sign of the work function is negative. The correlation is the same, nevertheless, where the incremental change in potential energy per unit time is analogous to the incremental variation in the external work to create new surfaces in a material. Using the energetics of Griffith[17] in amalgam with flaw theory, one can partition the fracture process into separate phases:

1) Slow isothermal phase with a stress and temperature dependence
2) Adiabatic phase occurring catastrophically leading to ultimate fracture

These concepts were developed by E.H. Andrews[3], in which he aspired to describe how flaws smaller than the critical size would somehow eventually achieve a critical value. A more rigorous energy balance for fatigue loading of polymers has been suggested by Kausch[27], and is given as:

$$dW = dU - TdS + Q_{ir}$$

The change in internal energy (U) of the specimen during cycling is[27]:

$$\delta U_n = dW_s - dW_r + Td_sS - Td_rS + Q_{irs} - Q_{irr}$$

As shown, these energy balance equations are more comprehensive in a sense that they contain both irreversibility and entropy (S) parameters, which are components that all materials possess to some degree.

4.2. Fracture in Polymers and Polymer Fibers

The fracture behavior of polymer materials is atypical to that of metals or ceramics, and thus an entirely different analysis is prescribed to illustrate the effects. In polymer systems, the processes of plasticity and fracture are normally independent,

whereas in metals the two mechanisms occur simultaneously. Nevertheless, molecular weight and molecular structure are the main determinants in the rupture behavior of polymer systems and determining these effects for various materials can be a confounding task. Becht et al.[5] considered that fracture in nylon fibers from an atomistic viewpoint occurs mainly by chain scission. They determined that this deformation occurs mainly in the amorphous regions of the polymer, and normally results in free radical production that is detectable by electron spin resonance (ESR). Ward and Hadley[58] discussed how the crystalline bridges that connect adjacent crystalline blocks are a key factor in determining the axial stiffness of a semi-crystalline polymer. Because of this, researchers have examined chain fracture in oriented polymers using electron paramagnetic resonance to detect the free radicals produced. Infrared spectroscopy is another method commonly used in the analysis of polymer fracture. This method seeks to identify aldehyde end groups in polymers, which suggests chain scission. Kausch[58,28] has investigated such studies and provided a synopsis of the results. These findings are concomitant with flaw theory[3] in polymers, which expresses that stress concentrations at the crack tip produce dilatation which aids in the production of corrosive molecules. Additionally, Bershtein et al.[7] confirmed from an extensive investigational procedure on thin polyamide samples that molecular weight and structure can be altered under a combination of stress conditions. All of these studies are good from a molecular perspective, but are inadequate for solving real world fracture mechanics problems. In solitary form, these atomistic assessments can not lead to results for the critical strain energy release rate or nonlinear energy release rate. Therefore, some researchers in the

past have performed experiments on polymers and attempted to quantify the effects of fracture and develop fracture mechanics protocols.

Analogous to the results for yield phenomena in polyamide 6,6 fibers, the fracture performance is affected by the hydrostatic pressure to a great extent. Kausch et al.[29] concluded that in nylon 6,6, the fracture stress increases with increasing pressure. The behavior of the fracture strain is the exact antithesis of the fracture stress, in which decreases occur for augments in the hydrostatic pressure. These observations are what one would expect, since in theory the hydrostatic pressure creates a triaxial state of stress at the crack tip and would thus initiate an expansion in the fracture stress value. As a consequence, the fracture strain would obviously experience a decrease in quantity. These conjectures are based on concepts in simple mechanics theory, in which the hydrostatic pressure invokes a state of dilatation due to changes in volume of the sample.

The direction of the propagation path in polyamide fibers can be described as meandering and aberrant in nature, as compared to other structural materials. Whether in uniaxial tension or fatigue, the path is similar and as discussed earlier is strictly governed by the effects of anisotropy in the sample. Hearle[19] has performed a rigorous investigation on fiber failure, and has provided a progression of events that govern the ductile rupture process in tension. A schematic is shown below in Figure 4.3.

Understanding the chain of events in this schematic is vital to the development of fracture techniques to describe the strength limitations of nylon fibers. As shown, the fiber is loaded in uniaxial tension (a) and a crack forms orthogonal to the fiber axis of symmetry (b1). Upon further loading (b2), the orthogonal flaw transmutes to a v-shaped notch and opens up further (c). At the critical juncture, the flaw ruptures orthogonal to

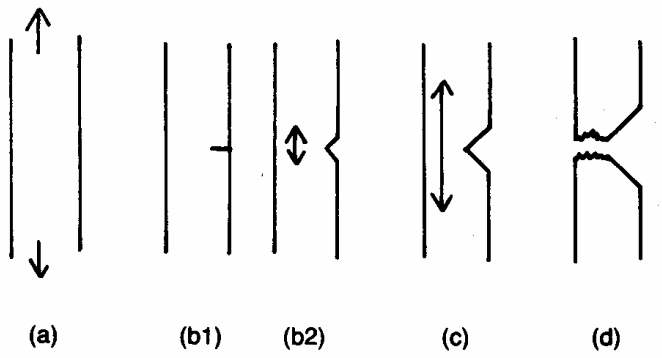

Figure 4.3. Ductile Rupture Process in Fibers for Case of Uniaxial Tension[19]

the fiber axis which constitutes final fracture (d). One should pay careful attention to the separate fiber ends and notice that a mirror image is produced from the fracture of ductile fibers when viewing in the 2-D plane shown. This is important for S.E.M. study, because when viewing the individual fiber surfaces next to one another it appears that a segment of material is missing. In actuality, this façade is produced by the ductile v-shaped rupture process described in Figure 4.3. The fractographs of nylon 6,6 fibers in uniaxial tension conform to this process unequivocally. Hearle[19] has done an extensive S.E.M. investigation on nylon 6,6 fibers, and Figure 4.5 in the following pages provides a clear micrograph showing an isometric view of the fracture surface. Schematics 1 and 2 show the opposite ends of the same fiber that was loaded at a strain rate of 1.67E-02 s^{-1}. The schematics in 3 and 4 represent a fiber that was deformed at a strain rate 100 times lower than the fiber in Figure 1 and 2. However, notice how the fracture surface is not significantly altered by this variable change. The main difference is the larger remaining ligament length at the initiation of critical crack propagation.

Hearle[19] has also provided the chain of events that describe the crack propagation path for ductile fatigue in nylon 6,6 fibers. As shown in Figure 4.4., the sequence of

events is similar; however, notice the dramatic effect of the shear lip that is produced in stage (c) and further progression to final fracture orthogonal to the fiber axis of symmetry (e). In addition, Hearle[19] has provided a variation of the effects of tensile fatigue in stage (f), which depicts the fracture path of ductile tensile fatigue as bi-directionally propagating. S.E.M. fractographs of nylon 6,6 fibers at 50Hz for 62,000 cycles between zero load and 71% of the fracture load substantiate this theory, and are depicted in Figure 4.6. Notice the resemblance in nature to the uniaxial tension case, but how the tensile fatigue forms a long shear ligament prior to ultimate deformation. The fibers in the current study were not tested under such extreme conditions. Rather, the frequency and quantity of cycles prior to deformation was much lower. As an observation, the S.E.M. fractographs obtained in the current investigation resembled that of Hearle's results for uniaxial tension as opposed to uniaxial fatigue.

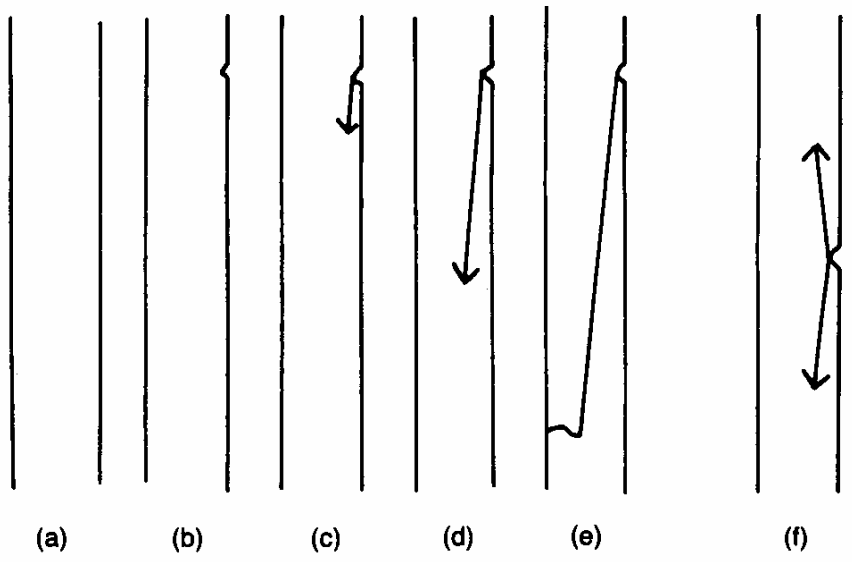

Figure 4.4. Ductile Rupture Process in Fibers for Case of Uniaxial Fatigue[44]

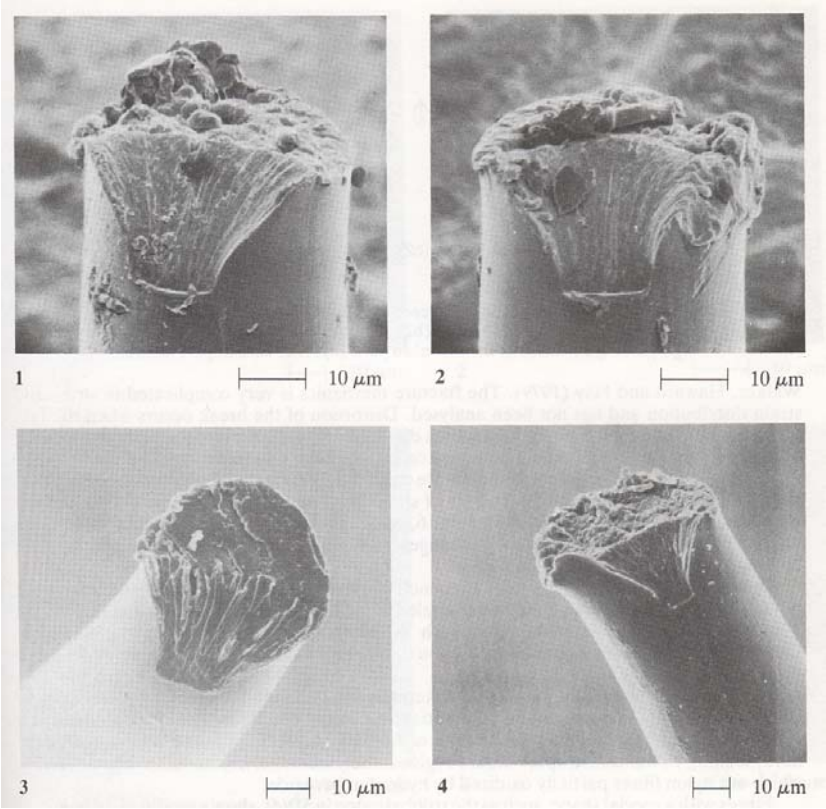

Figure 4.5. S.E.M. Fractograph Depicting Uniaxial Tensile Break of Nylon 6,6 Fibers[19]

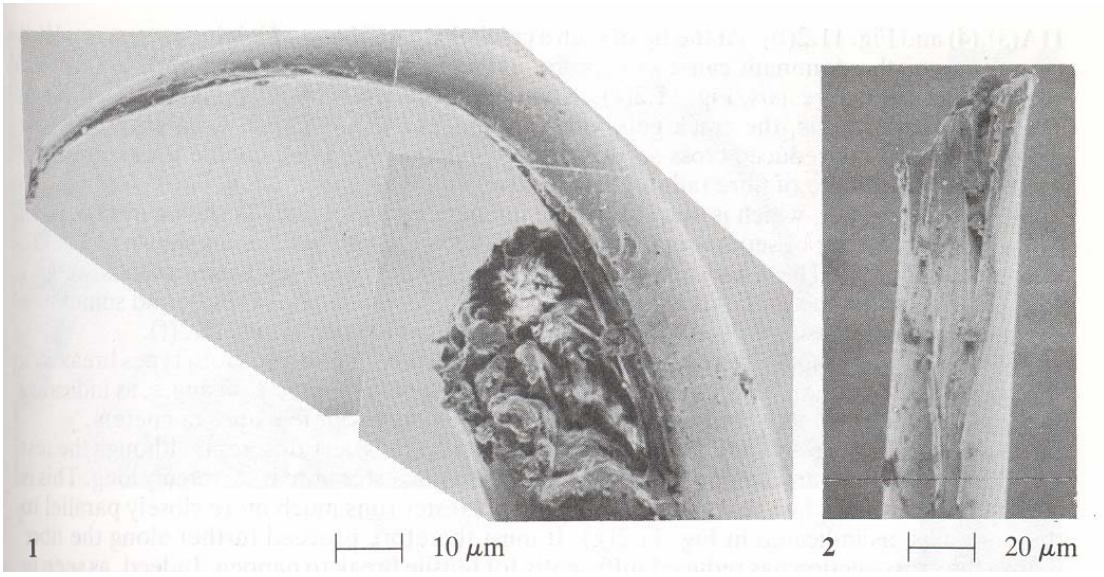

Figure 4.6. S.E.M. Fractograph of Uniaxial Fatigue of Nylon 6,6 Fibers (50Hz, 62,000 Cycles)[19]

4.3. Theories of Strain Energy Release Rate (G) and Nonlinear Energy Release Rate (J)

Irwin later defined the Griffith concept as an energy release rate, which is essentially derived as[2]:

$$G = -\frac{d\Pi}{dA}$$

Here, Π represents the potential energy of the specimen and A represents the crack surface area. Instability in the material occurs when the energy release rate attains a critical value, and is given by:

$$G_c = \frac{dW_s}{dA} = 2w_f$$

This entire formulary serves as the underpinnings of the field of fracture mechanics, because it evinces that when energy limitations are exceeded in a solid body, ultimate material deformation will occur. Griffith and Irwin made their observations based on linear-elastic, brittle materials in the absence of yielding. Nevertheless, what is necessary for the study of fracture in polymeric fibers is a parameter that can quantify the effects of plasticity and yielding. J. R. Rice[50] developed the J- contour integral to achieve this, in which he idealized an elastic-plastic material as nonlinear-elastic for the case of uniaxial tension. Similar to Irwin, he used the concepts of energy and irreversibility to formulate a path-independent line integral that can be used to determine the strength limitations of nonlinear-elastic and elastic-plastic materials. In its rigorous mathematical form, the J-integral is given as:

$$J = \int_{\Gamma} \left(w dy - T_i \frac{\partial u_i}{\partial x} ds \right)$$

A schematic of the integration around the contour of a crack is presented in Figure 4.7. In this equation, Γ represents the contour around the crack, w represents the strain energy

density function of the material, T_i are the surface tractions on the crack front, $\frac{\partial u_i}{\partial x}$ are the displacement gradient (strain) quantities, *dy* is the infinitesimal distance in the y-direction, and *ds* is the infinitesimal arc length in the counterclockwise rotation direction. This line integral demonstrates that the aggregate of the strain energy density terms minus the external work function done by tractions on the crack surface are independent of the path taken[6]. As with the strain energy release rate, *G*, the J-integral is an energy parameter for characterizing stable and unstable propagation in cracked configurations.

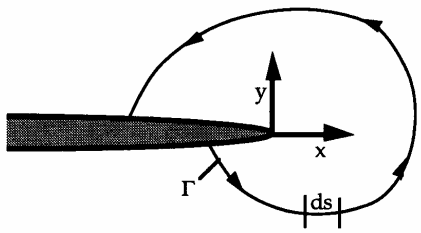

Figure 4.7. Contour for J-Integral Enclosing Crack Tip[2]

Rice[50] made these observations on path independence for elastic-plastic materials by employing a beam configuration idealized in 1) constant displacements and 2) pure bending. The derivation is exhaustive; nevertheless, it has applications that range from the assessment of material resistance behavior to determining strain concentrations at notch tips in elastic or elastic-plastic materials. For the case of elastic behavior or small-scale yielding, Rice theorized that *J* is equivalent to *G*. By assuming a semi-infinite crack in an infinite body and imposing appropriate elastic crack tip boundary conditions, the following relationship was obtained:

$$J = G = \frac{1-\nu^2}{E} K_I^2 \qquad \textit{(elastic materials \& small scale yielding)}$$

This is one of the essential features of the J-integral that is pertinent to the study of fracture in nylon 6,6 fibers. The fact that this parameter can be sequestered into elastic and plastic components has significant implications on how the critical nonlinear energy release rate can be computed from laboratory trials.

Hutchinson[23] was later successful at utilizing these results from Rice to determine stress singularities at the forefront of the crack tip for elastic-plastic, power-law hardening materials. He was further able to deduce that the value of the singularity ahead of the crack tip was lower for the case of plane stress in comparison to plane strain for a hardening material. This is clearly demonstrated in Figure 4.8, in which the ratio of the stresses in plane strain and plane stress increases as a function of the power law hardening coefficient, *n*. This is extremely vital to the case of fracture in minute polyamide fibers, where there is a possible mixed mode of plane stress and plane strain due to the specimen geometry and crack configuration.

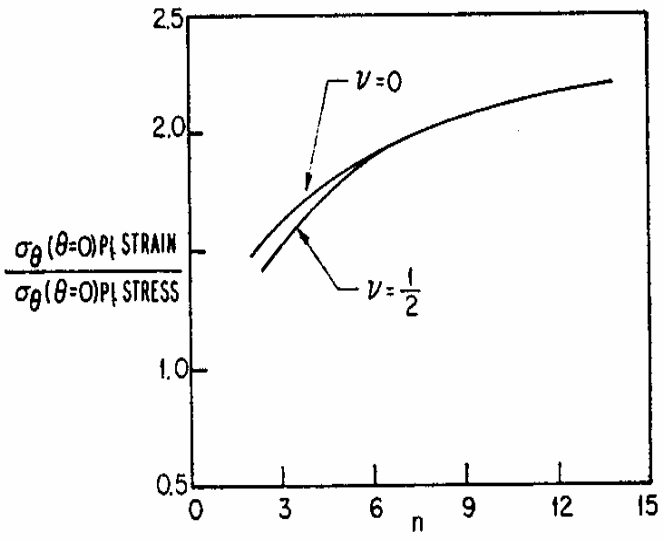

Figure 4.8. Ratio of the Stress in Plane Strain to Plane Stress as a Function of the Power Law Hardening Coefficient[23]

CHAPTER 5

METHODOLOGY

5.1. Sample Preparation

The development of a method that is appropriate for experimentation in individual fiber research is exacting; however, it is the most significant portion of the research. Two different configurations of single filament nylon 6,6 fibers were exploited in this research for range and breadth of application. For the first configuration, a single fiber approximately 35μm in diameter was used. The fibers were extremely small in magnitude, and thus could not be placed directly into the grips for mechanical loading. To circumvent this problem, a Scotch brand adhesive capable of bonding to polymeric materials was applied to the specimen. Next, the assembly was allowed to equilibrate overnight and to permit the adhesive to bond permanently to the gasket. At the end of the 24-hr. period, the fibers were considered ready for experimentation. Tabs were used as a fixture to mount the sample and for direct placement into the grips. The tabs were also utilized in an attempt to set the correct gauge length. The gauge length used in the experiments was 25.4mm, which is equivalent to a 1" gauge. The DuPont Corporation supplied the industrial nylon fibers and the tabs were purchased from the Ohio Valley Gasket Company. These fibers possessed a draw ratio of 2.5X and a picture of the tab with a single fiber attached via epoxide adhesive is displayed in Figure 5.1.

One key component that is associated with the preparation of these samples is being certain that the fiber is aligned parallel to the gasket. Because of the veneer attributes of these nylon fibers, one can not always be certain that the fiber is oriented properly. Without the proper orientation of the fiber, the sample could experience other

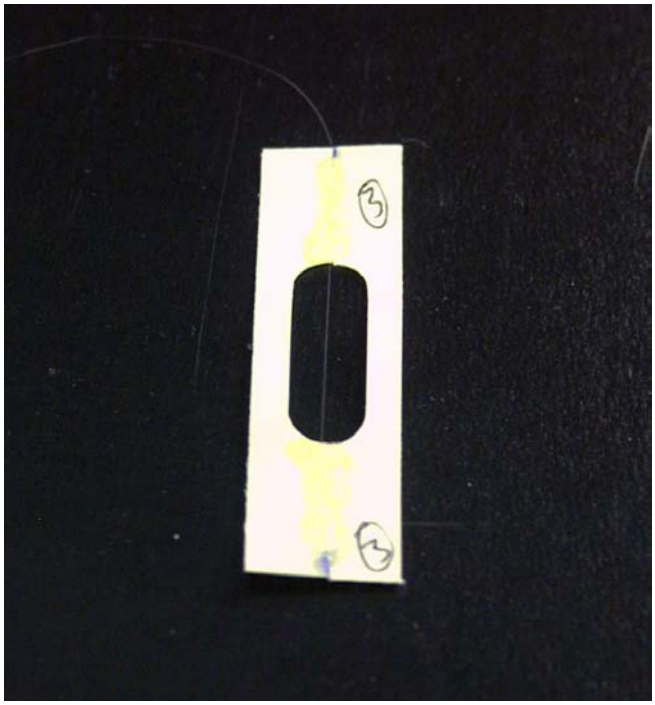

Figure 5.1. 1” Tab With Single Filament Attached

modes of deformation (Mode II, Mode III) that are not accounted for in a normal uniaxial tensile experiment. This could lead to erroneous results when the fracture calculations are performed.

One must use assiduousness when handling the fibers so as not to introduce artificial flaws or imperfections. Special tweezers for handling single fibers were used and latex gloves were worn in an effort not to add artificial weight from the oil produced by human skin. Other researchers in fiber testing have employed a method analogous to the one described for this research. Zinck et al.[64] utilized a similar method in preparing E-glass fibers for mechanical testing, where they mounted the fibers on a paper box and attached it via an epoxide adhesive. However, adhesive attachment is not the only available method for testing single filament polymer samples. Other techniques were attempted, and in particular an alternate method proved to be modestly successful. This

procedure involved the use of a capstan, in which the fiber was wound several times and mounted on the tab via double-sided tape. The results were shown to be closely correlated; however, the capstan did not mount into the grips easily which proved to be time consuming and problematic.

In the second configuration, a larger fiber was used that possessed an obround shape with the same chemical structure. The dissimilarity in the small and large fibers was the amount of drawing that was done during the processing of the fibers. These larger fibers possessed a more highly oriented structure, and thus behaved as pseudo linear-elastic, brittle materials. Michielsen[68] performed research on these fibers and determined the Mode I critical strain energy release rate using a range of initial flaw sizes. For the current research, experiments were carried out to help substantiate the results of the smaller fiber experiments. Tensile experiments were carried out on these fibers in the absence of prior fatigue loading. Fatigue experiments were unnecessary in the larger fibers experiments because the specimens contained a flaw of a known size. These defects were introduced by means of a sharp razor and an apparatus that ensured the proper orthogonal alignment of the flaw in respect to the fiber axis. Initial crack lengths were obtained by means of an optical microscope and energy computations were derived from integration of the load-displacement curve for determination of the work done during the deformation process. The goal was to validate the theory of the strain energy release rate, which basically reveals that an increase in ligament area produces a decrease in the energy available to the structure to perform mechanical work. This was pertinent to the current investigation, because in the smaller fibers there was not a simple method of determining the initial flaw size. A schematic of the geometrical shape of the

obround filament is depicted in Figure 5.2 as well as the apparatus used for achieving the various flaw sizes (Figure 5.3).

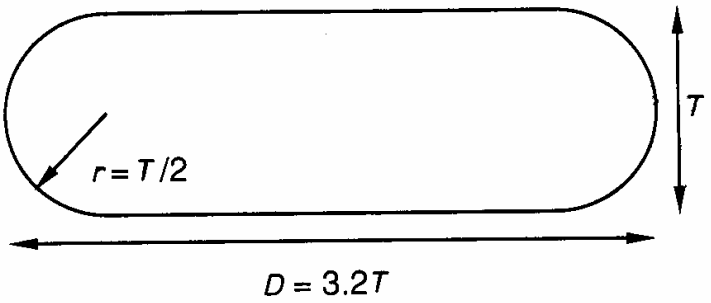

Figure 5.2. Schematic of Obround Fiber Used in Large Fiber Experiments[68]

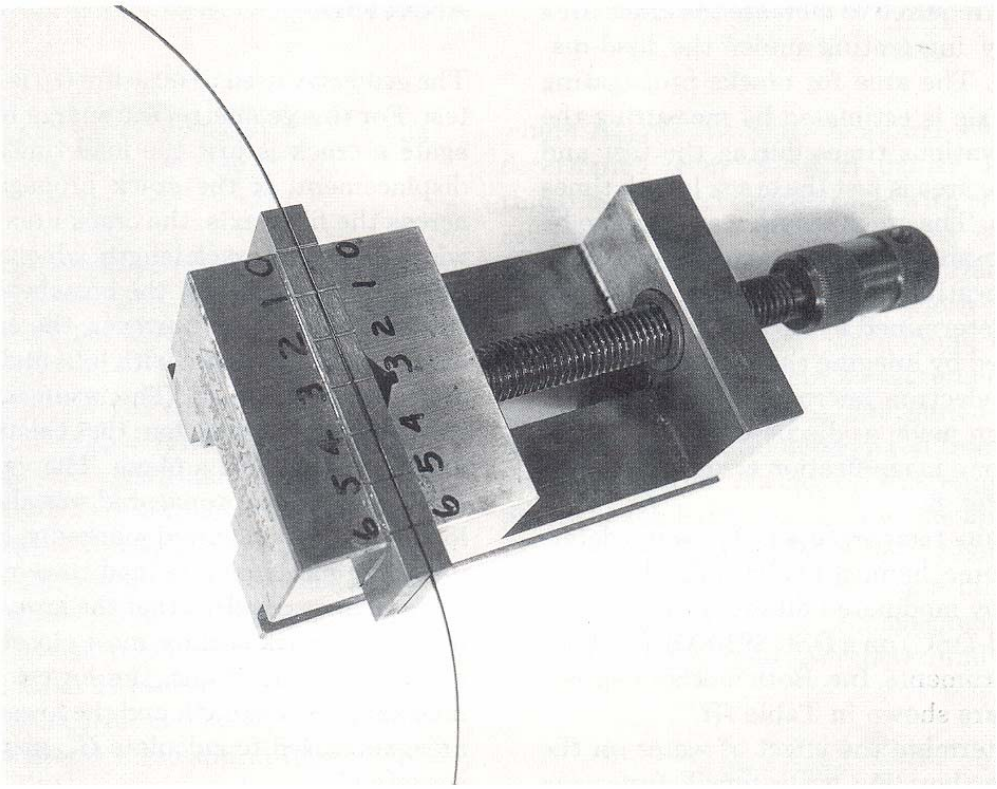

Figure 5.3. Apparatus Used to Introduce Various Initial Flaw Sizes in Large Fiber Samples[34]

5.2. Method of Research/Experimental Procedures

A device capable of performing uniaxial tensile tests and low/high cycle fatigue was necessary for the completion of this investigation. To accomplish this, the Enduratec ELF 3200 was purchased, which is a multi-purpose mechanical tester useful for characterizing a wide variety of materials. Many researchers have used the device for testing metals, composites, and biomaterials, but the interest of researchers in single fiber testing is growing rapidly. Figure 5.4 provides a general schematic of the Enduratec ELF 3200 used for experimentation. The Enduratec machine is controlled by a low distortion actuator from the Bose® corporation, which is capable of performing a multitude of waveforms at various frequencies with precision.

All experiments for the small fibers were conducted on the ELF 3200. In response to the aforementioned issue on slippage, it was important to achieve proper grasping of the small fiber during mechanical loading. There is a scarcity of manufacturers in the development of grips for single fiber testing, so a simple design was conceived that was adaptable to the Enduratec ELF 3200 and capable of gripping the single filaments appropriately. Aluminum was used in the fabrication of the components for the grips, due to its low density attributes and damage durability. This low density, and consequently lightweight, was an extremely important feature since the load cell used for these tests had a maximum rating of 2.5N. Using larger and heavier grips for testing these fibers interfered significantly with the PID controllers, which resulted in noise and undampening of the signal. A description of this error that is generated during testing is provided on a load-displacement graph in Figure 5.5. The scatter that is seen in the diagram is a direct consequence of the "ringing" that is produced when the system goes

slightly unstable. Figure 5.5 also demonstrates the effects of improper gripping during mechanical loading, as shown by the precipitous decreases in load value. Thus when performing mechanical tests on fibers of this magnitude, one should pay special attention to the load cell rating and weight of the grips. The PID controllers were often adjusted on the Enduratec ELF 3200, so as to diminish the effects of noise and scatter on the oscilloscope. In the testing of the larger nylon fibers, a standard Instron machine with a larger load cell was utilized. Also, serrated grips were used and the fibers were placed directly in the gripping apparatus during testing.

5.3. Fatigue Experiments

Fatigue tests were conducted on the small fibers for different cycle times in an effort to propagate a dominant congenital flaw in the specimen. As discussed in the aforementioned literature review, this defect was assumed to be of the semi-elliptical form and is normally engendered through imperfections in the polymer extrusion process. The technique of using fatigue to proliferate flaws in a stable and controlled manner in a specimen is known as "precracking." In theory, different crack lengths can be obtained through precise control of the cyclic loads. In the 1960's Paris et al.[2,45,46] demonstrated that fracture mechanics is a useful tool for characterizing crack growth by fatigue in engineering materials. Since that time, fracture mechanics has been applied to fatigue problems customarily. However, large-scale plasticity is involved in this problem, and the interest lies in elucidating this phenomenon. Because of the extensive plasticity, it was theorized that the J-integral could be used to characterize the crack growth for a prescribed number of cycles in nylon 6,6 fibers. The equations are described as:

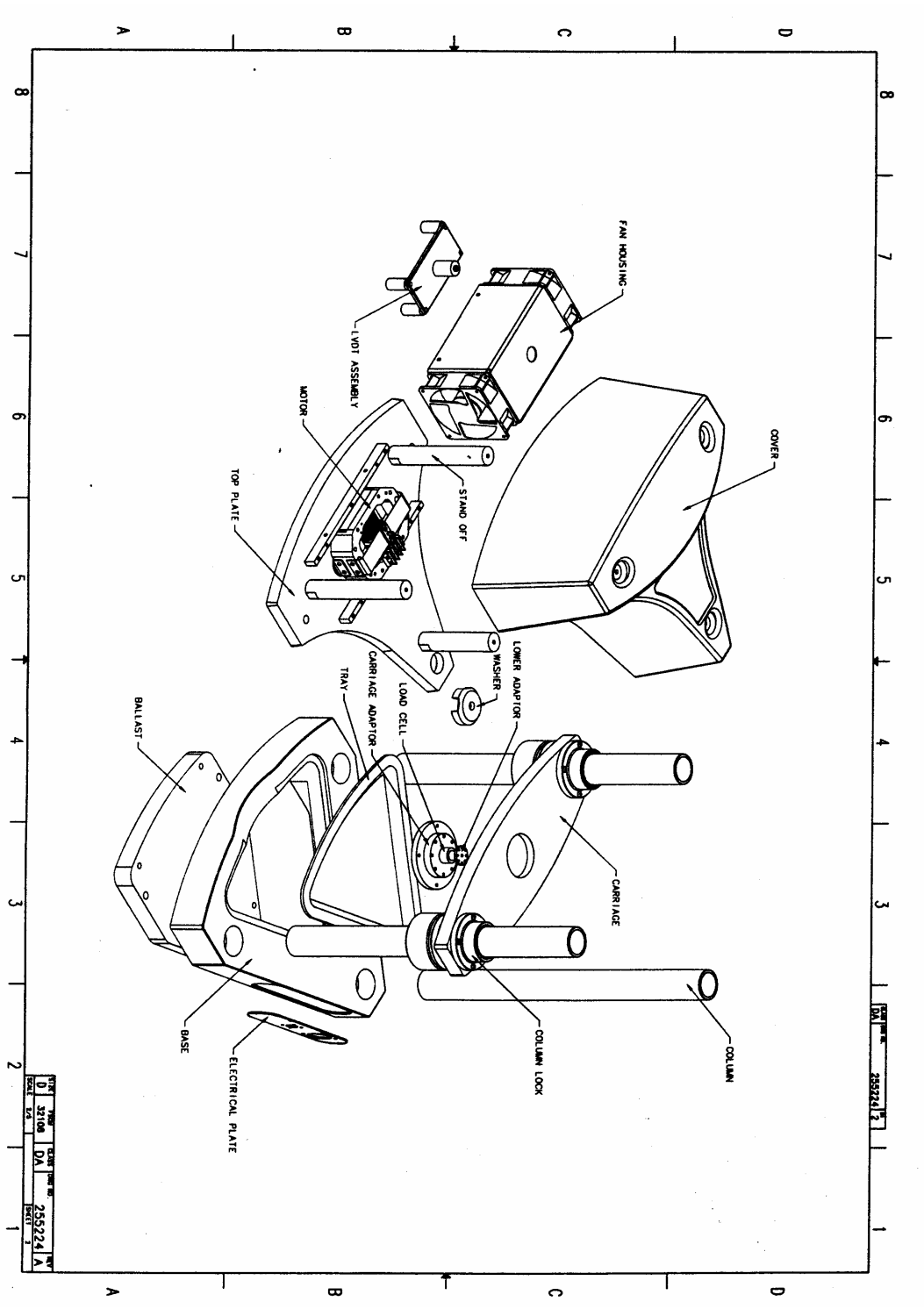

Figure 5.4. Schematic of Enduratec ELF 3200

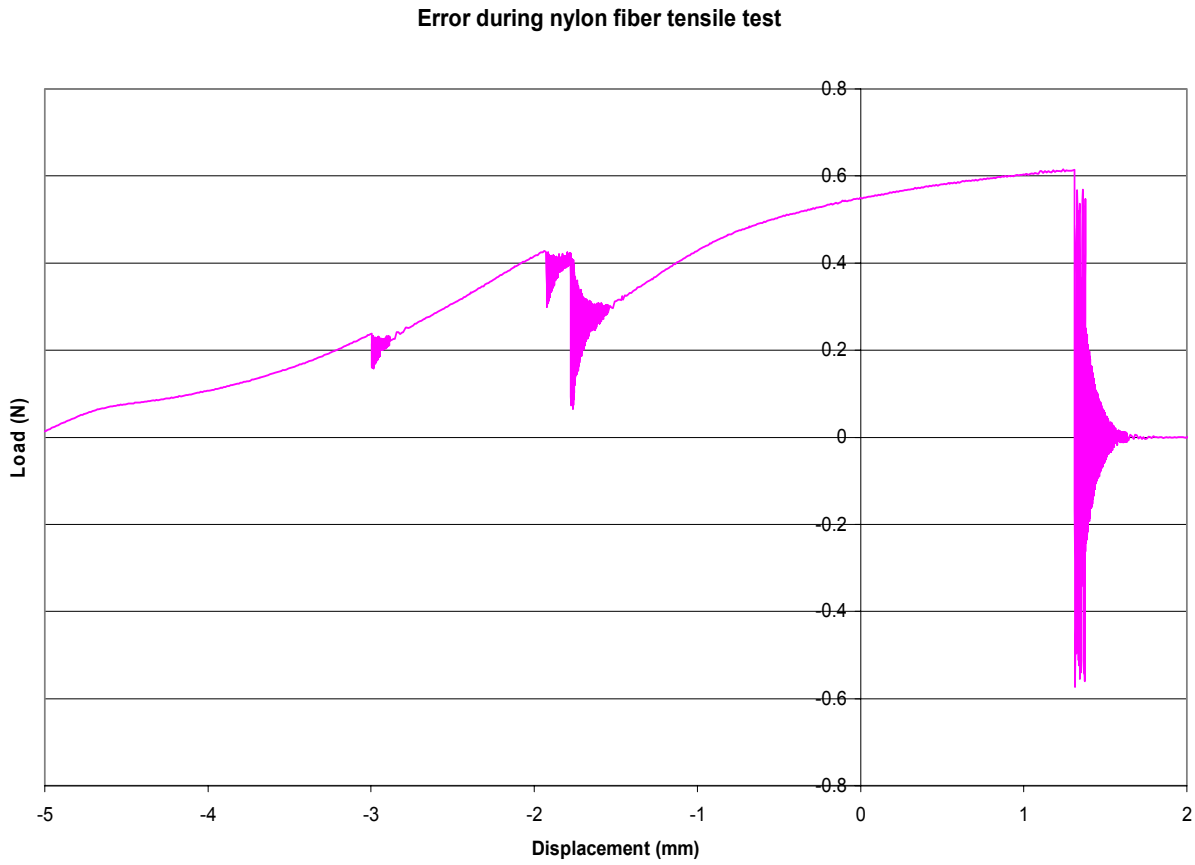

Figure 5.5. Error Produced in Signal During Single Fiber Test With Heavy Grips

$$\frac{da}{dN} = C\Delta J^{m}$$

This equation is reminiscent of the well-known Paris-Erdogan law for characterizing crack growth in brittle materials. In this expression, ΔJ replaces ΔK in the conventional fracture toughness expression. Dowling and Begley[2,13] applied the J-integral to fatigue crack growth under large scale yielding where K is no longer applicable. This expression can be rearranged and integrated to obtain the number of cycles required to propagate a crack from an initial length to a final length, as described in the above power law expression:

$$N = \int_{a_0}^{a_f} \frac{da}{f(\Delta J, R)}$$

In this expression, R represents the ratio of the maximum applied J to the minimum J (J_{max}/J_{min}). Since it is possible to estimate J experimentally from a load displacement curve, ΔJ can be obtained from the cyclic load displacement curve. The ΔJ can be estimated in the following manner:

$$\Delta J = \frac{\eta}{ligament\_area} \int_{V_{min}}^{V_{max}} (P_{max} - P_{min}) dV$$

This equation reveals that if a specimen is cycled between the loads P_{min} and P_{max}, then ΔJ is equivalent to the work done in displacing the specimen from V_{min} to V_{max} multiplied by a dimensionless constant η per unit crack area. η is based on the geometry of the configuration, where the width (W) of a rectangular sample was assumed to be equivalent to the diameter (D) in these round samples. The ligament area represents the area of the material remaining from the formation of the crack. Combining the results from Paris[45,46] with the cyclic J-integral, one achieves the following relationship:

$$dN = C\left[\frac{\eta}{ligament\_area}\int_{V_{min}}^{V_{max}} (P_{max} - P_{min}) dV\right]^{-m} da$$

$$N_f = \int_{a_0}^{a_f}\left[C\left[\frac{\eta}{ligament\_area}\int_{V_{min}}^{V_{max}} (P_{max} - P_{min}) dV\right]^{-m}\right] da$$

Here, the number of cycles to failure for the fiber cycled between a minimum and maximum load is represented by N_f. The drawback in these models for this investigation is that they require a priori knowledge of the size of the dominant initial flaw, which was not determined for the smaller fiber investigation.

A specific model for assessment of the damage accumulation experienced by a polymer fiber in cyclic tension was established by Regel et al.[27] and is provided as:

$$\int_0^{2\pi N_F/\omega} dt / \tau(\sigma[t]) = 1$$

Here, ω represents the frequency of the test, N_f is the number of cycles to failure as described in the aforementioned, τ is the expected time to break, and $\sigma[t]$ represents the stress equation as a function of time. When combined with the well-established Arrhenius equation, the expression becomes[27]:

$$\int_0^{2\pi N_f/\omega} dt / \tau_0 \exp[(U_0 - \gamma\sigma[t]) / RT] = 1$$

In this modified expression, γ represents the activation volume and T is the ambient temperature of the process.

One caveat that has been established throughout the years in polymer testing is the frequency that is prescribed during experimentation. At high frequencies, hysteresis heating occurs and could potentially cause melting of the sample at the crack tip where the stress concentration is high. Many researchers have grappled with this phenomenon in polyamide testing, and have made some discoveries that should be adhered to during testing of polymer fibers. Boukhili et al.[8] performed experiments on polyamide-12 and concluded that the fatigue crack propagation increases with increasing frequency. They performed experiments from 0.3Hz to 5Hz to make those observations. ASTM[78] recommends that plastic materials be tested at frequencies of 4Hz or less due to hysteretic heating. For the samples in this investigation, some benefit was given to the diminutive nature of the fiber in respect to other materials. As an estimate, the volume of the fiber was only 2.44×10^{-11} m^3 and it was assumed that the sample could dissipate heat at an

accelerated rate in comparison to a bulkier sample. Kausch[27] has confirmed this conjecture for sinusoidal loading of polymer samples, where the rate of energy exchange to the surroundings via heat transfer modes is:

$$\Delta W = \pi \sigma_0 \varepsilon_0 \sin \delta$$

He also confirmed that a cylindrical polymer sample equilibrates when the following condition approaches zero[27]:

$$\frac{\partial T(r,t)}{\partial t} = \frac{\omega \sigma_0^2 \sin \delta}{2 \rho c_p E'} + \frac{k}{\rho c_p}\left(\frac{\partial^2 T}{\partial r^2} + \frac{1}{r}\frac{\partial T}{\partial r}\right)$$

Here ω is the testing frequency, and ρ, c_p, and k are the density, specific heat, and conductivity of the sample, respectively. By inference, one notices that when this equation reaches a near-zero value heat transfer no longer occurs from the sample to the surroundings. From this relationship and knowledge of Fourier's Law, it is also evident that the rate of heat transfer per unit time escalates for low density samples. Because of these assumptions in heat transfer, a frequency of 10Hz in pseudo-load control was used for the fatigue tests. The phrase "pseudo-load control" is apposite because the Enduratec ELF 3200 requires input of the minimum and maximum load values desired, as well as minimum and maximum displacement values for the system to respond to. In reality, the Enduratec is not capable of performing a true load control test on a small-scale fiber with a minimal fracture load. The system is not able to respond instantaneously, and thus displacements that correspond to these loads are required parameters for input. These "pseudo-load control" experiments constituted the high cycle fatigue phase of the experiment, and the goal was to generate striations on the crack front that could be characterized by the modified Paris Law. Displacement control tests were also conducted for low cycles, and the objective was analogous to that of the "pseudo-load control"

experiments. The two experimental techniques produce similar results for uniaxial tensile tests, which is concomitant with the theory of the nonlinear energy release rate, J, for load-control and displacement control. Anderson[2] proved this mathematically, by illustrating on a load-displacement curve that the two phenomena are essentially equivalent. Figure 5.6 illustrates this general concept.

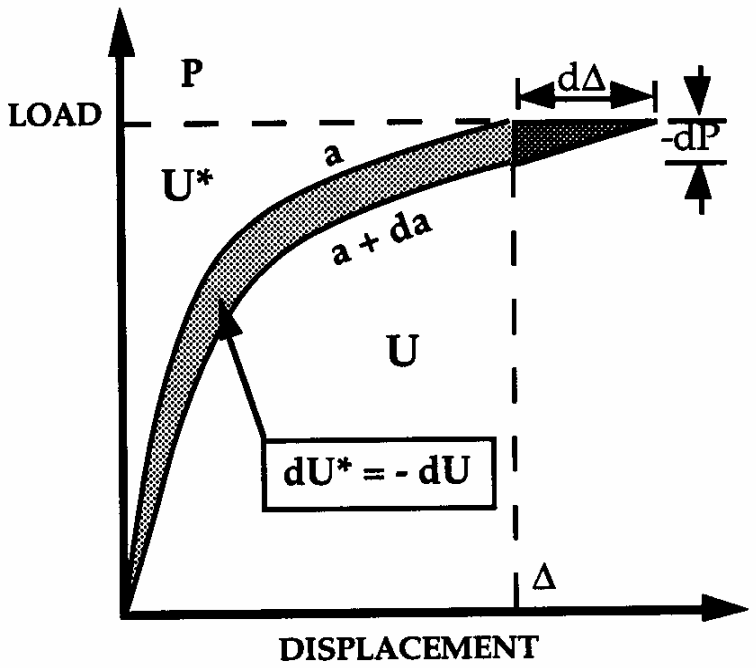

Figure 5.6. Schematic of the J-Integral for Load-Control and Displacement Control[2]

Equivalence of the two methods is easily shown from the following relationships on load-control and displacement-control of the J-integral:

$$J = \int_0^P \left(\frac{\partial \Delta}{\partial a}\right)_P dP \qquad \textit{(load control)}$$

$$J = -\int_0^\Delta \left(\frac{\partial P}{\partial a}\right)_\Delta d\Delta \qquad \textit{(displacement control)}$$

5.4. Post-Fatigue Experiments

After fatigue experiments, tensile tests were performed on the smaller specimens in an effort to obtain the critical nonlinear energy release rate, J_c. The equations that govern the nonlinear energy release rate are described as[69]:

$$J_{TOT} = J_{el} + J_{pl}$$

$$J_{TOT} = \frac{K_I{}^2\left(1-\nu^2\right)}{E} + \frac{\eta_p U_p}{ligament\_area}$$

This expression gives the nonlinear energy release rate in terms of the plastic energy absorbed by the specimen, U_p. It is a useful experimental tool for evaluating nonlinear elastic and elastic-plastic materials, because the plastic energy is directly proportional to the area under the load-displacement curve and can be solved by the following equation[2]:

$$U_P = \int_0^{\Delta_P} P d\Delta_P$$

$P = C\Delta_P{}^N$ (load-displacement curve obeys power law)

$$U_P = C\int_0^{\Delta_P} \Delta_P{}^N d\Delta_P = \frac{P\Delta_P}{N+1}$$

If the elastic component of the equation is computed for the plane strain criterion, J_{TOT} can be simplified as:

$$J_{TOT} = J_{EL} + J_{PL} = \frac{Y^2 P^2 \pi a\left(1-\nu^2\right)}{\left(ligament\_area\right)^2} + \frac{C\Delta_P{}^{N+1}\eta_P}{(N+1)ligament\_area}$$

Where Y = geometry constant

P = applied load

ν = Poisson's ratio

a = initial crack length

E = Young's modulus

C, N = material constants from power law expression

η_P = "plastic" dimensionless constant based on geometry.

Since all other terms are known, the critical nonlinear energy release rate, J, was found by experimentally determining the plastic area under the stress-strain curve and the measurement of the critical crack length, a_c through usage of microscopy techniques.

This gave a critical nonlinear energy release rate for the fibers as well as a critical flaw size that led to unstable crack growth. In mathematical terms, this critical flaw size occurs when the slope of the driving force curve and the slope of the material resistance curve are equivalent. These slopes can be expressed in terms of a dimensionless tearing modulus T.

$$T_R = \frac{E}{\sigma_0^{\,2}} \frac{dJ_R}{da}$$

$$T_{app} = \frac{E}{\sigma_0^{\,2}} \left(\frac{dJ}{da} \right)_{\Delta T}$$

As discussed earlier, these relationships can be utilized if the initial flaw size is known for the sample. Huang[70,71] developed a method for using J-R curves to characterize larger nylon 6,6 samples (10×25×1.2cm), which can be employed when the initial flaw size is known. These techniques allow one to evaluate the critical incremental crack advance quantity and corresponding nonlinear energy release rate for a material. Since the material resistance curve obeys a power law and the applied driving force obeys a law of the form,

$$J = -\frac{1}{B} \left(\frac{\partial U}{\partial a} \right)_{\Delta}$$

an expression can be obtained to equate the slopes of the two curves and thus a critical

value of flaw size (a_c) and driving force (J_c) can be established.

5.5. Elongation (Strain) Rate Effect in Polyamide Fibers

The strain rate was an important factor in determining critical nonlinear energy release rate values. For single nylon 6,6 fibers, the ultimate tensile strength increases linearly as a function of increasing load rate. This is shown below in Figure 5.7, which also provides results for a bundle of fibers for comparison[27]:

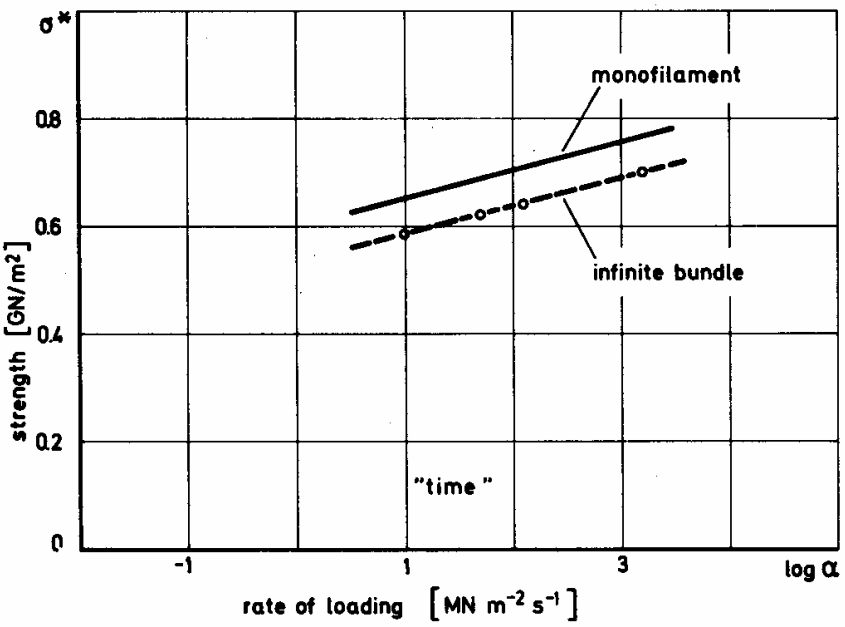

Figure 5.7. Effect of Strain Rate on Ultimate Strength of Nylon 6,6 Fibers[27]

This strain rate effect is normally accompanied by a decrease in the plasticity of the sample, in which the stress-strain response is indicative of a pseudo-brittle nonlinear behavior. Molecular theories of polymers clearly authenticate these results, as the polymer chains are not given proper time to orient themselves along the fiber axis in high strain rate experiments which leads to a premature and brittle failure mode.

5.6. S.E.M. (Scanning Electron Microscopy) Techniques

Scanning electron microscope (S.E.M.) techniques along with image processing were used to analyze the fracture surface of the small nylon 6,6 specimens. It was important to look at both fracture surfaces of the fiber, since they contained vital information about the failure process and crack propagation mechanism. Since the S.E.M. fractograph provides a visual of the fiber surface, it aided in the correlation between the theory of fracture mechanics and laboratory experiments. From viewing the cross-section of the fiber, it was assumed that a relationship could be made between the crack growth and number of fatigue cycles. An illustration is shown in Figure 5.8 of what was anticipated after cyclic loading preceded a tensile test:

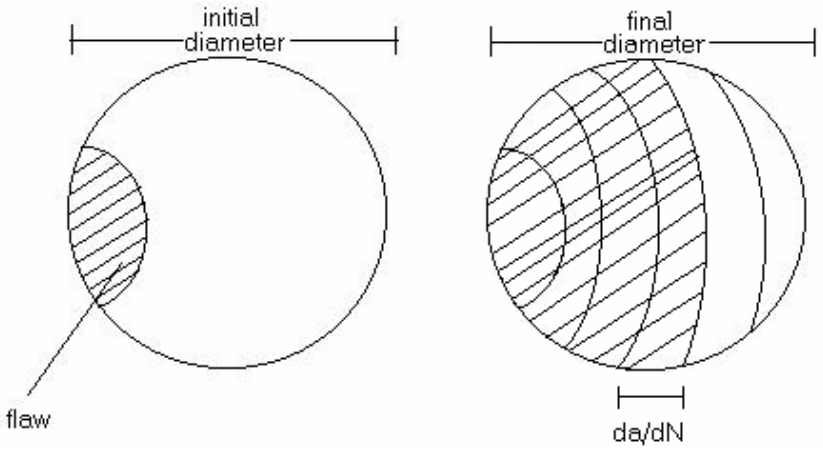

Figure 5.8. Proposed Illustration of Fiber Cross-Section After Fatigue and Tensile Loading

In this diagram, an initial flaw is present in the sample before cycling (left). After *N* cycles, the crack propagates to some final size and finally breaks (right). It was assumed that there would be striations on the surface of the crack and a relationship could be made as to the rate of crack advance. This assumption was made based on case studies in

striation markings for fatigue loading of various polymer and metallic materials. Previous fractography studies on bulk nylon 6,6 samples reveal a similar phenomenon to that of metals, in which striations are visible for a prescribed number of fatigue cycles. To produce these diacritical effects, a stress slightly higher than the peak stress is normally achieved after a certain number of cycles so that one can infer the actual crack growth rate data from fractography. An actual fractograph of a nylon 6,6 sample with fatigue striations is illustrated in Figure 5.9.

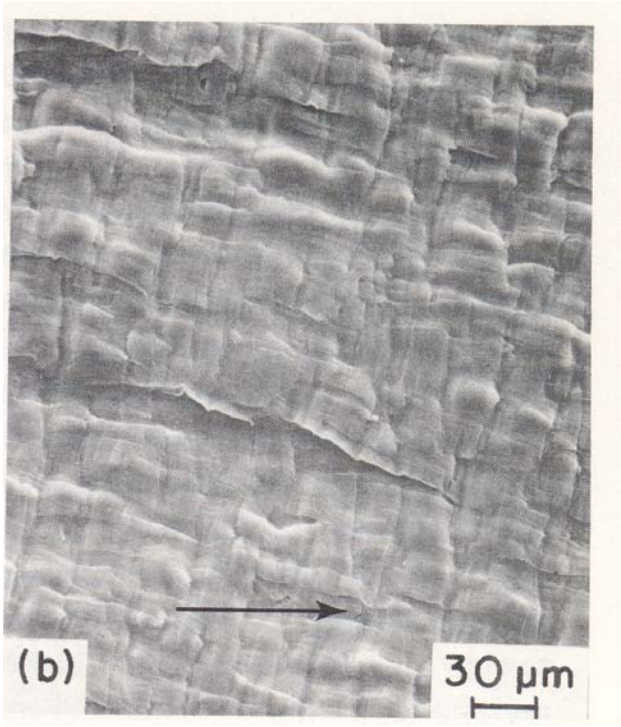

Figure 5.9. S.E.M. Fractograph of Bulk Nylon 6,6 Sample[21]

From Figure 5.9, one can clearly discern the fracture propagation direction and the striation accentuations in the sample. For larger samples such as these, this information can be used directly with the Paris relationship to establish fatigue crack growth rate data.

However, these striation marks were not observed in the diminutive fibers used in this investigation. This could be due to inadequacies in the magnification device used, which did not provide the clarity for striations to be detected by the naked eye. The S.E.M. device used in this study was an LEO 1530 thermally-assisted FEG scanning electron microscope (S.E.M.). The instrument possesses a 1 nm resolution at 20 kV and a 3 nm resolution at 1 kV. The device has an operating voltage range of 200 V – 30 kV. A picture of the S.E.M. is shown in Figure 5.10.

The samples were prepared for microscopy analysis in the following manner:

1) Using precision gripping tweezers, the fibers were dismantled from the tab and mounted onto a cylindrical S.E.M. mount. The fiber was mounted orthogonal to the mounting plane in order to establish a cross-sectional view of the fiber from the S.E.M. Non-conducting tape was used to secure the fiber to the mount.
2) Sputter coater (Edwards) with a gold target was used to coat the samples in an effort to reduce electron charge density during the S.E.M. process. Samples were coated for approximately 150s to achieve proper thickness.
3) Samples were loaded into LEO electron microscope device for fractography analysis.

This is a succinct account of the S.E.M. micrograph process used for this investigation. The process of preparing the samples for S.E.M. analysis is highly time consuming, where the main quandary rests in ensuring the orthogonal alignment of the fiber with respect to the mounting plane. Even though assiduous attempts were made to guarantee this proper orientation, in many instances the fiber was coiled at the fracture end. This did not allow for the production of a utilizable S.E.M. image for J_c analysis. In fact, the

Figure 5.10. Picture of S.E.M. Device Used in This Study[16]

percentage of fibers that resulted in valid fractographs for J_c analysis was below 20%.

5.7. Method for Determining Fiber Diameter

The determination of the fiber diameter was essential for this study, because its value was used for all calculations pertaining to the crack surface area. An optical microscope in conjunction with computer techniques were used to measure the fiber diameter and an average was obtained for several measurements. The steps taken to achieve this process are as follows:

1) Fiber was aligned on S.E.M. mount perpendicular to the surface
2) Optical microscope was used to capture cross-sectional image of fiber

3) Image was imported onto computer and measurements were made

4) Process was iterated for five times and an average fiber diameter was obtained

The average diameter obtained was 35μm which resulted in a cross-sectional area of 9.6E-10 m^2. All fracture calculations were based on this diameter, since its value could not be obtained prior to or following final deformation. Due to the isochoric assumption, the instantaneous diameter for a given strain value was calculated based on initial length and area calculations of the sample.

Section 5.8. Method for Determining Critical Crack Length, a_c

Utilization of the S.E.M. in conjunction with ruler measurements were used to determine the critical crack length of the fiber after final deformation. Due to the severe anisotropic effects of these semi-crystalline nylon fibers, this was proven to be a problematic task. For the small fibers, the orthogonal ligament of the crack path was used for the determination of fracture parameters, since this represented the commencement of unstable crack propagation.

After mechanical testing, the fractured fiber was placed in the S.E.M. and aligned perpendicular to the viewing area. Next, the image was captured and after the proper magnification was obtained, an appropriate length of measurement was recorded on the photograph. The entire fractograph was printed on a laser-quality printer for visual clarity. Physical measurements of the critical crack length were performed manually through usage of the scale length and a ruler. An actual S.E.M. fractograph obtained for this study is shown in Figure 5.11, as well as an estimate of how the critical crack length was obtained. The fractograph shows a marker scale of 10μm, which was used in the

determination of the critical crack length a_c. Notice from the figure the resemblance in the results from Hearle[19] and Kausch[27] and the distinct regions of stable and unstable crack growth. The unstable crack plane is differentiated from the stable region of growth by distorted features that resemble clouded effects.

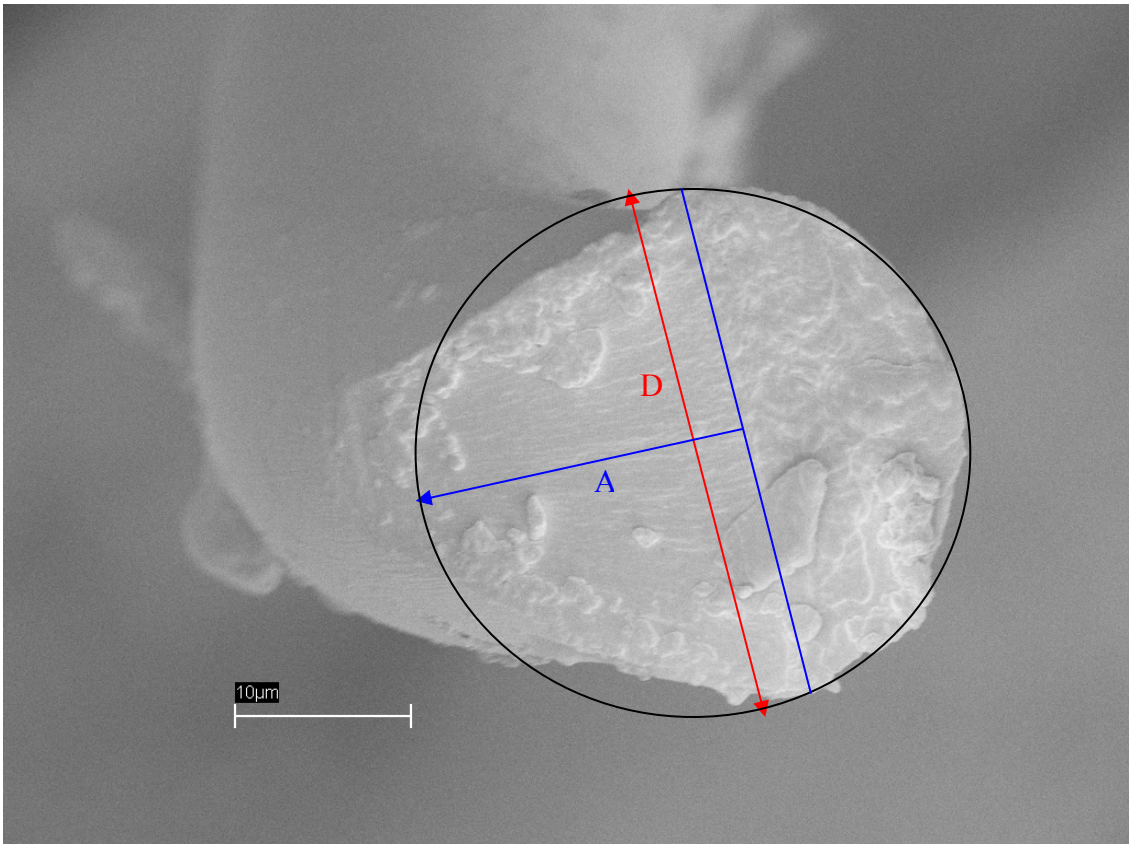

Figure 5.11. Experimental S.E.M. Fractograph and Estimates of the Fiber Diameter (D) and Critical Crack Length, a_c (A)

5.9. Method for Determining Area of Ligament

The determination of the ligament area was also necessary for the calculation of the critical nonlinear energy release rate J_c. Trigonometric identities were used to establish these relationships, and two separate derivations were necessary for the completion of the formulary. One notices a minor variation in the formulae, depending

on whether the critical crack length is less or greater than the radius of the fiber. The basic result of the ligament area of the fiber is provided as:

Ligament area = entire area of fiber cross-section – crack surface area

In mathematical terms, the ligament area is prescribed as:

$$Ligament\ area = \pi r^2 - \left[r^2 \left(\arctan \left(\frac{\left(2a_c r - a_c{}^2\right)^{1/2}}{r - a_c} \right) - \frac{\left(2a_c r - a_c{}^2\right)^{1/2}\left(r - a_c\right)}{r^2} \right) \right] \qquad r \le a_c$$

$$Ligament\ area = \left[r^2 \arctan \left(\frac{\left(2a_c r - a_c{}^2\right)^{1/2}}{a_c - r} \right) - \left(a_c - r\right)\left(2a_c r - a_c{}^2\right)^{1/2} \right] \qquad r > a_c$$

The important factor in the determination of these equations was that the trigonometric relationships had to be associated with a measurable quantity. Thus, $r\cos\theta$, $r\sin\theta$, and θ were defined in terms of the critical crack length and the fiber diameter (radius), which were measured via S.E.M. techniques. An extensive derivation of these quantities is provided in the Appendix.

CHAPTER 6

RESULTS FROM TENSILE TESTS

6.1. Load-Elongation Curves for Different Elongation (Strain) Rates

Uniaxial tensile tests were conducted on the single filament nylon 6,6 fibers in an effort to determine the strength limitations and their response under various elongation (strain) rates. Figure 6.1 provides a sample graph of a load-elongation experiment conducted on the small fibers for three different elongation (strain) rates. The fibers tested reveal significant amounts of plasticity and plastic strain preceding ultimate tensile failure. As also shown in the figure, the implications of an increase in strain rate approximately five times the value for a 2.5X fiber with no prior loading history are minimal. Table 6.1 in the proceeding pages provides results from the load-elongation experiments that are apposite for understanding the fracture limitations of nylon 6,6 fibers.

6.2. Linear-Elastic Strain Hardening Response

The stress-strain response of the fibers in the absence of prior loading is characteristic of a linear-elastic, strain hardening material. The piecewise equation that governs this response is given as:

$$\sigma = \begin{cases} E\varepsilon & \varepsilon \le \dfrac{\sigma_Y}{E} \\ \sigma_Y + H\left(\varepsilon + \dfrac{\sigma_Y}{E}\right) & \varepsilon \ge \dfrac{\sigma_Y}{E} \end{cases}$$

In this piecewise model, E represents the initial elastic modulus, H represents the strain hardening modulus, σ_Y is the initial yield stress, and ε is the strain value corresponding to

the stress value σ. The model was used to delineate the empirical response of the nylon 6,6 fibers tested and is provided in Figure 6.2. The graph provides actual data from an experiment conducted at 0.33mm/s and the ensuing linear-elastic, strain-hardening empirical equation. As shown from the figure, the empirical model was in close agreement with the experimental results.

The method used in the computation of the stress and strain values for all experiments was based on the Lagrangian (reference) configuration. In addition, the second Piola-Kirchoff stress tensor was used in the determination of the uniaxial stress component. Based on simple concepts in mechanics, this second order tensor is given as[30]:

$$\Sigma_{II} = \det\left(\tilde{\tilde{F}}\right) F^{\tilde{\tilde{-1}}} \cdot \sigma \cdot \left(F^{\tilde{\tilde{-1}}}\right)^{T} = \begin{bmatrix} \frac{P}{\lambda_1 A_0} & 0 & 0 \\ 0 & 0 & 0 \\ 0 & 0 & 0 \end{bmatrix}$$

Here, $\boldsymbol{F}$ is the second-order deformation tensor, $\boldsymbol{\sigma}$ is the corresponding stress tensor, P is the instantaneous load, A_0 is the area in the reference (undeformed) state, and λ_1 is the stretch ratio. For the case of incompressibility, λ_1 is assumed to be unity. A derivation of this relationship is provided in the Appendix for a fiber under the case of simple uniaxial tension.

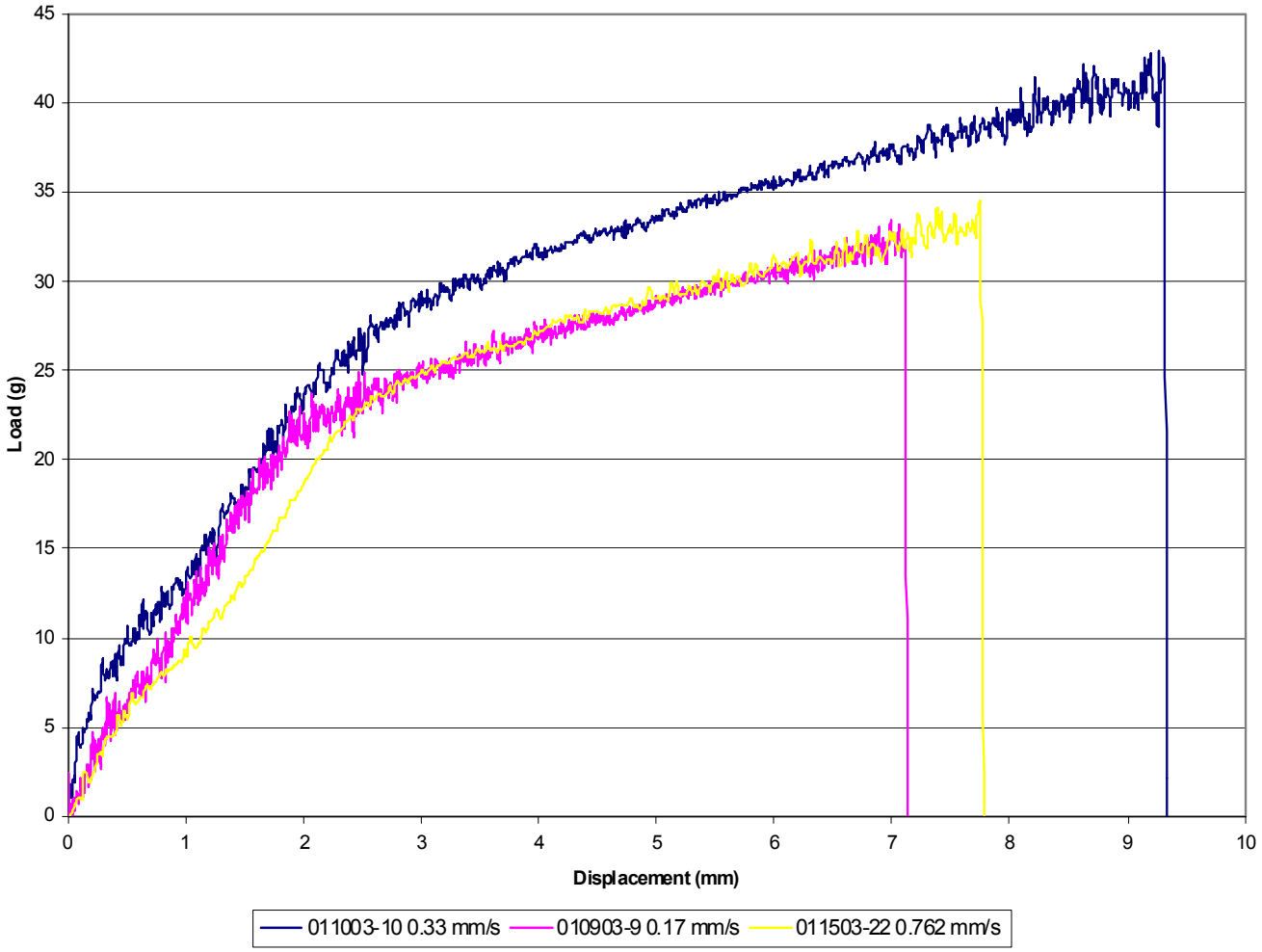

Figure 6.1. Load-Displacement Curves for Small Nylon Fibers Exhibiting the Effect of Elongation (Strain) Rate

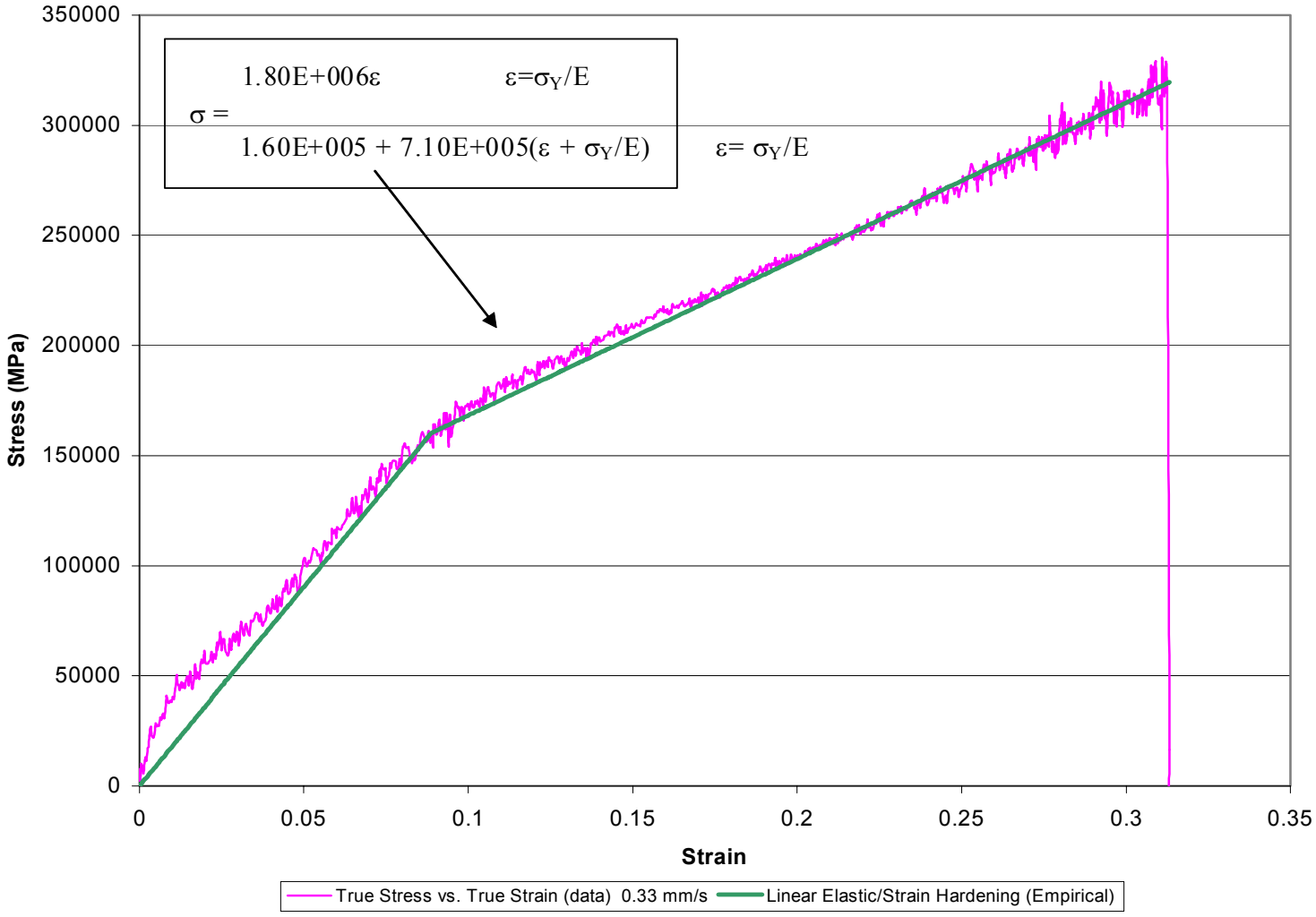

Figure 6.2. Actual Stress-Strain Curve and Empirical Data for Uniaxial Tensile Test of Small Fiber

Table 6.1. Results From Uniaxial Tensile Tests Conducted at Different Elongation (Strain) Rates

Sample name	Draw Ratio	Tensile Test		
		Elong. Rate (mm/s)	Strain Rate (1/s)	Breaking load (g)
010903-1	2.5X	0.17	0.006693	36.47
010903-3	2.5X	0.17	0.006693	36.17
010903-4	2.5X	0.17	0.006693	32.98
010903-5	2.5X	0.17	0.006693	35.69
010903-6	2.5X	0.17	0.006693	42.49
010903-7	2.5X	0.17	0.006693	31.60
8010803-1	2.5X	0.17	0.006693	34.83
8010803-2	2.5X	0.17	0.006693	42.28
8010803-3	2.5X	0.17	0.006693	38.25
010903-9	2.5X	0.17	0.006693	32.37
011003-10	2.5X	0.33	0.012992	41.33
011003-11	2.5X	0.33	0.012992	39.45
011003-12	2.5X	0.33	0.012992	30.65
011003-14	2.5X	0.33	0.012992	30.49
011003-15	2.5X	0.33	0.012992	31.94
011003-16	2.5X	0.33	0.012992	35.12
011503-20	2.5X	0.33	0.012992	34.83
011503-22	2.5X	0.762	0.030000	32.95
011503-23	2.5X	0.762	0.030000	35.40
011503-24	2.5X	0.762	0.030000	39.02
011503-26	2.5X	0.762	0.030000	29.91
011503-27	2.5X	0.762	0.030000	34.10

CHAPTER 7

FATIGUE RESULTS

Section 7.1. High Cycle Fatigue

The fatigue process used in this study was ancillary in nature, in which propagation of the dominant congenital flaw was the main objective. These fatigue experiments were carried out under stable conditions in an attempt to achieve smooth and controlled crack growth. High cycle fatigue trials were conducted for as many as 20,000 cycles to achieve this stable crack growth. More commonly, cycles between 500 and 5000 were used to achieve fatigue crack growth prior to fracture. Sinusoidal loading of the form

$$\sigma = |\sigma_A| \sin \omega t$$

was conducted on the Enduratec ELF 3200 instrument. A frequency of 10 Hz was employed and the experiments were carried out in pseudo-load control. As expected from this type of loading, the *load vs. time* response exhibited a constant amplitude over the prescribed time interval, whereas the *displacement vs. time* indicated an increasing response as time elapsed. Under invariable temperature conditions, this response is reminiscent of the strain response for time dependent, viscoelastic materials under a constant, dead-weight load. As shown in Figure 7.1, a material exposed to conditions under constant stress will ultimately increase in strain value due to an increased demand for load as time elapses. A schematic of the *load vs. time* and *displacement vs. time* responses for load-controlled fatigue are shown in Figures 7.4 and 7.5, respectively. The more appropriate equation that governs the stress response of nylon 6,6 fibers in pseudo-load control fatigue contains time dependent parameters, and is given as:

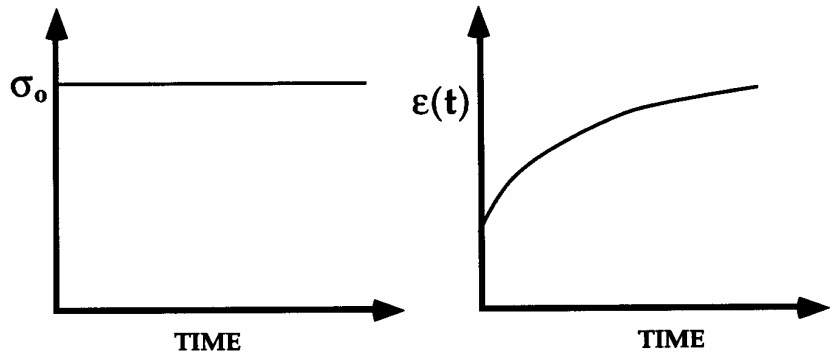

Figure 7.1. Constant Stress Experiment and Accompanying Creep Response[2]

$$\sigma(t) = E(t)\varepsilon_0 \sin \omega t$$

Here the modulus is given as a function of time, which results in the stress value possessing a time-dependent parameter. This phenomenon is anticipated for most polymers, where the time-dependent deformation is a consequence of the molecular structure[2].

Of particular importance was also the response of stress to strain for load-controlled cycling. Due to viscoelastic effects, one would expect to see a difference in the load and unload behavior for the single polymeric filaments. In Figure 7.6, the effects of hysteresis are quite discernible. Also notice from the figure the time dependent effects of the modulus upon loading and reloading of the sample. The modulus decreases upon subsequent loading and this effect can be directly attributed to the time dependent response of the modulus. Figure 7.2 shows a log-log plot of how the modulus of typical polymers varies as a function of time in the inelastic region.

S-N curve analysis was done on the fibers to determine their fatigue life. These models produce a plot of the stress amplitude vs. the *log* of the number of cycles to failure, and are useful at predicting the duration of life that a specimen can sustain under

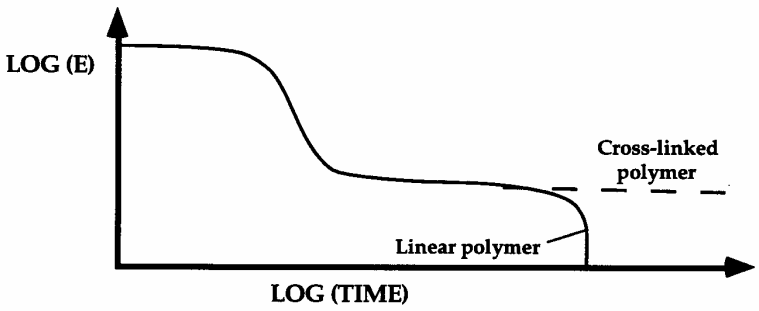

Figure 7.2. Response of Modulus as a Function of Time for Linear and Cross-Linked Polymers[2]

particular stress loads. Dowling[12,13] has provided a mathematical expression that can be employed to represent the stress amplitude of materials on a linear-log plot[12]:

$$\sigma_A = C + D \log N_f$$

Hertzberg and Manson[21] have provided an S-N curve for DAM (dry as moulded) nylon samples, which conforms to the above model introduced by Dowling. A diagram is shown below in Figure 7.3.

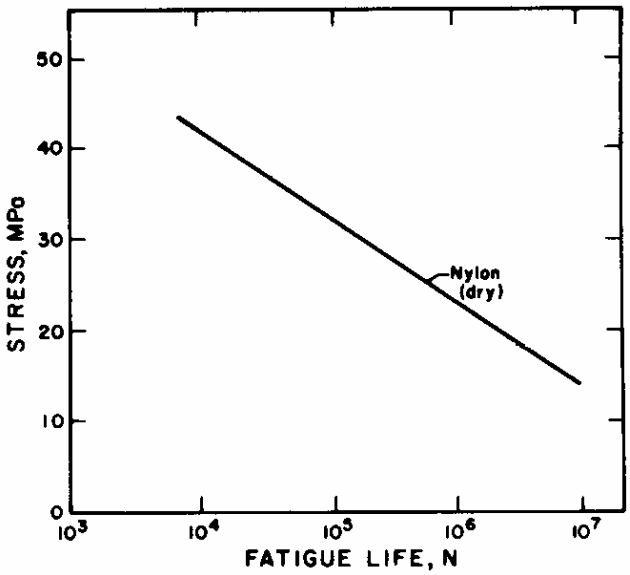

Figure 7.3. S-N Curve for Bulk Nylon[21]

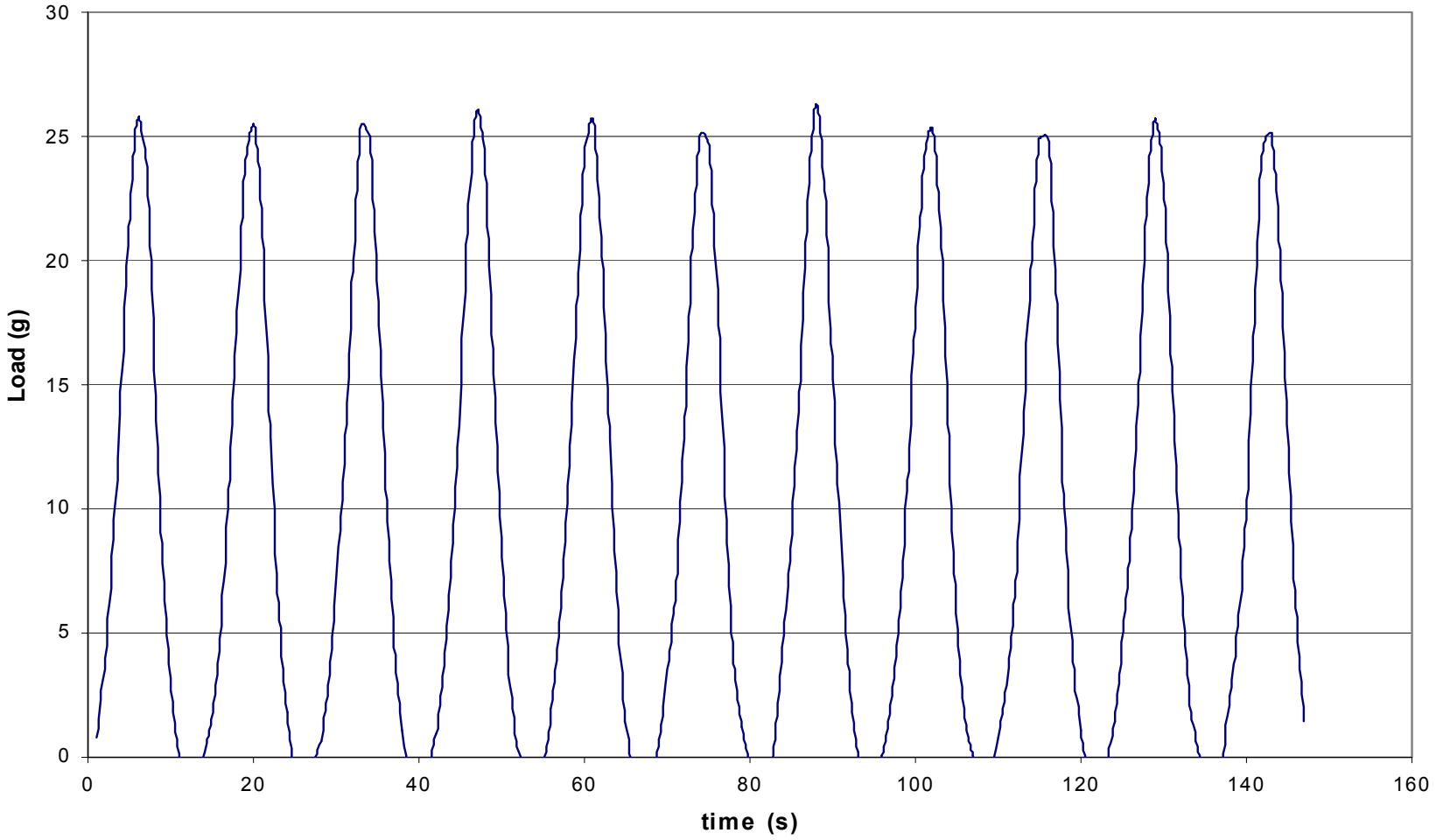

Figure 7.4. Load vs. Time Response of Small Fiber in Cyclic Tension for Pseudo-Load Controlled Conditions

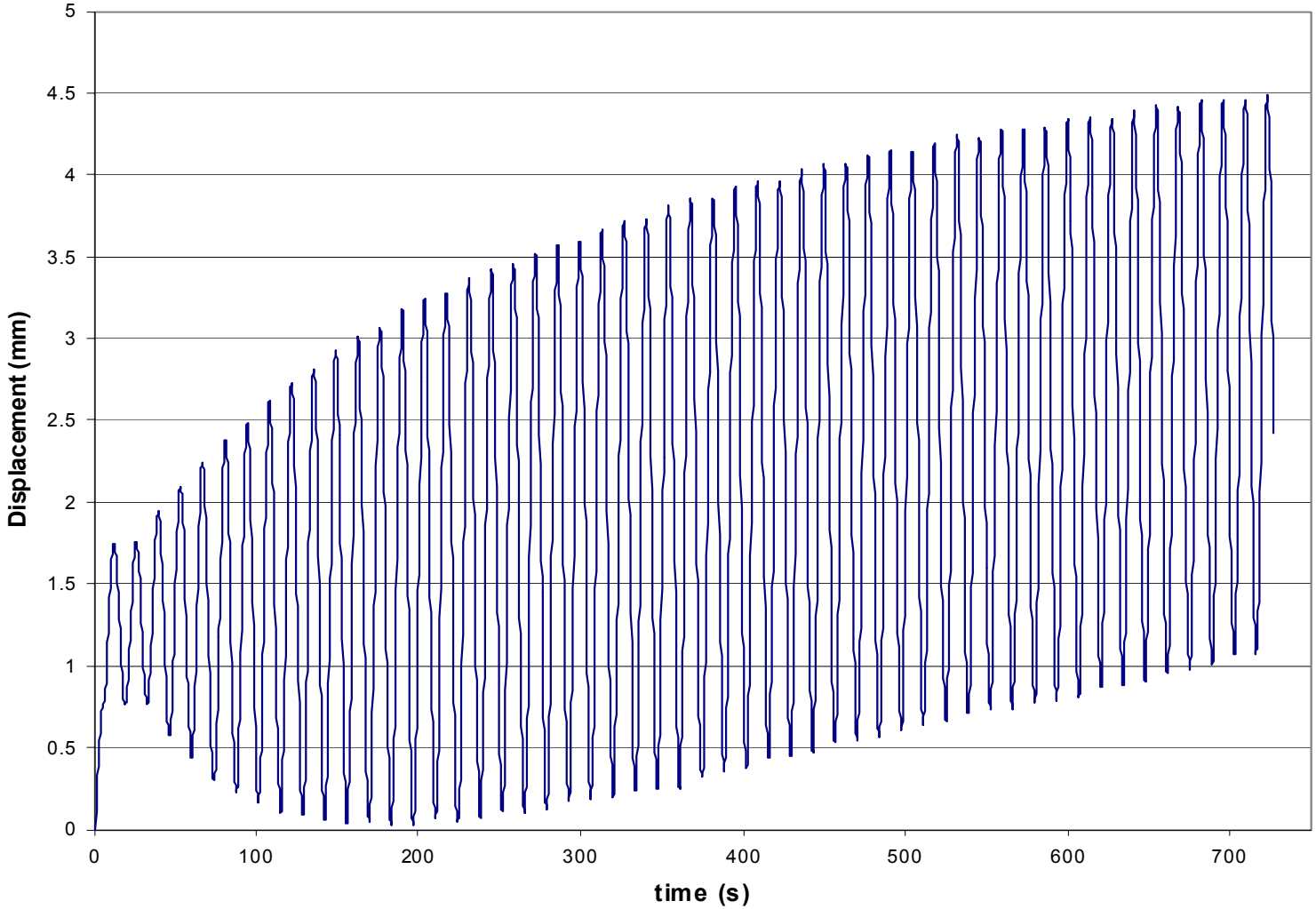

Figure 7.5. Displacement vs. Time Response of Small Fiber Under Pseudo-Load Controlled Fatigue Conditions

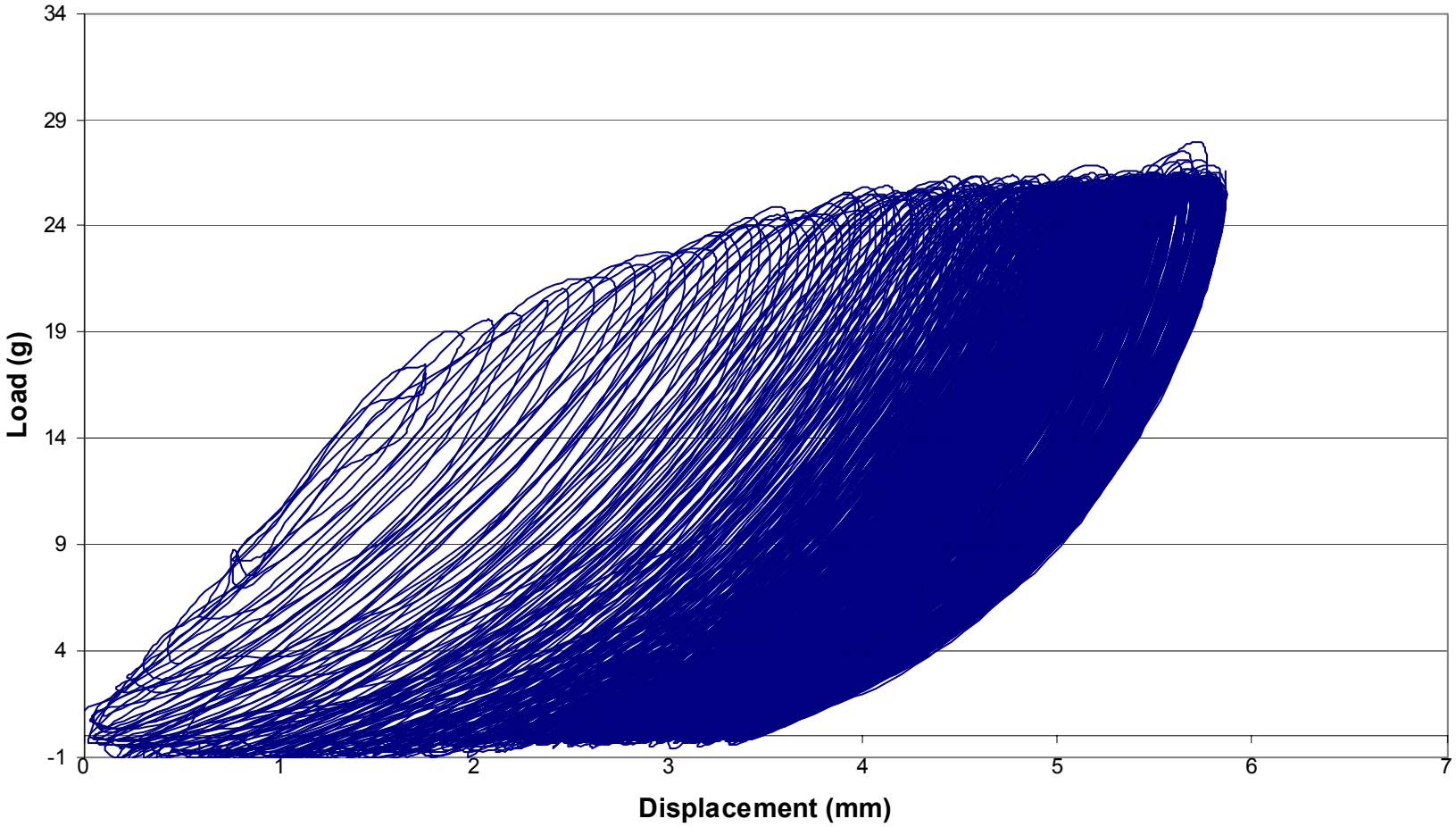

Figure 7.6. Load-Displacement Response of Fiber Undergoing Pseudo-Load Controlled Cyclic Deformation

The material used in the construction of the S-N plot in Figure 7.3 was a larger bulk sample of nylon that was undrawn. The tests conducted for this investigation show similar attributes to the trend displayed in Figure 7.3. All experiments were conducted in uniaxial tension and a representation of the fatigue life of nylon 6,6 fibers for the current study is provided in Figure 7.7. The figure shows the load amplitude of the samples versus the number of cycles to failure. From the linear curve fit, one notices that the trend corresponds closely to the model proposed by Dowling[12,13].

7.2. Low Cycle Fatigue

Low-cycle fatigue experiments were conducted on the small fibers under uniaxial loading and unloading conditions in displacement control. The purpose of the experiments was to expectantly create discernible striations on the crack front that resembled those observed in Figure 5.9 of the Methods section. As stated, this crack growth data in theory could be utilized to calculate the amount of crack growth and subsequently the critical nonlinear energy release rate, J_c. As with the results of the high cycle fatigue experiments, no striations were identified on the surface of the crack front with the use of the microscopy techniques discussed in the methodology section.

Figures 7.8 and 7.9 demonstrate a graph of the *load vs. time* and *displacement vs. time* response for low-cycle fatigue of 2.5X drawn fibers, respectively. To achieve the prescribed displacements for the experiment, the load responded accordingly, as shown in Figure 7.8. To induce further yielding in the sample upon successive loading iterations, proper displacements were imposed in the Enduratec ELF 3200. The number of fatigue iterations ranged between 2 and 5, and the last iteration constituted the critical cycle used

for calculation of the critical nonlinear energy release rate, J_c. Anderson[2] has theorized that the load-unload behavior in a typical polymer sample can complicate J_c measurement. This serves as justification for employing only the last cycle in the critical deformation analysis of the nylon 6,6 fibers. If using foregoing fatigue iterations in the analysis, one should pay careful attention during the integration scheme of the *load vs. displacement* not to include the energy from hysteresis effects in the calculation. A graphic representation of the *load vs. displacement* curve for a low-cycle fatigue experiment is depicted in Figure 7.10. Aside from hysteresis, notice the more apparent effects of the decrease in modulus upon subsequent loading, which is concomitant to the case of high-cycle fatigue loading. The modulus gradually decreases upon successive loading, due to the molecular orientation effects of nylon 6,6. As described in the aforementioned literature investigation, the theory of plasticity in polymeric fibers ratifies the full recovery claim. Basically, it evinces that the sample should recover from the effects of hysteresis upon an infinite time interval of zero load after subsequent loading. This was not observed for the samples tested, as shown in Figure 7.11 from a 24-hr recovery period for a sample tested after low-cycle fatigue. The effects of hysteresis are rather apparent, and are due to the fact that the hydrogen bonds in the polymer sample were not able to fully recover from the mechanical deformation process. Notice in Figure 7.11 how the initial modulus in the sample after 24 hrs increases initially, but plateaus after increased straining. This proves that the sample attempted to traverse its original deformation path, but due to bonding deficiencies was unable to achieve this. Also notice from this load-elongation curve how the sample exhibited a nonlinear-elastic, brittle response for the last cycle. This is due to the cumulative effect of inelastic deformation

of the sample during prior cycles, and the subsequent energy that was released during this process. These effects are also displayed in Figure A.1 in the Appendix, which show low-cycle fatigue experiments conducted at various elongation (strain) rates.

7.3. Effect of Fatigue on Load-Elongation (Stress-Strain) Response

The process of fatigue is actually similar to that of drawing in nylon 6,6 fibers, in which the molecules of the fiber attempt to align themselves preferentially along the fiber axis. For this investigation, this led to the removal of the extensive plasticity that was observed in Figures 6.1 and 6.2 of an unfatigued sample. As a comparison, Figure 7.12 provides a depiction of the difference in load-elongation response for materials that possess no prior fatigue history to those that have been fatigued. Notice also from Figure 7.12 how the tensile test without prior fatigue (blue, pink, turquoise) exhibited a linear elastic, strain hardening behavior, while the specimens with prior fatigue exhibited a nonlinear elastic, perfectly plastic behavior (green, orange). This clearly indicates that the morphology of the fiber is altered during the fatigue process. The uniaxial tensile test was performed immediately following the fatigue experiments. Thus the material did not have sufficient time to recover from the prior loading. Figure 7.12 also indicates how a specimen with a higher load (stress) amplitude in fatigue will generally fracture at a value higher than that of a specimen with a lower load (stress) amplitude.

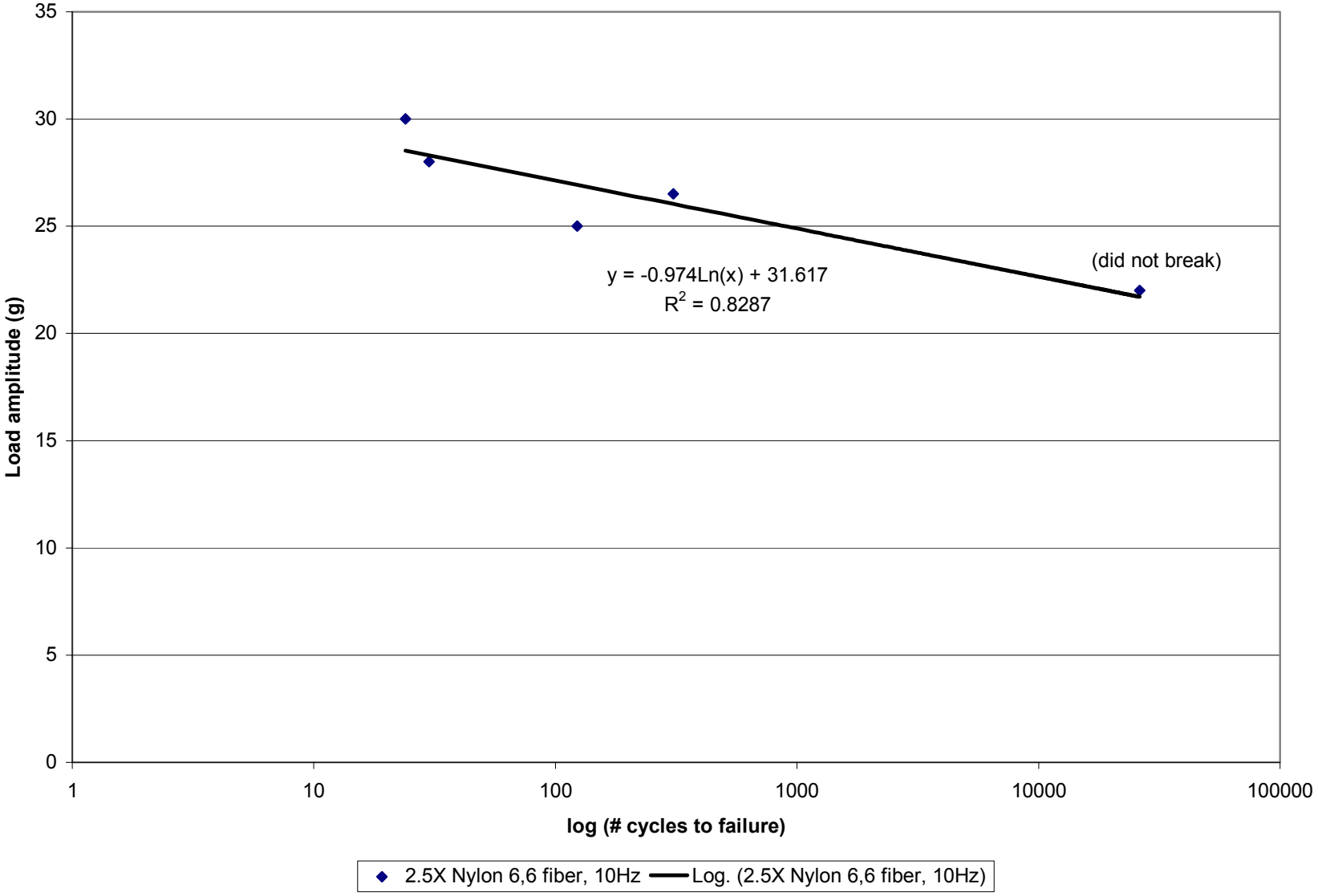

Figure 7.7. Experimental S-N Curve for Small Nylon 6,6 Fiber

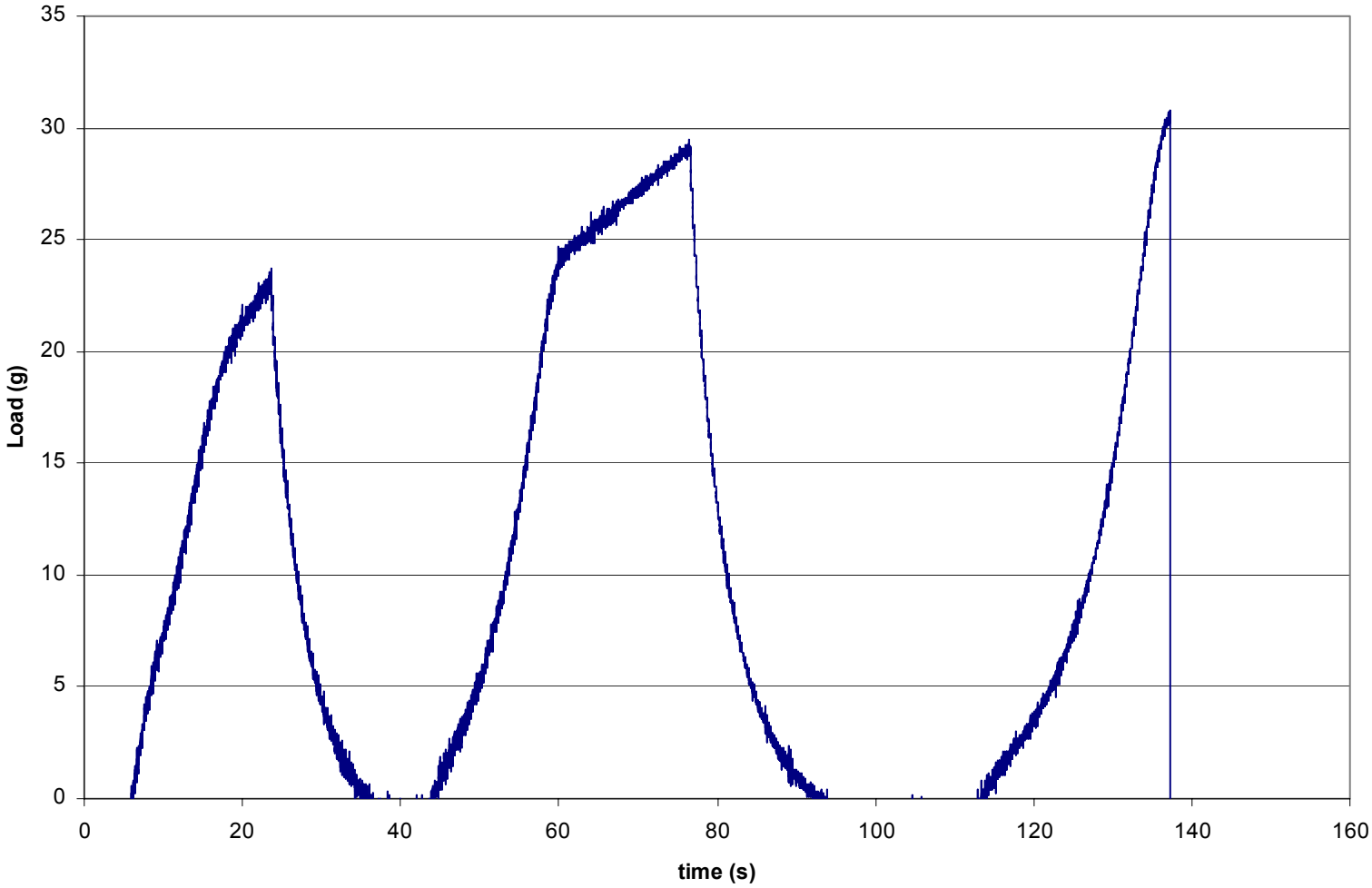

Figure 7.8. Load vs. Time Response of Small Fiber in Low-Cycle Fatigue

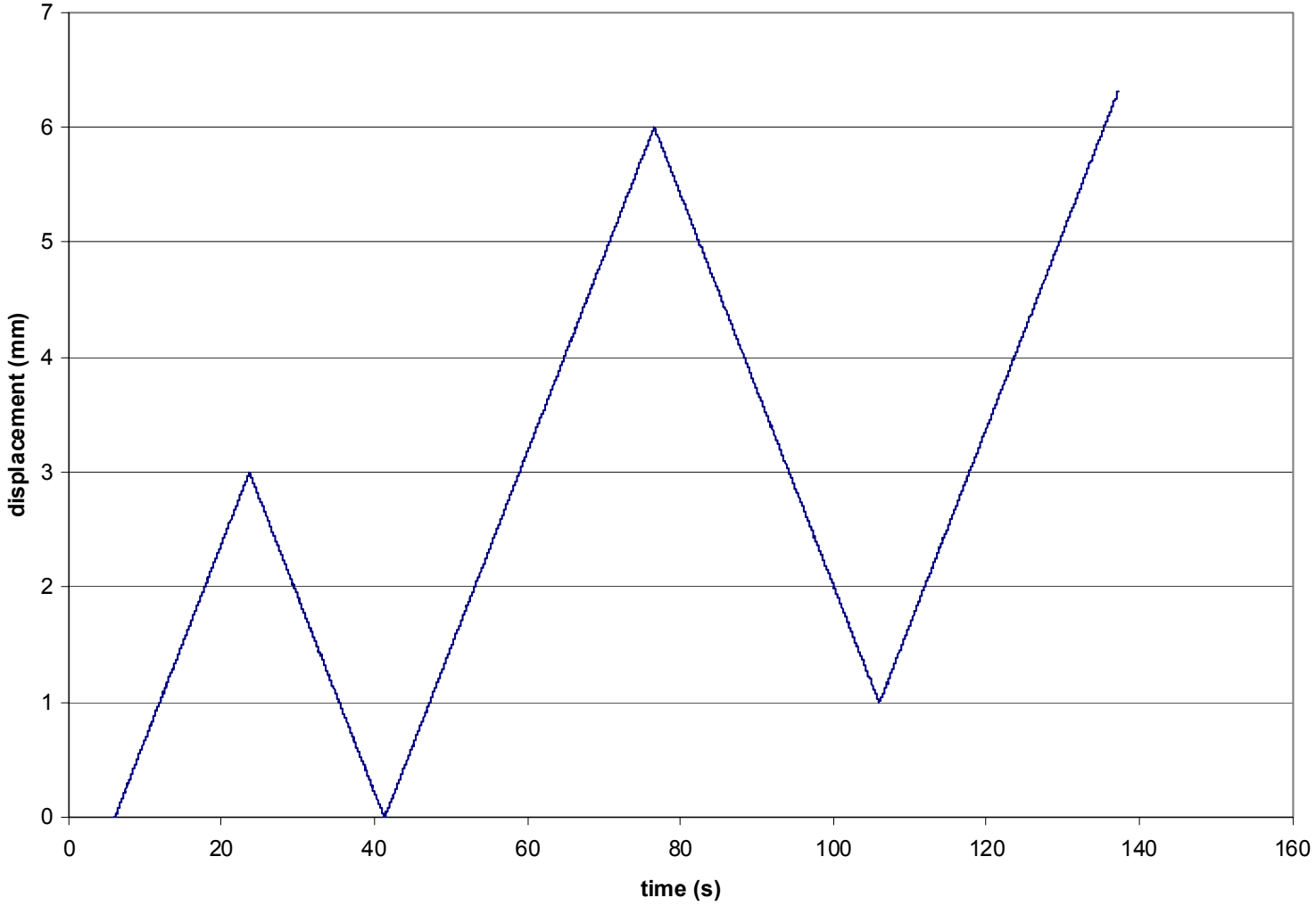

Figure 7.9. Displacement vs. Time Response of Small Fiber in Low-Cycle Fatigue

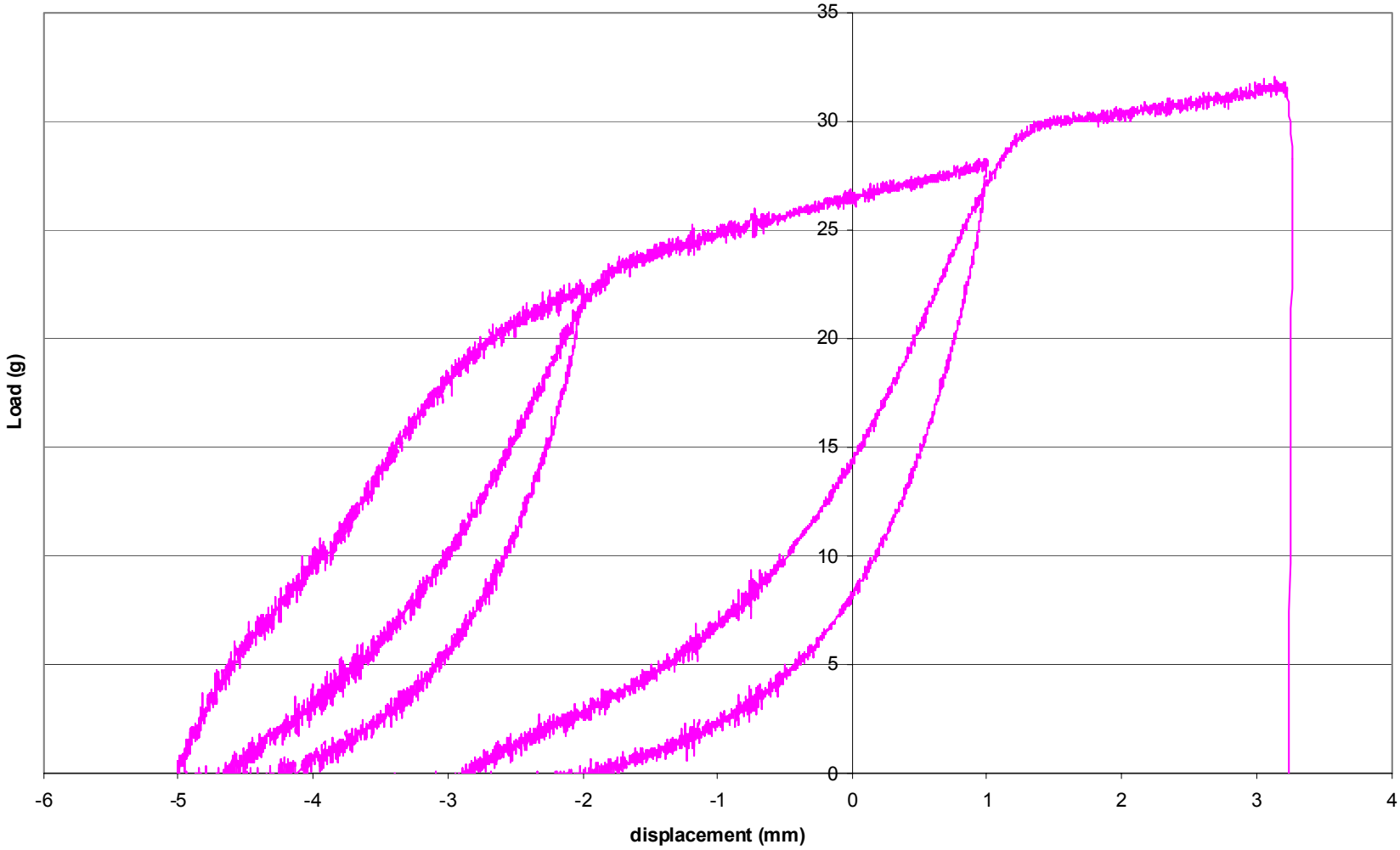

Figure 7.10. Load-Displacement Response of Small Fiber in Low-Cycle Fatigue

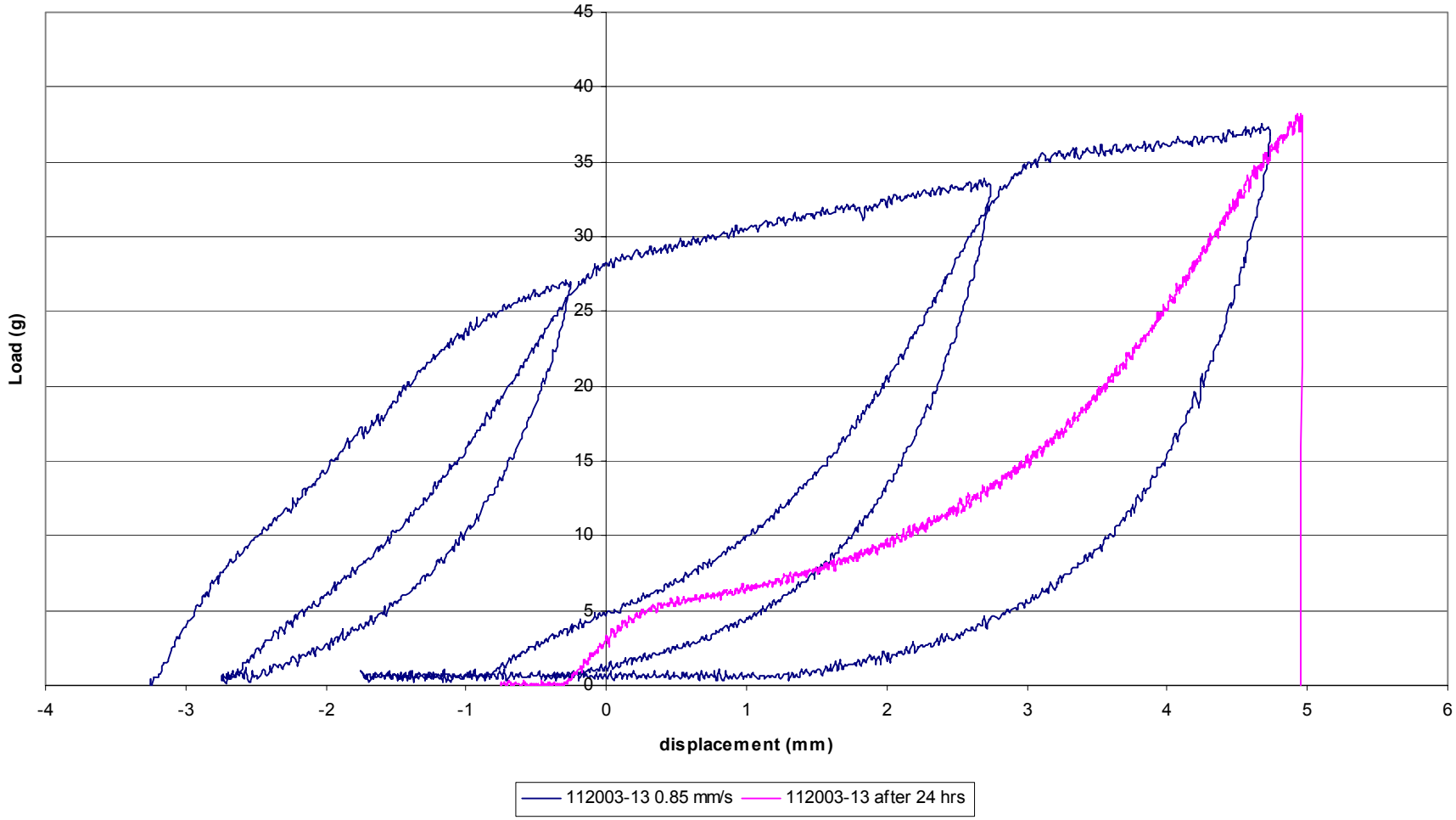

Figure 7.11. Figure Showing Recovery of Nylon 6,6 Sample After 24 hrs. (blue) Original Load-Unload Curve (pink) Re-load After 24 hrs.

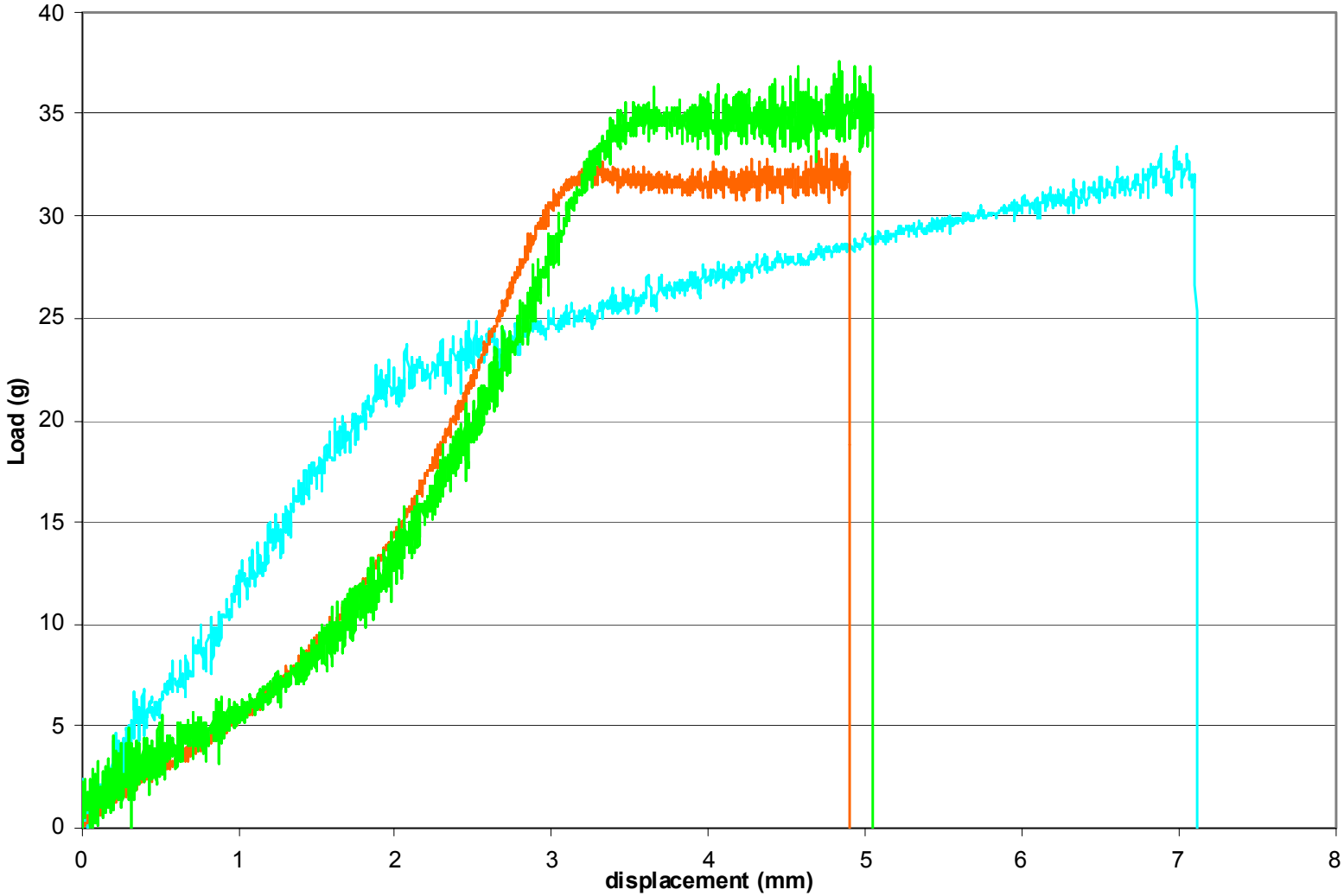

Figure 7.12. Figure Showing Drastic Difference in Unfatigued and Fatigued Small Nylon Samples. (turquoise) Unfatigued Sample (green – 30 g amplitude, 500 cycles, orange – 25 g amplitude, 750 cycles) Samples With Prior High Cycle Fatigue

CHAPTER 8

POST-FRACTURE RESULTS – DETERMINATION OF K_C, G_C, AND J_C

8.1. Linear-Elastic Fracture Mechanics Analysis – Determination of K_c and G_c ($J_{c,el}$)

The determination of the linear elastic fracture mechanics (LEFM) parameters was a straightforward and uncomplicated process, assuming that an accurate measurement was recorded for the critical crack length, a_c. The congenital flaw was assumed to be semi-elliptical in nature, and the stress intensity solution that governs this behavior for Mode I loading is given as[6]:

$$K = \sigma(\pi a)^{1/2}\left(\frac{1.12}{\phi^{1/2}}\right)$$

Here, σ represents the stress value, a represents the instantaneous crack length, and ϕ represents the ratio of the width to depth of the semi-elliptical flaw, as shown below in Figure 8.1. A graph showing how the dimensionless factor ϕ can be determined is provided alongside the pictorial representation of the flaw configuration.

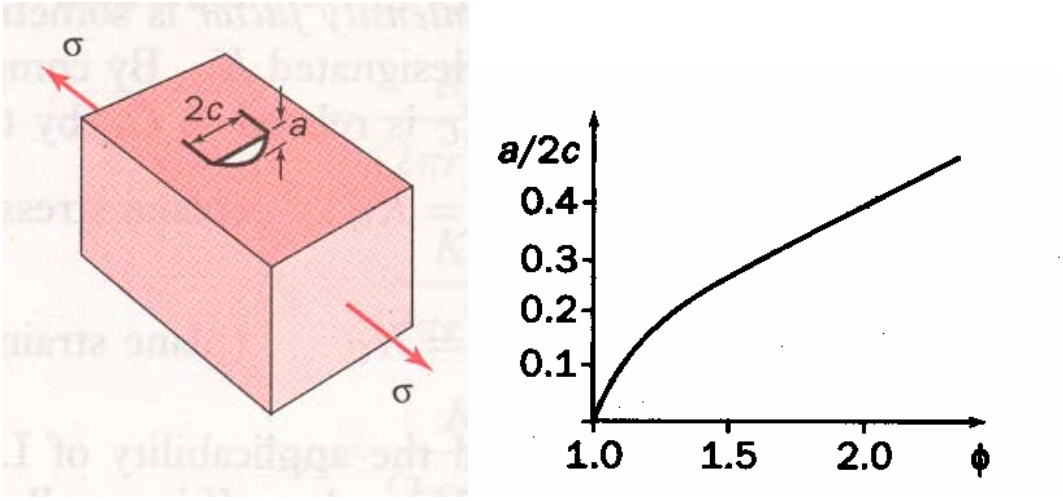

Figure 8.1. Semi-Elliptical Surface Flaw Configuration for Mode I Loading of a Sample[6]

For direct computation of the critical stress intensity factor solution, critical values were substituted into the stress intensity solution to obtain the following expression:

$$K_c = \sigma_c (\pi a_c)^{1/2} \left(\frac{1.12}{\phi^{1/2}} \right)$$

In this expression, the fracture strength represented the critical stress value (σ_c) and the critical crack length (a_c) was obtained via microscopy techniques described in the aforementioned methodology section. The ratio of the crack width to crack depth (*a/2c*) was assumed to be unity. A Microsoft Excel worksheet was generated that allowed the input of several key parameters from the stress-strain curves and the determination of the critical stress intensity factor solution. A sample of the worksheet that was generated in Microsoft Excel is provided in Table 8.2. Several measurements were made and the average value of the critical stress intensity solution, K_c, was 4.0 MPa$\sqrt{m}$. The value for the critical stress intensity solution of undrawn nylon 6,6 is 3.7 MPa$\sqrt{m}$[77]. This value represents a material property for nylon 6,6, whereas the value obtained in this research is specimen and geometry dependent. What is noticeable from this finding is that the critical stress intensity solution for this geometry and loading configuration is in close magnitude to the material property for undrawn, bulk nylon samples. The stress intensity values were computed with plastic zone correction, due to the presence of the plastic zone at the crack tip in these nylon fiber samples. The plastic zone correction employed was of the following form:

$$r_p = \frac{1}{6\pi} \left(\frac{K}{\sigma_f} \right)^2$$

Here, K represents the stress intensity factor and σ_f represents the fracture stress value.

Because the critical strain energy release rate (G_c) is directly related to the critical stress intensity solution, a simple computation was performed to determine its value. Although there is a possibility of a mixed mode of plane stress/strain conditions for this geometry, the plane strain case was assumed to be dominant for this particular geometry. Thus the following relationship was employed in the determination of the strain energy release rate:

$$G_c = \frac{1-\nu^2}{E} K_c{}^2$$

Basically, the critical stress intensity solution was substituted into the ensuing expression in addition to the initial loading modulus (E) of the sample. This process was performed for several samples, and an example of the Microsoft Excel worksheet is shown in Table 8.1 that was used to compute this value. The average value of the critical strain energy release rate was 6.8 kJ/m^2. For undrawn, DAM (dry as moulded), bulk nylon samples, the value of the critical strain energy release rate is 3.9 kJ/m^2, which also represents a material property[77]. As with the outcome in the stress intensity solution, one also notices the close proximity in magnitude of the load/geometry dependent strain energy release rate to the material property of the undrawn bulk sample. In both LEFM analyses of the fracture parameters, one must be admonished that the anisotropic nature of the crack propagation could have introduced minor errors in the calculations. However, the remaining orthogonal ligament in the fiber samples is consistent with the ligament area for samples in conventional LEFM techniques, which indicates that the value is accurate to a good degree.

Since the value of the congenital flaw was not found for the smaller nylon samples, a side investigation was done on larger nylon 6,6 samples to confirm the energy

theory proposed earlier. These samples possessed an obround shape and were approximately 840 μm in width with a thickness of 260 μm. A schematic of the load vs. elongation curves are provided in Figure 8.2, which portrays how the fracture strength of nylon 6,6 fibers varies with initial flaw size. Figure 8.3 in the following graph displays how the ultimate energy required to fully fracture the sample decreases as a function of increasing initial crack length. In tandem, these results (Figures 8.2 and 8.3) clearly evince that the Griffith Energy balance is applicable to fibers of various initial flaw sizes. One clearly notices from the graphs that an infinitesimal increase in initial crack surface area engenders a decrease in the potential energy available to the specimen for tensile work.

Table 8.1. Example Calculation in the Determination of Critical Strain Energy Release Rate, G_c, from Excel Worksheet

Critical Strain Energy Release Rate, Gc (plane strain case)

$$G_c = \frac{1.25\pi\sigma_f{}^2 a_c \left(1-\nu^2\right)}{E} \quad = \quad 5.5 \quad \text{kJ/m2}$$

Critical Strain Energy Release Rate, Gc (plane strain case) w/ plastic zone correction

$$G_c = \frac{1.25\pi\sigma_f{}^2 (a_c + r_p)\left(1-\nu^2\right)}{E} = \quad 6.8 \quad \text{kJ/m2}$$

Section 8.2. Elastic-Plastic Fracture Mechanics Analysis - Determination of J_c ($J_{c,pl}$)

The final determination of the critical nonlinear energy release rate for a particular loading configuration of the nylon 6,6 fibers was not an easy task. Several mathematical expressions were used, and most importantly an integration scheme was utilized to

determine the plastic energy under the load-displacement curve for the final deformation cycle. Anderson[2] has shown how the critical nonlinear energy release rate in polymers increases with increasing strain rate. Thus in the determination of the fracture mechanics parameters for this investigation, only one strain rate of 0.00669 s^{-1} was employed. Basically, the elastic portion of the critical nonlinear energy release rate was provided

Table 8.2. Example Excel Worksheet for Determination of Critical Stress Intensity Solution, K_c

Stress intensity solution for a semi-elliptical surface flaw

$$K = \sigma \sqrt{\pi a} \left(\frac{1.12}{\phi^{1/2}} \right)$$

critical stress intensity factor

$$K = \sigma_y \sqrt{\pi a_c} \left(\frac{1.12}{\phi^{1/2}} \right)$$

Nylon 6,6 (DAM) bars

KIc = 3.7 MPa*m1/2

Sample Name: 012803-20

Fiber properties		
diameter, d =	3.50E-05	m
critical crack length, ac =	1.70E-05	m
yield load, Py =	22.4	g
fracture load, Pf =	33.3	g
Fracture stress, σf =	4.48E+02	MPa
Strain at fracture, εf =	0.3205	
Yield eng. strain, ε =	0.0734	
Yield stress, σy =	2.4E+02	MPa
Area, A =	9.6E-10	m2
Young's Modulus, E =	1.8E+03	MPa
Poisson's ratio, ν =	0.41	

Critical stress intensity calculation

$K_c = 1.12 \sigma_f \sqrt{\pi a_c}$ = 3.7 Mpa*m^1/2

Plastic zone correction

$$r_p = \frac{1}{6\pi} \left(\frac{K}{\sigma_f} \right)^2 = 3.6E\text{-}06 \text{ m}$$

Critical stress intensity calculation, w/ plastic zone correction

$K_c = 1.12 \sigma_f \sqrt{\pi (a_c + r_p)}$ = 4.0 Mpa*m^1/2

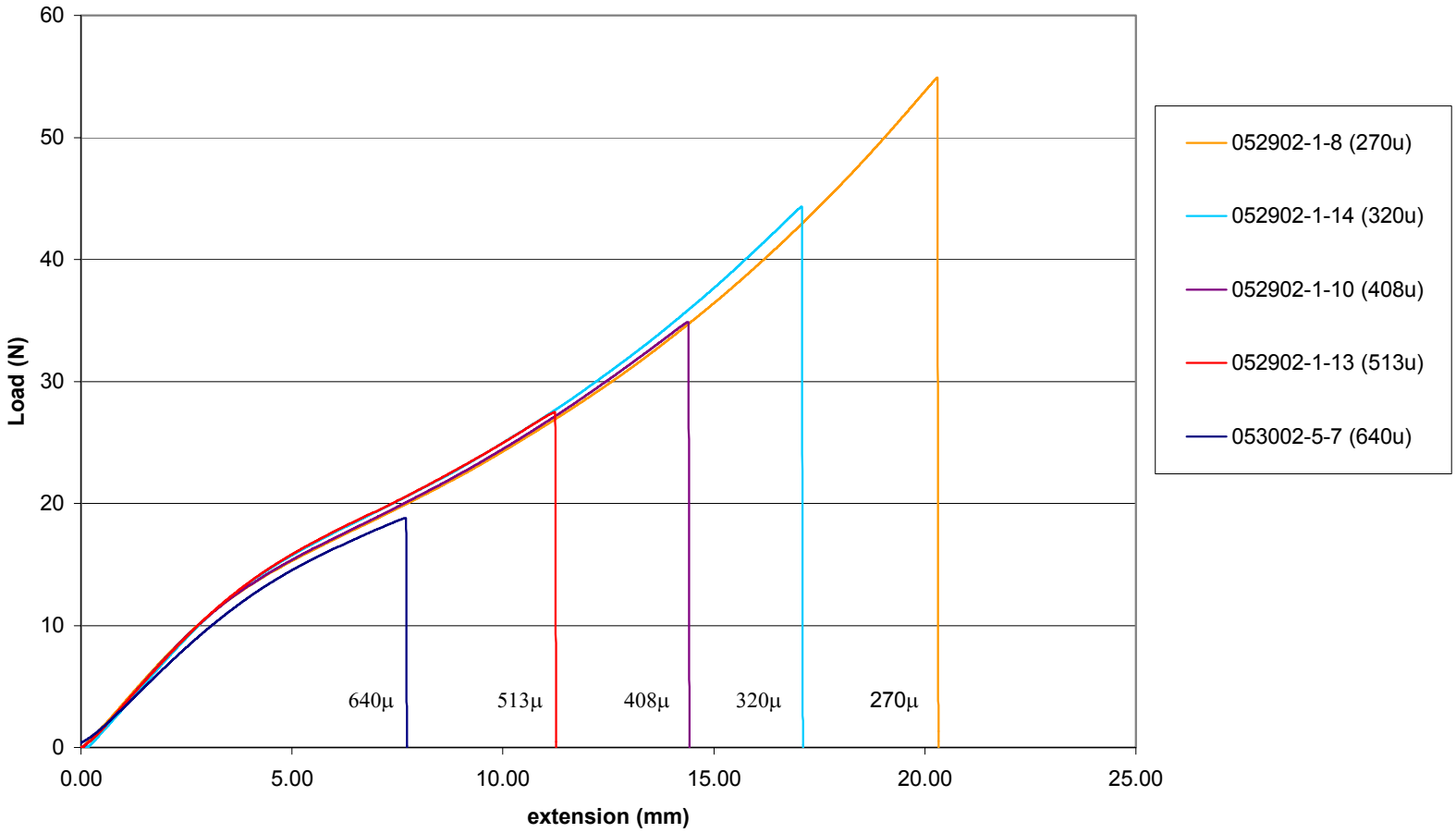

Figure 8.2. Load-Displacement Curves from Larger (Obround) Fiber Experiments with Varying Initial Flaw Sizes

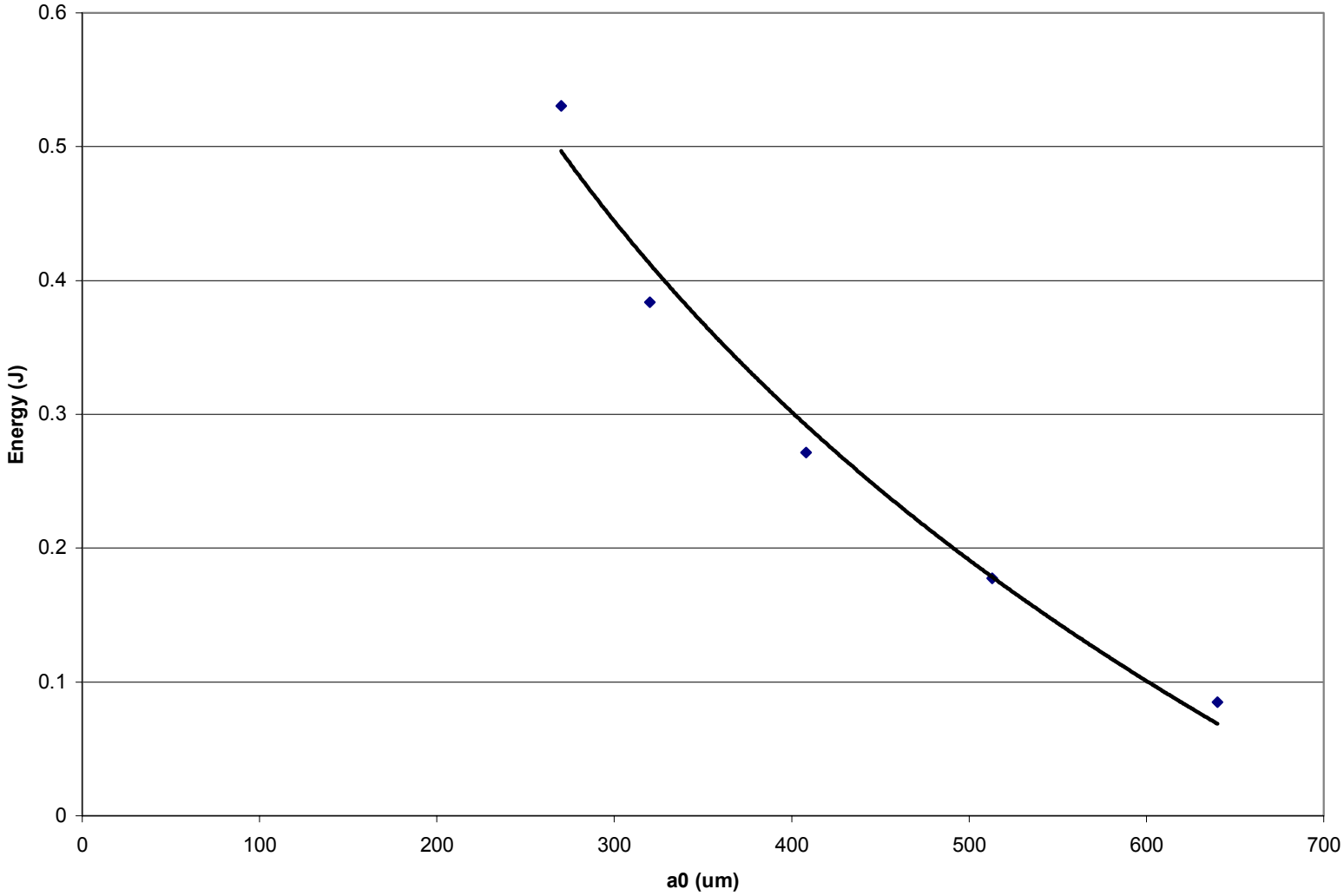

Figure 8.3. Graph Showing how Total Energy Required to Fracture a Nylon 6,6 Sample Decreases for Increasing Initial Crack Length

from the results of the critical strain energy release rate, G_c. The plastic component was computed from the following parameters:

1) dimensionless constant η

2) plastic energy under stress-strain curve

3) ligament area of the sample

For the determination of the dimensionless constant η, the following relationship was employed:

$$\eta = 2 + \frac{0.522(W - a)}{W}$$

Here W represents the width of the sample and a represents the critical crack length. This relationship was derived on the basis of a rectangular sample. Due to the round cross-sectional area of these small nylon filaments, the width (W) was assumed to be equivalent to the diameter of the sample. Likewise, the crack length (a) was measured from the edge of the sample, similar to the method of measurement in rectangular specimens.

A pictorial representation is shown in Figure 8.4 of how the plastic area under the load-elongation curve was obtained via simple integration techniques. With the aid of Microsoft Excel, the energy under the curve for the elastic and plastic portions was obtained from the following relationships:

$$Elastic\_Energy = \int_0^{\Delta_e} P d\Delta_e$$

$$Plastic\_Energy = \int_0^{\Delta_P} P d\Delta_P$$

In these relationships, P represents the load, and Δ_e and Δ_P represent the elastic and plastic displacement limits, respectively. The aggregate energy parameter was obtained

from the summation of the elastic and plastic energy quantities. This constituted the total mechanical work that was done by the specimen during the tensile loading process.

The ligament area constituted the final parameter needed for calculation of the critical nonlinear energy release rate, $J_{c,pl}$. As described earlier, trigonometric identities were used to calculate this value, and an example of the worksheet employed for determination of the ligament area is presented in Table 8.3. As with the other fracture parameters, Microsoft Excel was used in the computation of the nonlinear energy release rate. The average value of the critical crack length observed via S.E.M. fractography analysis was 21 μm with a standard deviation of 2 μm. This represents a critical crack length to width (a_c/W) ratio of 0.6. This value includes results from both high-cycle and low-cycle fatigue experiments prior to tensile deformation at a strain rate of 0.00669 s^{-1}. This proves that the critical crack length of the fiber is not altered by its fatigue history, if the frequency is kept at or below 10Hz. Rather, Hearle[19] has already shown that the critical crack length is altered by changes in the tensile loading rate, which was not a factor in this study. As depicted in the literature investigation from the S.E.M. fractographs of nylon 6,6 fibers, a high frequency coupled with a large number of load cycles can also engender a transmutation of the fiber fracture surface. However, alterations in the frequency were not a variable in this research investigation.

The average value of the critical crack length, and consequently the critical a/W ratio, was shown to be in close alliance with the theoretical estimates from the Griffith Energy Balance. The total energy of the nylon 6,6 sample is given by:

$$U = U_s + U_e$$

where U_s = surface energy stored in the material due to the presence of the crack and U_e =

elastic strain energy released by the formation of the crack. In mathematical notation, this value is computed in the following manner[6]:

$$U = 2aG - \frac{\pi\sigma^2 a^2}{E}k$$

Here, $k = 1-\nu^2$ for plane strain or $k = 1$ for plane stress. As expected, the critical condition occurs when $dU/da = 0$. Using this criterion with the plane strain case, the critical crack length was obtained from the following relationship[6]:

$$\frac{d}{da}\left(2aG - \frac{\pi\sigma^2 a^2}{E}(1-\nu^2)\right) = 0$$

$$a = \frac{EG_c}{\pi\sigma_f^2(1-\nu^2)}$$

Table 8.3. Example Calculation in the Determination of Ligament Area and Critical Nonlinear Energy Release Rate, $J_{c,pl}$, via Microsoft Excel Worksheet

$$J_{pl} = \frac{\eta A_{pl}}{ligament\_area}$$

$$\eta = 2 + \frac{0.522(W-a)}{W}$$

$$ligament\_area = \pi r^2 - \left[r^2\left(\tan^{-1}\left(\frac{\left(2a_c r - a_c^2\right)^{1/2}}{r-a_c}\right) - \frac{\left(2a_c r - a_c^2\right)^{1/2}(r-a_c)}{r^2}\right)\right]$$

$$J_c = \frac{1-\nu^2}{E}\sigma_Y^2 \pi a_c + \frac{\left(2 + \frac{0.522(W-a)}{W}\right)A_{pl}}{\pi r^2 - \left[r^2\left(\tan^{-1}\left(\frac{\left(2a_c r - a_c^2\right)^{1/2}}{r-a_c}\right) - \frac{\left(2a_c r - a_c^2\right)^{1/2}(r-a_c)}{r^2}\right)\right]}$$

Gc =	5.73183010195	kJ/m2
η =	2.3132	
Apl =	8.92738E-07	kN-m
Area total	9.621128E-10	m2
Area 1	4.193905E-10	m2
Area 2	6.001250E-11	m2
Ligament Area	6.027347E-10	m2
Jc =	3432	kJ/m2

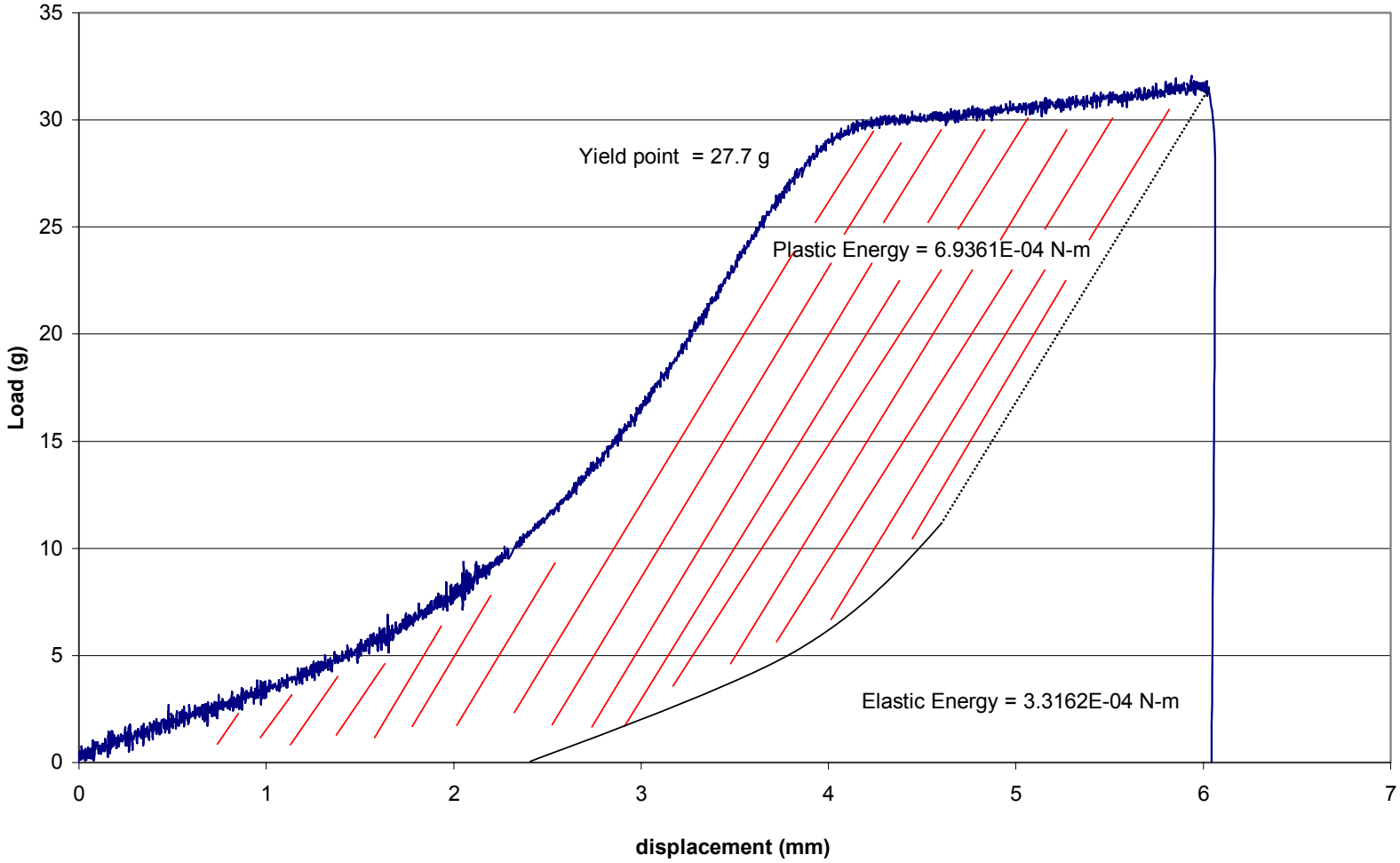

Figure 8.4. Determination of Plastic and Elastic Energy From Load-Elongation Curve in Small Nylon Fiber Sample

The fracture stress, σ_f, represents the strength of the fiber at failure and was found from the stress/strain curves of the uniaxial tensile test. From these curves, the average value of the fracture stress, σ_f, was approximately 380 MPa. Computing the value for the critical flaw size, the theoretical value of the critical crack length for this loading and geometry is:

$$a = \frac{\left(1.8\times10^{9}\right)\frac{N}{m^2}\left(3.9\times10^{3}\,\frac{J}{m^2}\right)}{\pi\left(380\times10^{6}\right)^2\left(1-0.41^2\right)} = 19\mu$$

This constitutes a critical crack length to fiber diameter (a/W) ratio of 0.54. This value is within 5% of the experimental value for the critical flaw size, which indicates that fracture mechanics is applicable to fibers of this magnitude.

The value of J_c for the loading conditions described was 3080 kJ/m^2 for the small samples tested in this experiment. This value is more than 450 times the critical strain energy release rate value; however, the effects of large scale yielding in such a small polymer sample substantiate this finding. The plastic component of the strain energy release rate scales according to the inelastic deformation in the sample, which was an enormous value in this investigation. A schematic of the linear curve fit is provided in Figure 8.5 that was used in the determination of this value. The following equation was used to obtain the linear curve fit and subsequently the plastic contribution of the critical nonlinear energy release rate:

$$J_{c,pl} \times ligament\_area = \eta \times A_{pl}$$

In this equation, the plastic area of the stress-strain curve multiplied by the geometrical constant, η, was plotted vs. the ligament area of the sample. The resulting slope represented the plastic entity of the critical nonlinear energy release rate, $J_{c,pl}$. One can

also use a spreadsheet function such as the one shown in Table 8.3 to calculate the nonlinear energy release rate, $J_{c,pl}$ when the appropriate parameters are specified. The extreme magnitude difference in the elastic and plastic components of the nonlinear energy release rate may pose uncertainty as to the validity of the methods and procedures employed for the determination of the plastic parameter. Nevertheless, this seemingly anomalous result can be clarified through the following observations:

1) In this analysis, the plastic component of the energy release rate is coterminous with the plastic energy under the load-elongation curve.
2) The elastic parameter is obtained strictly on the assumption that J=G for purely elastic behavior.
3) The former assumption does not include an energy parameter, and thus the elastic solution does not scale according to the elastic energy under the load-displacement curve.

What has been suggested by Bernal et al.[74] in a study conducted on ABS polymers is to express both the elastic and plastic components of J in terms of their respective energy quantities. In simple mathematical form, this relationship is provided as:

$$J = \frac{\eta_{el} A_{el}}{ligament\_area} + \frac{\eta_{pl} A_{pl}}{ligament\_area}$$

While this is a plausible solution, the utilization of the above relationship could generate misleading results for the samples tested in this research. The elastic parameter in the above equation is based on the aggregate elastic energy in the sample, which includes energy that is not accounted for in conventional LEFM techniques. Thus when the strain energy release rate is computed from this equation, it will lead to the overcompensation of energy and an abnormally high elastic parameter. However, the plastic component of

the equation can been utilized in the computation of the nonlinear energy release rate, since it has been established as a useful parameter in fracture testing of polymers[69,78]. Because the critical flaw size can not be visually inspected during mechanical testing, it has been hypothesized that the critical flaw size coincides with the yield point on the load-displacement curve (Figure 8.4). This validates the usage of the entire plastic energy parameter, and is a good assumption because of the demonstrated semi-perfectly plastic behavior beyond the elastic limit. This semi-perfectly plastic behavior can be viewed as the process of fast fracture, in which the dominant flaw has reached its critical value and propagates at an accelerated rate without an increase in load.

8.3. S.E.M. Fractography Analysis

The S.E.M. fractographs obtained for this work resemble the results of Hearle[19] to a large degree. This indicates to a great extent that the tensile experiments were conducted correctly and can be repeated by other investigators. Figures 8.6 and 8.7 depict an isometric view of a fiber as well as the cross-sectional area that underwent low-cycle fatigue for 2 cycles preceding ultimate deformation. Other S.E.M. fractographs are included in Figures 8.8 to 8.16 for fibers that underwent low-cycle and high-cycle fatigue deformation prior to tensile loading. As shown, all of the fractographs display the same general attributes, with minor alterations in the appearance of the fracture surface and ligament length. This fractography study leads to a general hypothesis for the low-cycle and high-cycle fatigue experiments conducted in this study. It is confirmed from these fractographs and the results of Hearle[19] that the cyclic portion of this experimentation phase did not produce a substantial amount of crack growth in the sample.

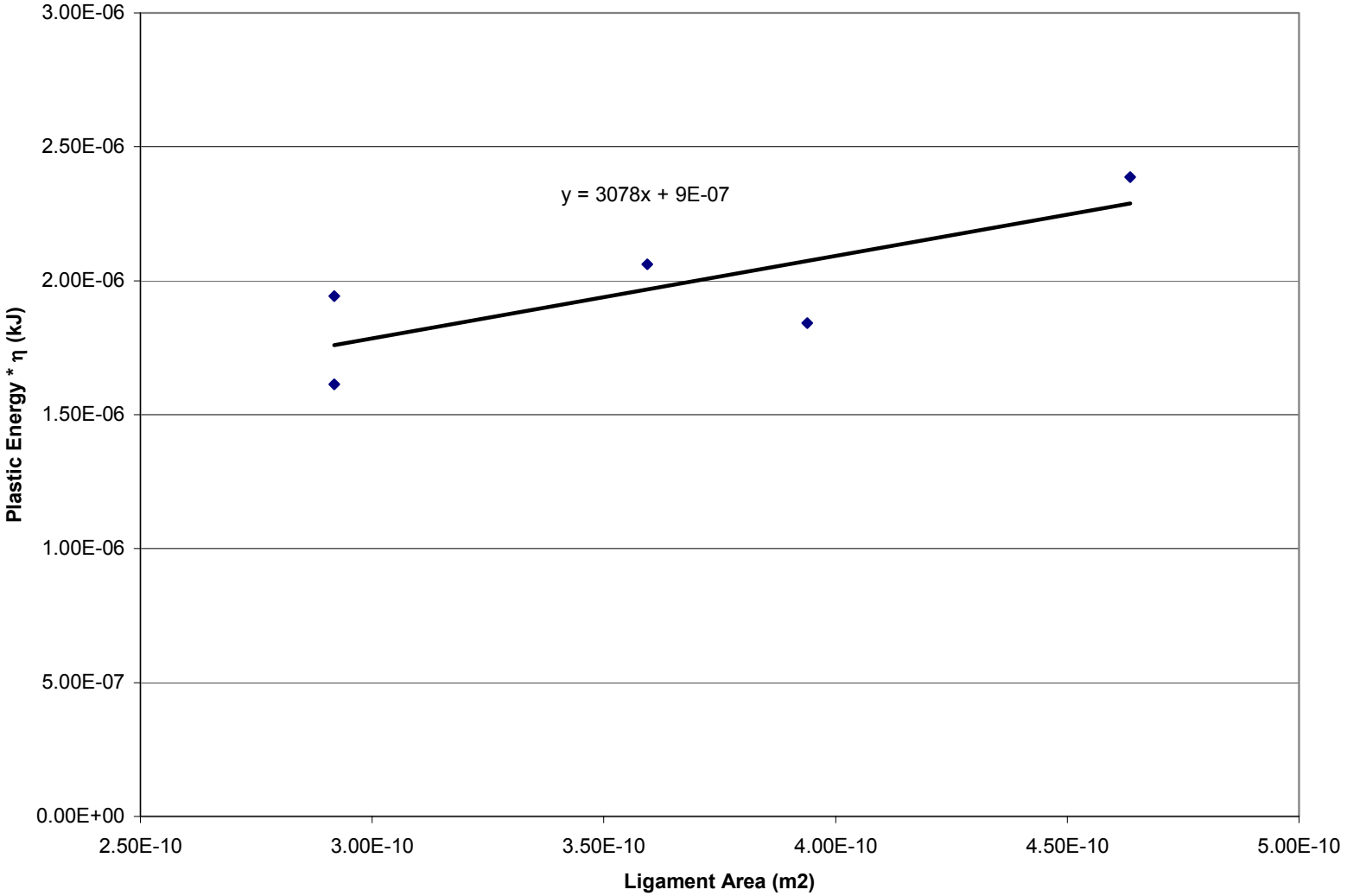

Figure 8.5. Determination of the Plastic Entity of the Critical Nonlinear Energy Release Rate ($J_{c,pl}$) via Linear Curve Fit

Rather, the ancillary technique only contributed to a small amount of crack growth, in which the uniaxial tensile mode was the main contributor of crack growth. In addition, what is clearly delineated from these fractographs (8.6 – 8.16) and the results from Hearle[19] is that the crack growth for the fatigue and tensile phases of this experiment was smooth and controlled. This is best depicted in Figure 8.6, where the fracture surface appears smooth from an isometric view at a distance. Upon close view of the crack surface area (Figure 8.7), however, one notices the distinct regions of stable and unstable (catastrophic) crack propagation. These results clearly indicate that there are two distinct phases in the crack growth mechanism of nylon 6,6 fibers. The first phase of the crack growth is fairly stable, resulting from the initial loading of the sample. For this research, the first mode occurred due to a small contribution from the cyclic loading, but was predominantly governed by the initial tensile loading phase. The second phase is deleterious in nature, and is likely the result of further loading of the sample beyond the elastic limit. This constitutes the catastrophic, or unstable crack propagation region on the fracture surface of the fiber.

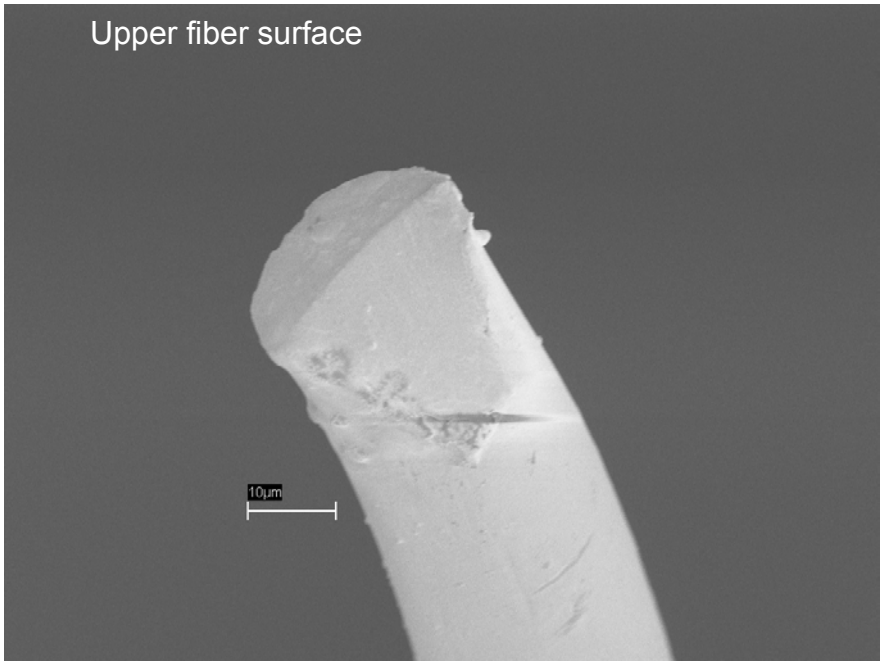

Figure 8.6. Upper Fiber Surface of Fiber Tested in Displacement Control for 2 Cycles Preceding Ultimate Deformation

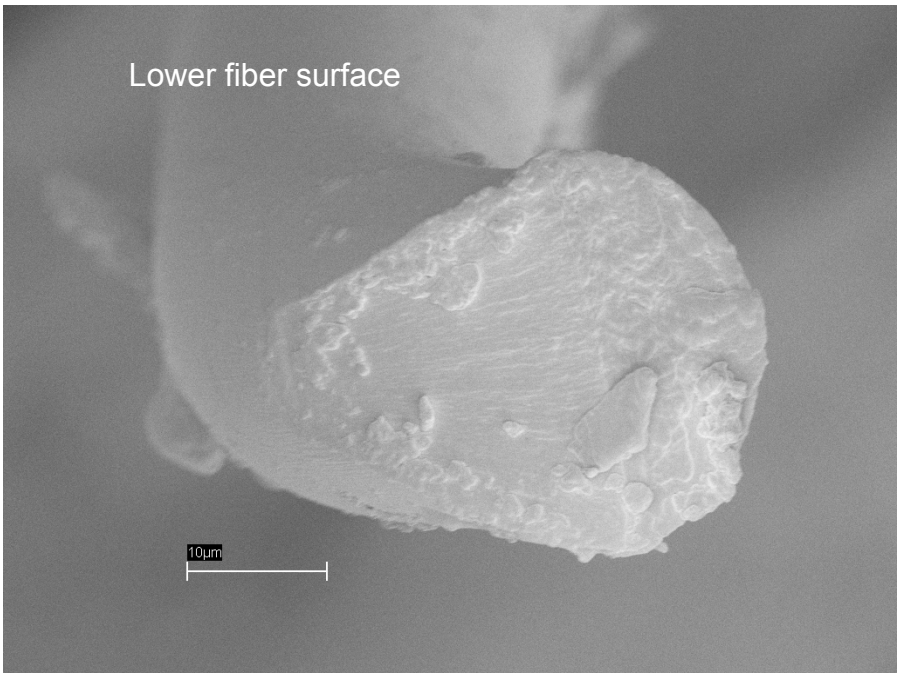

Figure 8.7. Lower Fiber Surface of the Fiber in Figure 8.6 Showing Cross-Sectional Area

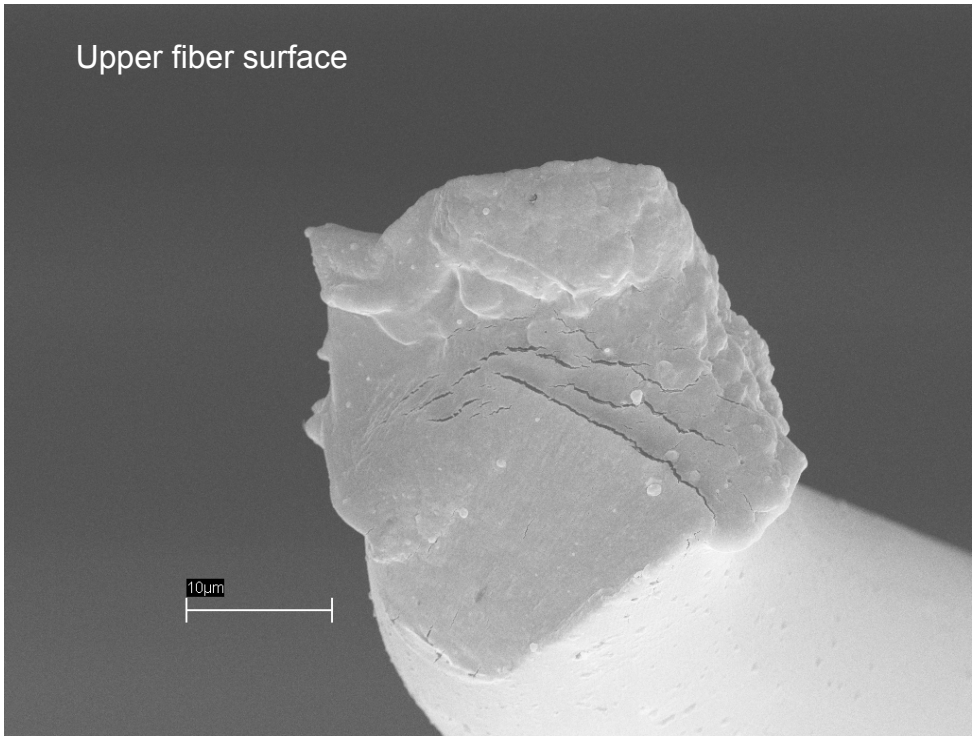

Figure 8.8. Fractograph Showing Cross-Section of Sample Loaded in High-Cycle Fatigue (5Hz, 0 to 25g) for 500 Cycles Prior to Tensile Deformation

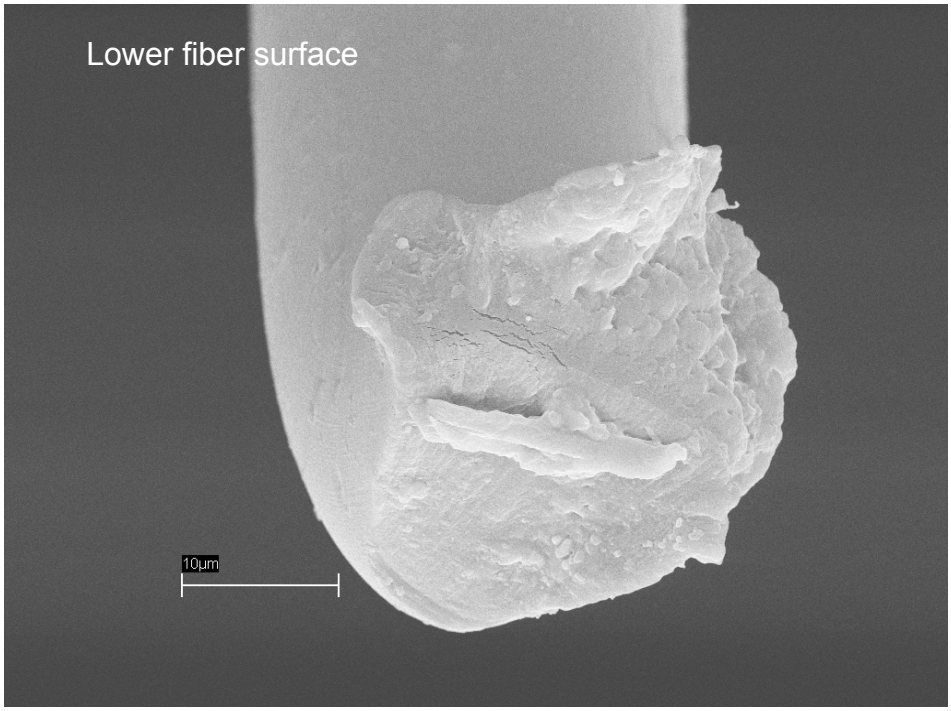

Figure 8.9. Lower Surface of the Fiber Described in Figure 8.8 Above

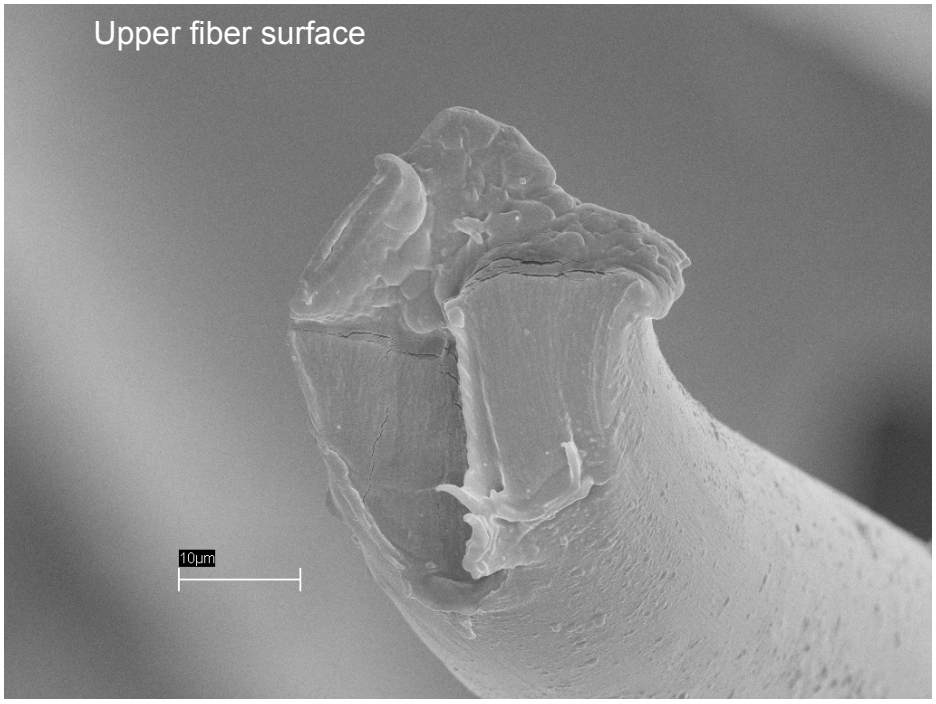

Figure 8.10. Fractograph Showing Cross-Section of Fiber with Prior High-Cycle Fatigue Loading (5Hz, 0 to 25g) for 500 Cycles

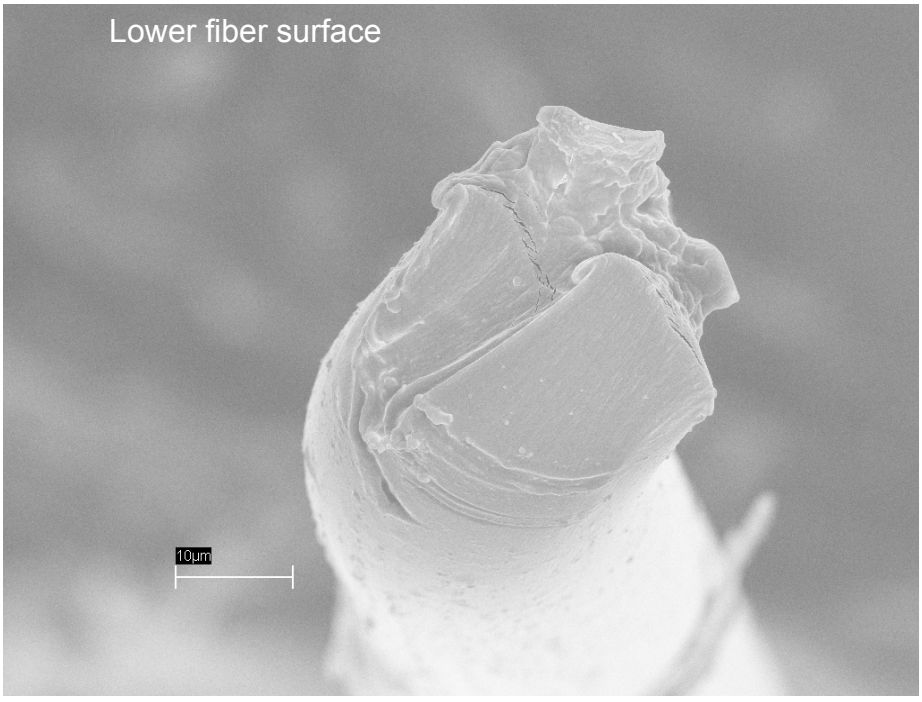

Figure 8.11. Lower Fiber Surface of Specimen Depicted in Figure 8.10

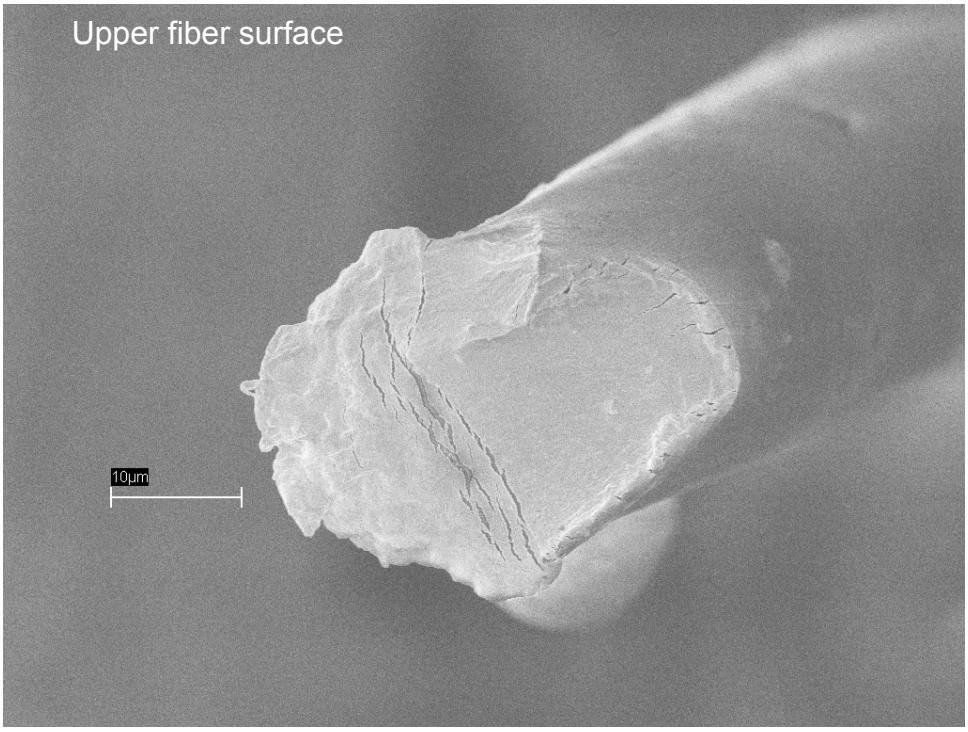

Figure 8.12. Fractograph Showing Upper Fiber Cross-Section of Sample that Underwent High-Cycle Fatigue (5Hz, 15 to 20g) for 1000 Cycles

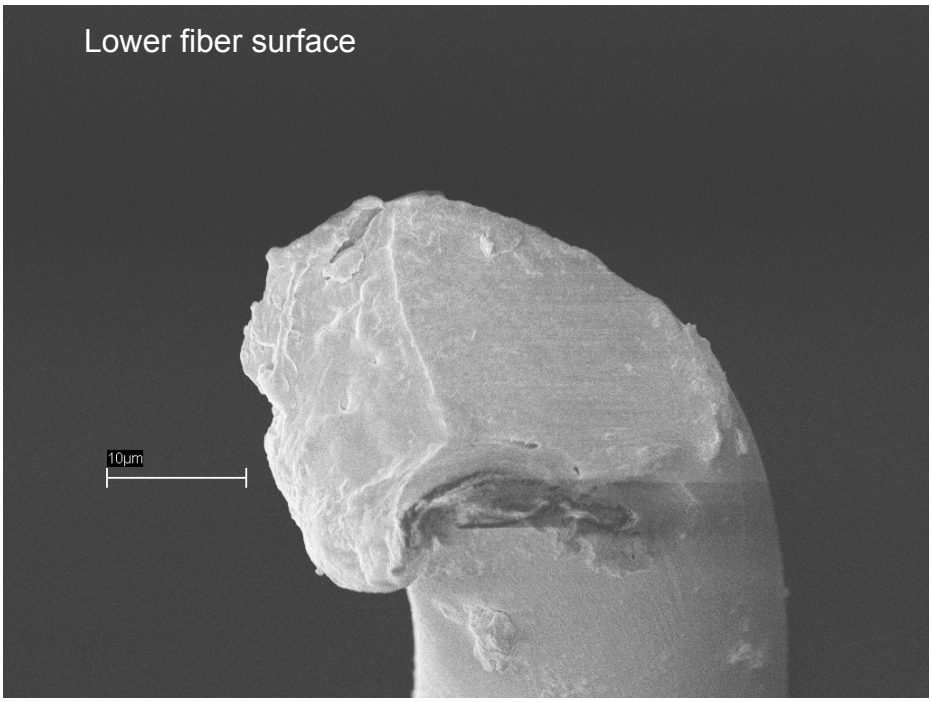

Figure 8.13. Lower Fiber Surface of Fiber Depicted in Figure 8.12

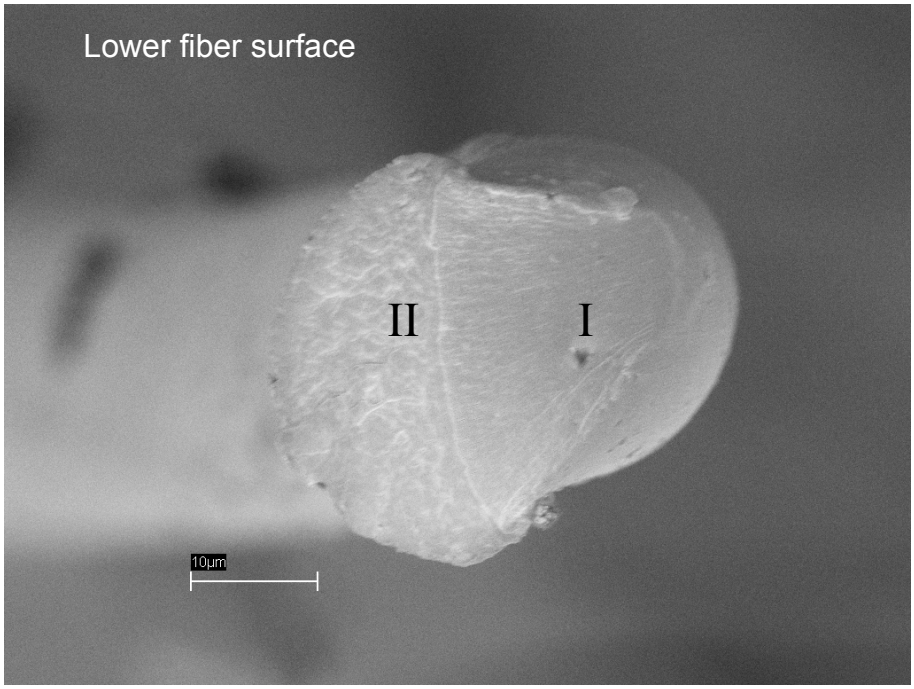

Figure 8.14. Fractograph Showing Cross-Section of Lower Fiber Surface of Fiber That Underwent Low-Cycle Fatigue (3 cycles) Preceding Ultimate Tensile Fracture (Notice the distinct regions of stable (I) and unstable (II) crack growth)

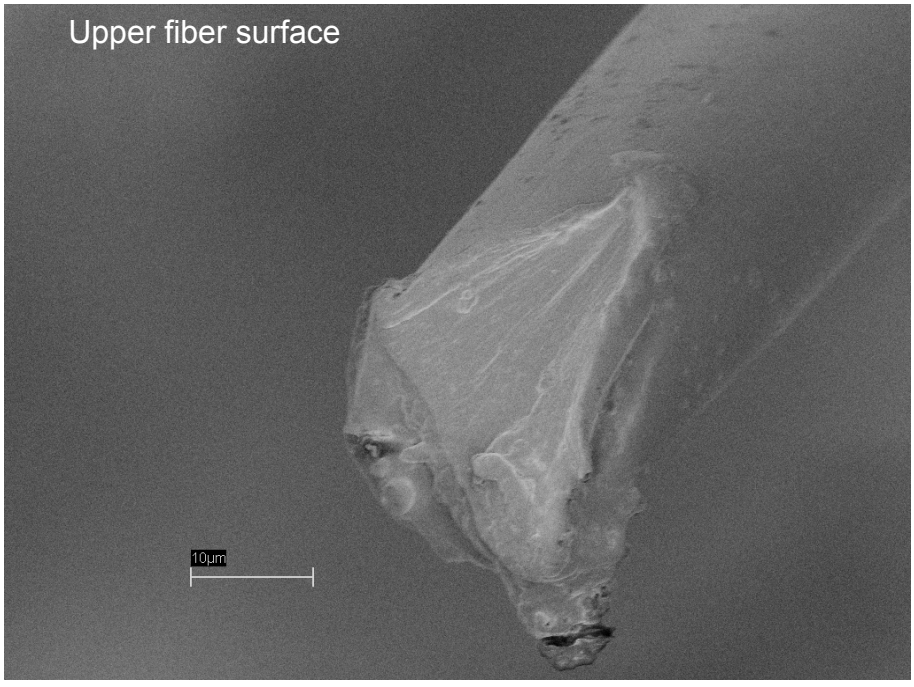

Figure 8.15. Fractograph Showing Isometric View of Upper Surface of Fiber that Underwent Prior Low-Cycle Fatigue (3 cycles)

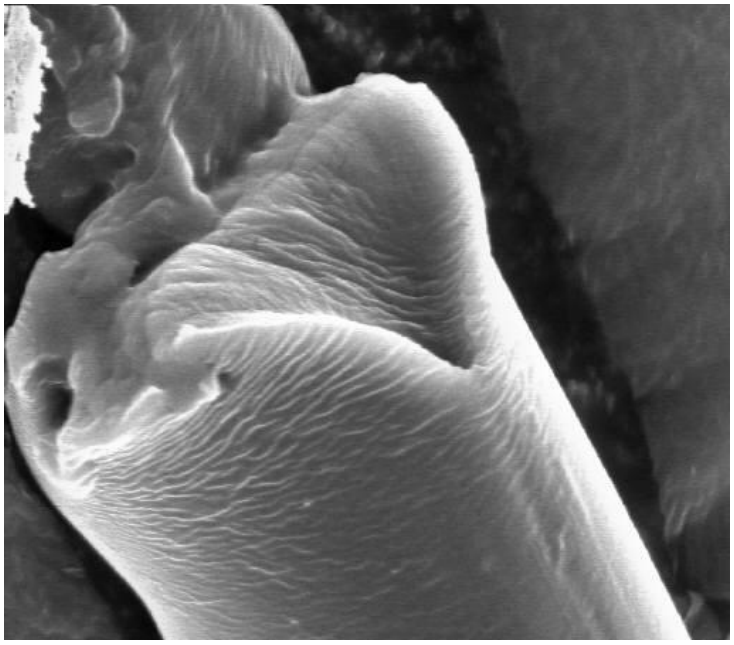

Figure 8.16. Isometric View of Fiber that Underwent Prior High Cycle Fatigue (0 to 25g) for 500 Cycles (Notice the v-shaped notch representing the initiation of crack growth)

CHAPTER 9

CONCLUSIONS & FUTURE WORK

9.1 Conclusions

The purpose of this study was to develop a fracture mechanics procedure useful for characterizing nylon 6,6 fibers of a small cross-section. In particular, an exacting testing methodology has been established that generates repeatable results. This includes sample preparation, mechanical testing, and fractography methods, which are the main constituents in fiber testing and research. From the fracture mechanics research, it has been shown that the results of LEFM are in alliance with previously published material values for bulk, undrawn nylon 6,6. More importantly, the Griffith Energy Balance was shown to predict the critical flaw size within 5% of the experimental value for this material. The results from EPFM indicate a large critical nonlinear energy release rate, but this is expected from these fibers due to the low draw ratio (2.5X) that was employed, and more significantly the amount of inelastic deformation during mechanical loading. These studies were performed with no prior knowledge of the initial flaw size in the material; however, a side study was done on larger samples to show how the potential energy of nylon 6,6 decreases as a function of increasing initial flaw size. This side study proves that the Griffith Energy Balance is applicable to nylon 6,6 fibers and can be used to determine the strength and energy limitations when necessary. This entire study helps to corroborate the initial assumption of similitude in fracture mechanics of polyamide samples and proves that existing LEFM and EPFM techniques can be utilized to describe the failure processes in nylon 6,6 fibers.

9.2. Future Work

Because these fibers possessed large quantities of inelastic deformation prior to fracture, an autonomous study should be conducted to ascertain how plasticity interacts with fracture mechanics of nylon 6,6 fibers. Some models and suggestions have been provided in the literature review that can help to illuminate these perplexities. In addition, the molecular aspects of fracture in nylon 6,6 fibers should be expounded, in which the results from existing literature can be coupled with these findings to develop a more rigorous deformation framework. Thus a synergistic approach can be developed in which one can ascertain how the molecular aspects, inelastic deformation, and fracture mechanics of nylon 6,6 fibers are interrelated. This would allow for modeling of the fiber its entirety, and these results could be used by researchers and developers to simulate how the fiber reciprocates under certain stress conditions. These techniques would be of great benefit to manufacturers, in which they would have advanced knowledge of how the individual fibers will behave at the conclusion of processing.

APPENDIX

Ligament Area Calculations ($r \leq a_c$)

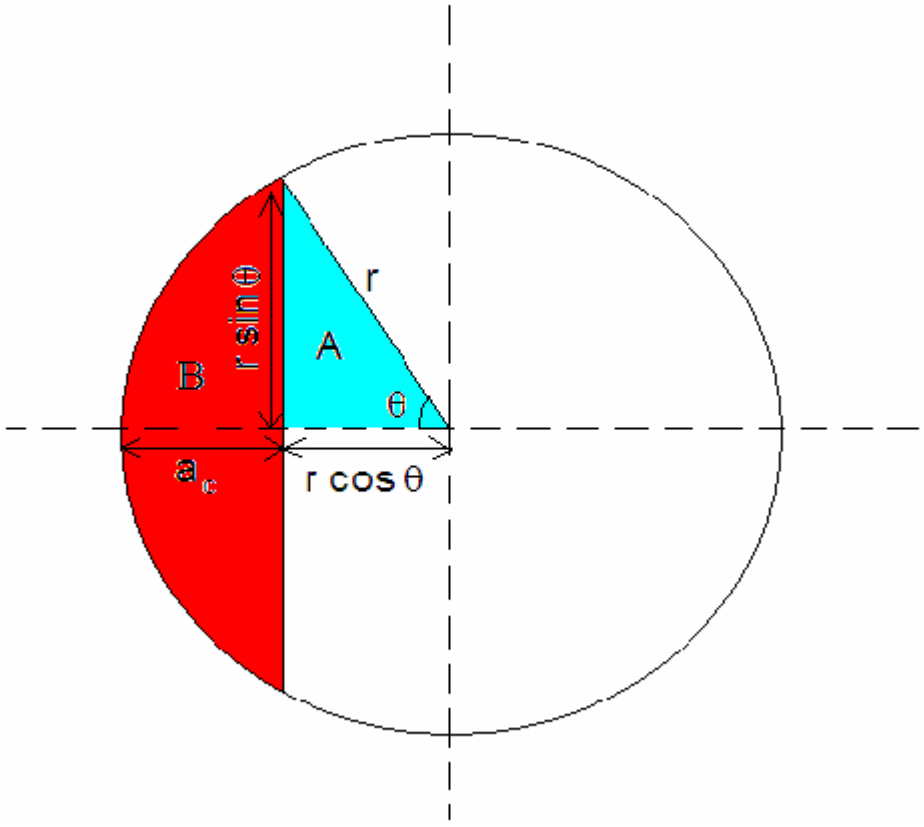

$$\text{Area A} = \frac{1}{2} r \sin\theta r \cos\theta = \frac{1}{2} r^2 \sin\theta\cos\theta$$

$$\text{Area sector} = \pi r^2 \frac{\theta}{2\pi} = \frac{r^2\theta}{2}$$

$$\text{Area B} = \text{crack surface area} = 2 \times (\text{Area sector} - \text{Area A}) = r^2\theta - r^2 \sin\theta\cos\theta$$

$$\text{crack surface area} = \boxed{r^2(\theta - \sin\theta\cos\theta)} \quad (1)$$

$$r\cos\theta = r - a_c$$

$$\boxed{\cos\theta = \frac{r - a_c}{r}} \quad (2)$$

For $\sin\theta$, use the following relationship:

$$(r\cos\theta)^2 + (r\sin\theta)^2 = r^2$$

$$(r\sin\theta)^2 = r^2 - (r\cos\theta)^2$$

$$r\sin\theta = \sqrt{r^2 - (r - a_c)^2} = \sqrt{r^2 - \left(r^2 - 2a_c r + a_c{}^2\right)}$$

$$r\sin\theta = \sqrt{2a_c r - a_c{}^2}$$

$$\boxed{\sin\theta = \frac{\sqrt{2a_c r - a_c{}^2}}{r}} \qquad (3)$$

$$\tan\theta = \frac{\sin\theta}{\cos\theta} = \frac{\sqrt{2a_c r - a_c{}^2}}{r - a_c}$$

$$\boxed{\theta = \arctan\left(\frac{\left(2a_c r - a_c{}^2\right)^{1/2}}{r - a_c}\right)} \qquad (4)$$

Ligament area = entire area of circle – crack surface area

$$\text{Ligament area} = \pi r^2 - \left[r^2 \left(\arctan\left(\frac{\left(2a_c r - a_c{}^2\right)^{1/2}}{r - a_c} \right) - \frac{\left(2a_c r - a_c{}^2\right)^{1/2}(r - a_c)}{r^2} \right) \right]$$

Finally, the nonlinear energy release rate, J, can be defined in terms of the ligament area and the plastic work done by the fiber:

$$J = J_{el} + J_{pl}$$

$$J = \frac{1-\nu^2}{E} K_I{}^2 + \frac{\eta A_{pl}}{\pi r^2 - \left[r^2 \left(\arctan\left(\frac{\left(2a_c r - a_c{}^2\right)^{1/2}}{r - a_c} \right) - \frac{\left(2a_c r - a_c{}^2\right)^{1/2}(r - a_c)}{r^2} \right) \right]} \quad \text{(plane strain)}$$

The critical nonlinear energy release rate is defined as:

$$J_c = \frac{1-\nu^2}{E}\sigma_Y{}^2 \pi a_c + \frac{\eta A_{pl}}{\pi r^2 - \left[r^2 \left(\arctan\left(\frac{\left(2a_c r - a_c{}^2\right)^{1/2}}{r - a_c} \right) - \frac{\left(2a_c r - a_c{}^2\right)^{1/2}(r - a_c)}{r^2} \right) \right]} \quad (5)$$

Ligament Area Calculations ($r > a_c$)

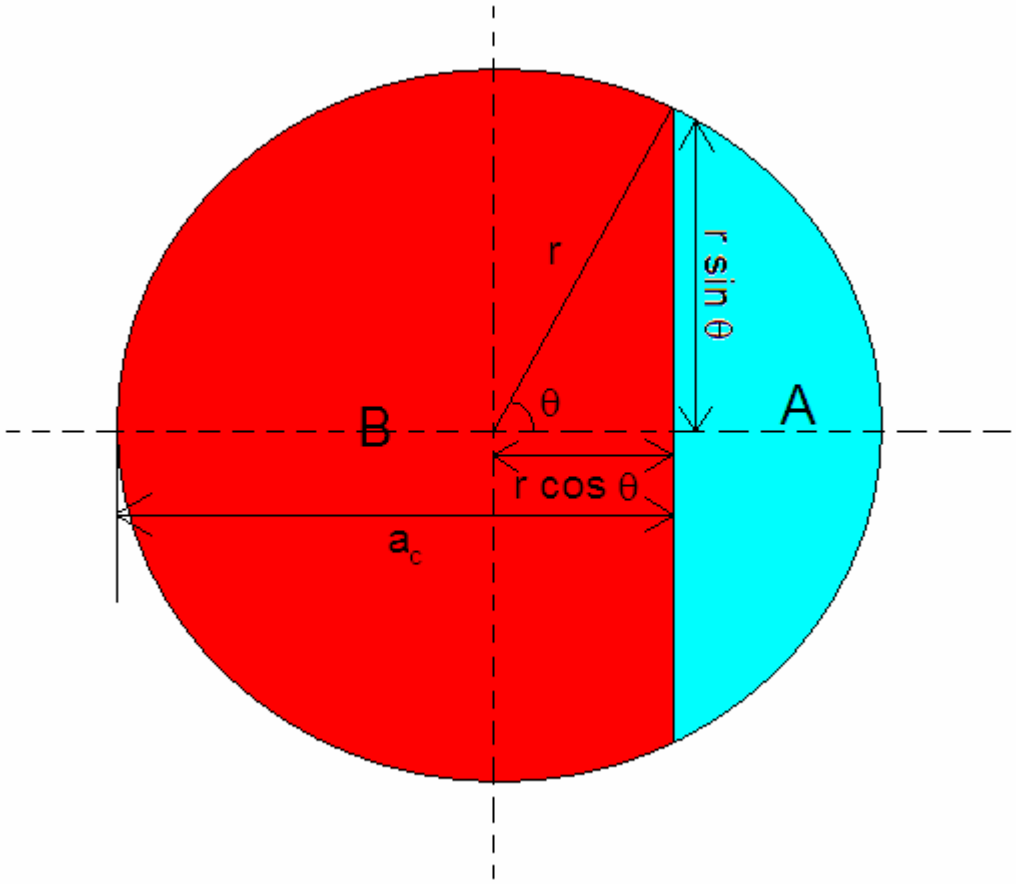

$$\text{Area sector} = \pi r^2 \frac{\theta}{2\pi} = \frac{r^2\theta}{2}$$

$$\text{Area A = ligament area} = 2 \times \left(\frac{r^2\theta}{2} - \frac{1}{2} r \sin\theta r \cos\theta \right) = r^2\theta - r^2 \sin\theta \cos\theta$$

Area B = crack surface area

$$\text{Ligament area} = \boxed{r^2(\theta - \sin\theta\cos\theta)} \qquad (1)$$

$$r\cos\theta = a_c - r$$

$$\boxed{\cos\theta = \frac{a_c - r}{r}} \quad (2)$$

For sinθ, use the following relationship:

$$(r\cos\theta)^2 + (r\sin\theta)^2 = r^2$$

$$(r\sin\theta)^2 = r^2 - (r\cos\theta)^2$$

$$r\sin\theta = \sqrt{r^2 - (a_c - r)^2} = \sqrt{r^2 - \left(a_c{}^2 - 2a_c r + r^2\right)}$$

$$r\sin\theta = \sqrt{2a_c r - a_c{}^2}$$

$$\boxed{\sin\theta = \frac{\sqrt{2a_c r - a_c{}^2}}{r}} \qquad (3)$$

$$\tan\theta = \frac{\sin\theta}{\cos\theta} = \frac{\sqrt{2a_c r - a_c{}^2}}{a_c - r}$$

$$\boxed{\theta = \arctan\left(\frac{\left(2a_c r - a_c{}^2\right)^{1/2}}{a_c - r}\right)} \qquad (4)$$

The ligament area can now be defined in terms of the critical flaw size:

$$\text{Ligament area} = \left[r^2 \arctan\left(\frac{\left(2a_c r - a_c{}^2\right)^{1/2}}{a_c - r}\right) - (a_c - r)\left(2a_c r - a_c{}^2\right)^{1/2}\right]$$

Finally, the nonlinear energy release rate, J, can be defined in terms of the ligament area and the plastic work done by the fiber:

$$J = J_{el} + J_{pl}$$

$$J = \frac{1-\nu^2}{E} K_I{}^2 + \frac{\eta A_{pl}}{\left[r^2 \arctan\left(\frac{\left(2a_c r - a_c{}^2\right)^{1/2}}{a_c - r} \right) - \left(a_c - r\right)\left(2a_c r - a_c{}^2\right)^{1/2} \right]} \quad \text{(plane strain)}$$

The critical nonlinear energy release rate is defined as:

$$J_c = \frac{1-\nu^2}{E} \sigma_Y{}^2 \pi a_c + \frac{\eta A_{pl}}{\left[r^2 \arctan\left(\frac{\left(2a_c r - a_c{}^2\right)^{1/2}}{a_c - r} \right) - \left(a_c - r\right)\left(2a_c r - a_c{}^2\right)^{1/2} \right]} \quad (5)$$

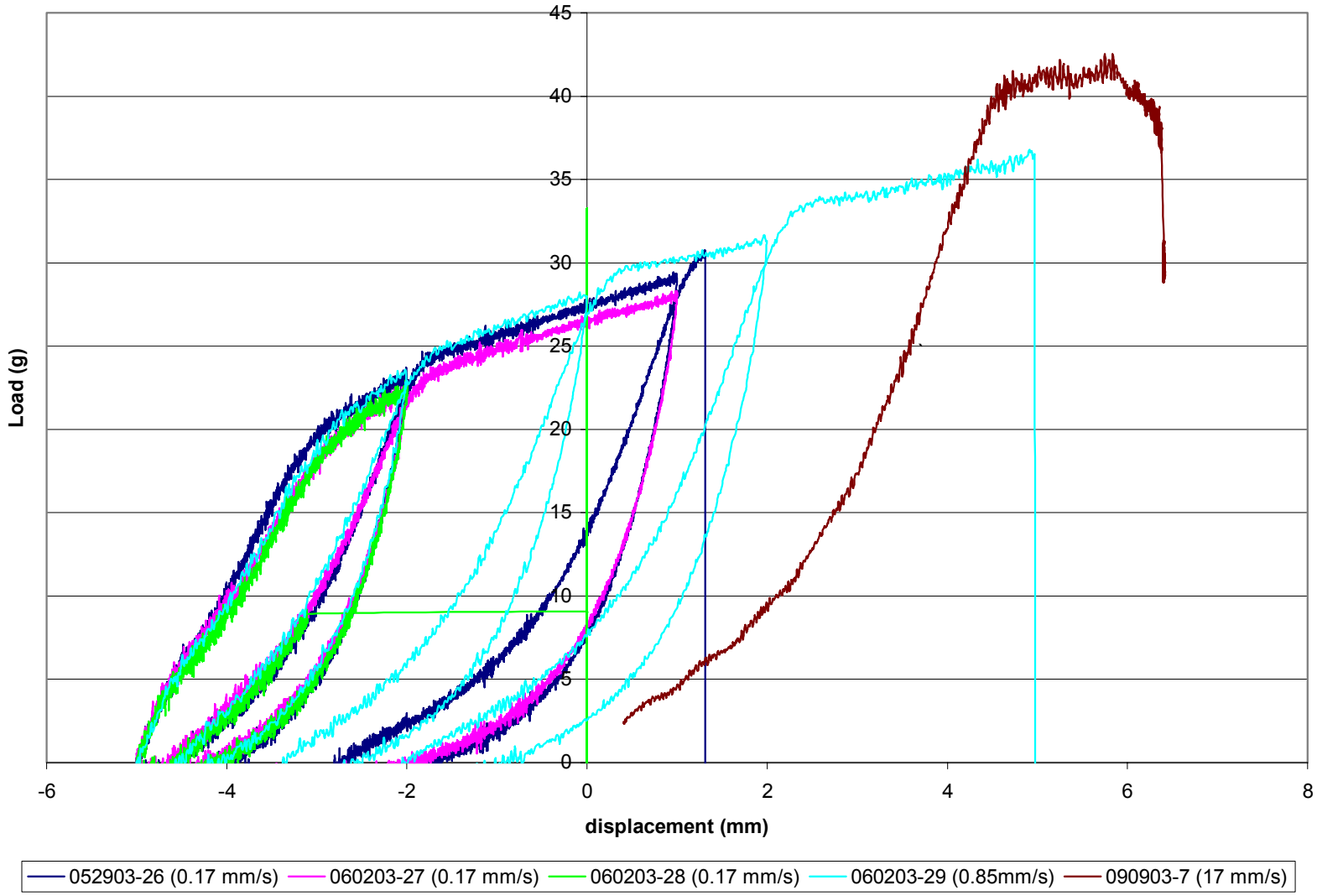

Figure A.1. Figure Showing Effects of Elongation (Strain) Rate of Nylon 6,6 Fibers Under Low-Cycle Fatigue Conditions

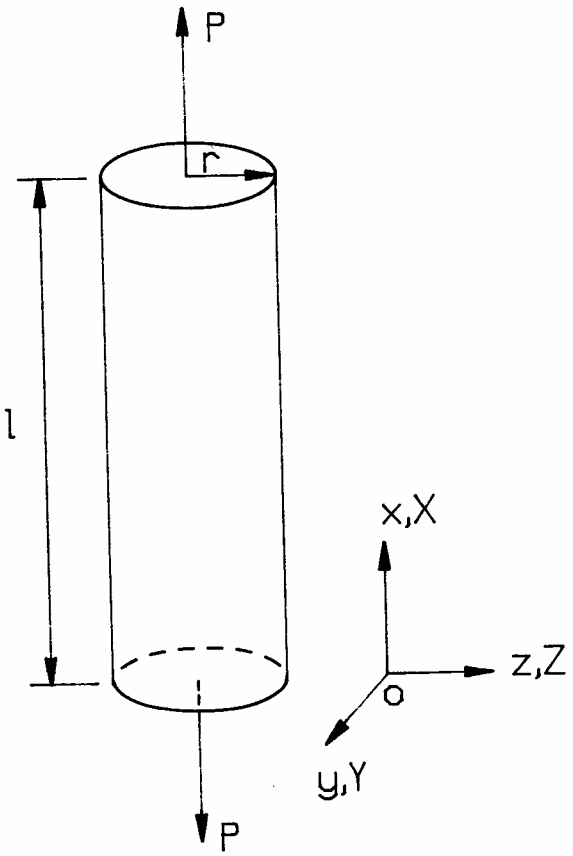

Figure A.2. Schematic of Fiber in Uniaxial Tension[30]

This figure represents a fiber in the case of uniaxial tension under applied load, *P*, with initial length, *l*, and radius, *r*. The coordinates X, Y, Z represent the material coordinates, or the coordinates in the undeformed configuration. x, y, z represent the coordinates in the deformed, or current configuration. To relate the coordinates, the following relationship can be inferred from Figure A.2:

$$x = \lambda_1 X$$

$$y = \lambda_2 Y$$

$$z = \lambda_2 Z$$

where

$$\lambda_1 = l/L$$

$$\lambda_2 = r/R$$

The rotation tensor, deformation gradient, Cauchy-Green tensors, and Lagrangian and Eulearian strain tensors, respectively, are equated as[30]:

$$\mathbf{R} = \mathbf{I}, \quad \mathbf{F} = \mathbf{U} = \mathbf{V} = \begin{bmatrix} \lambda_1 & 0 & 0 \\ 0 & \lambda_2 & 0 \\ 0 & 0 & \lambda_2 \end{bmatrix}, \quad \mathbf{F}^{-1} = \begin{bmatrix} \lambda_1^{-1} & 0 & 0 \\ 0 & \lambda_2^{-1} & 0 \\ 0 & 0 & \lambda_2^{-1} \end{bmatrix}$$

$$\mathbf{C} = \mathbf{U}^2 = \mathbf{F}^{\mathrm{T}} \cdot \mathbf{F} = \begin{bmatrix} \lambda_1^2 & 0 & 0 \\ 0 & \lambda_2^2 & 0 \\ 0 & 0 & \lambda_2^2 \end{bmatrix}$$

$$\mathbf{B}^{-1} = \mathbf{V}^{-2} = (\mathbf{F}^{-1})^{\mathrm{T}}(\mathbf{F}^{-1}) \begin{bmatrix} \frac{1}{\lambda_1^2} & 0 & 0 \\ 0 & \frac{1}{\lambda_2^2} & 0 \\ 0 & 0 & \frac{1}{\lambda_2^2} \end{bmatrix}$$

$$\mathbf{E} = \tfrac{1}{2}(\mathbf{B} - \mathbf{I}) = \tfrac{1}{2} \begin{bmatrix} \lambda_1^2 - 1 & 0 & 0 \\ 0 & \lambda_2^2 - 1 & 0 \\ 0 & 0 & \lambda_2^2 - 1 \end{bmatrix}$$

$$\mathbf{e} = \tfrac{1}{2}(\mathbf{I} - \mathbf{B}^{-1}) = \tfrac{1}{2} \begin{bmatrix} 1 - \frac{1}{\lambda_1^2} & 0 & 0 \\ 0 & 1 - \frac{1}{\lambda_2^2} & 0 \\ 0 & 0 & 1 - \frac{1}{\lambda_2^2} \end{bmatrix}$$

The true strain, velocity gradient, and strain rate are computed as[30]:

$$\bar{\mathbf{e}} = \ln \mathbf{V} = \begin{bmatrix} \ln \lambda_1 & 0 & 0 \\ 0 & \ln \lambda_2 & 0 \\ 0 & 0 & \ln \lambda_2 \end{bmatrix} = \begin{bmatrix} \ln \frac{l}{L} & 0 & 0 \\ 0 & \ln \frac{r}{R} & 0 \\ 0 & 0 & \ln \frac{r}{R} \end{bmatrix}$$

$$\mathbf{L} = \dot{\mathbf{F}} \cdot \mathbf{F}^{-1} = \begin{bmatrix} \dot{\lambda}_1 & 0 & 0 \\ 0 & \dot{\lambda}_2 & 0 \\ 0 & 0 & \dot{\lambda}_2 \end{bmatrix} \begin{bmatrix} \lambda_1^{-1} & 0 & 0 \\ 0 & \lambda_2^{-1} & 0 \\ 0 & 0 & \lambda_2^{-1} \end{bmatrix}$$

$$= \begin{bmatrix} \frac{\dot{\lambda}_1}{\lambda_1} & 0 & 0 \\ 0 & \frac{\dot{\lambda}_2}{\lambda_2} & 0 \\ 0 & 0 & \frac{\dot{\lambda}_2}{\lambda_2} \end{bmatrix} = \begin{bmatrix} \frac{\dot{l}}{l} & 0 & 0 \\ 0 & \frac{\dot{r}}{r} & 0 \\ 0 & 0 & \frac{\dot{r}}{r} \end{bmatrix}$$

$$\mathbf{L} = \mathbf{D}$$

$$\mathbf{W} = 0$$

$$\dot{\bar{\mathbf{e}}} = \begin{bmatrix} \frac{\dot{\lambda}_1}{\lambda_1} & 0 & 0 \\ 0 & \frac{\dot{\lambda}_2}{\lambda_2} & 0 \\ 0 & 0 & \frac{\dot{\lambda}_2}{\lambda_2} \end{bmatrix} = \mathbf{D}$$

L = D in the ensuing relationship because the spin tensor (W) is equal to zero. The engineering strain components are determined as[30]:

$$\hat{\mathbf{E}} = \begin{bmatrix} \frac{l-L}{L} & 0 & 0 \\ 0 & \frac{r-R}{R} & 0 \\ 0 & 0 & \frac{r-R}{R} \end{bmatrix} = \begin{bmatrix} \lambda_1 - 1 & 0 & 0 \\ 0 & \lambda_2 - 1 & 0 \\ 0 & 0 & \lambda_2 - 1 \end{bmatrix} = \mathbf{V} - \mathbf{I}$$

$$\dot{\hat{\mathbf{E}}} = \begin{bmatrix} \frac{\dot{l}}{L} & 0 & 0 \\ 0 & \frac{\dot{r}}{R} & 0 \\ 0 & 0 & \frac{\dot{r}}{R} \end{bmatrix}$$

$$\mathbf{D} = \dot{\hat{\mathbf{E}}} \cdot \left(\hat{\mathbf{E}} + I\right)^{-1}$$

$$\dot{\hat{\mathbf{E}}}\,\Delta\mathbf{t} \approx \begin{bmatrix} \frac{l_2 - l_1}{L} & 0 & 0 \\ 0 & \frac{r_2 - r_1}{R} & 0 \\ 0 & 0 & \frac{r_2 - r_1}{R} \end{bmatrix}$$

$$\mathbf{D}\,\Delta t \approx \begin{bmatrix} \frac{l_2 - l_1}{l_1} & 0 & 0 \\ 0 & \frac{r_2 - r_1}{r_1} & 0 \\ 0 & 0 & \frac{r_2 - r_1}{r_1} \end{bmatrix}$$

The final results of the relationships for the First and Second Piola Kirchoff stress tensors (Σ^{I}, Σ^{II}), respectively[30]:

$$\boldsymbol{\sigma} = \begin{bmatrix} \frac{P}{\pi r^2} & 0 & 0 \\ 0 & 0 & 0 \\ 0 & 0 & 0 \end{bmatrix} = \begin{bmatrix} \frac{P}{\lambda_2^2 \pi R^2} & 0 & 0 \\ 0 & 0 & 0 \\ 0 & 0 & 0 \end{bmatrix} = \begin{bmatrix} \frac{P}{\lambda_2^2 A_0} & 0 & 0 \\ 0 & 0 & 0 \\ 0 & 0 & 0 \end{bmatrix}$$

$$\boldsymbol{\Sigma}^{\mathbf{I}} = \det(\mathbf{F})\mathbf{F}^{-1} \cdot \boldsymbol{\sigma} = \lambda_1 \lambda_2^2 \begin{bmatrix} \frac{1}{\lambda_1} & 0 & 0 \\ 0 & \frac{1}{\lambda_2} & 0 \\ 0 & 0 & \frac{1}{\lambda_2} \end{bmatrix} \begin{bmatrix} \frac{P}{\lambda_2^2 A_0} & 0 & 0 \\ 0 & 0 & 0 \\ 0 & 0 & 0 \end{bmatrix}$$

$$= \begin{bmatrix} \frac{P}{A_0} & 0 & 0 \\ 0 & 0 & 0 \\ 0 & 0 & 0 \end{bmatrix}$$

$$\boldsymbol{\Sigma}^{\mathbf{II}} = \det(\mathbf{F})\mathbf{F}^{-1} \cdot \boldsymbol{\sigma} \cdot \left(\mathbf{F}^{-1}\right)^{\mathrm{T}} = \begin{bmatrix} \frac{P}{\lambda_1 A_0} & 0 & 0 \\ 0 & 0 & 0 \\ 0 & 0 & 0 \end{bmatrix}$$

REFERENCES

1. Ahzi, S., B. J. Lee, and R. J. Asaro. *Materials Science and Engineering*. A189, (1994), pp. 35-44.

2. Anderson, T.L. Fracture Mechanics: Fundamentals and Applications, 2nd Edition. CRC Press. Boca Raton, FL 1995.

3. Andrews, E. H. *Fracture in Polymers*. American Elsevier. New York, 1968, 204 p.

4. Atkins, A. G. and Y-W. Mai. Elastic and Plastic Fracture: Metals, Polymers, Ceramics, Composites, Biological Materials. Ellis Horwood Limited, Chichester, West Sussex, England. 1985.

5. Becht, J., K. L. DeVries, and H. H. Kausch. *European Polymer Journal*. Volume 71. 1971, pp. 105-114.

6. Benham, P.P, Crawford, R.J., Armstrong, C.G. Mechanics of Engineering Materials, 2nd Edition. Longman Group Limited. London, 1996.

7. Bershtein, V. A. et al. *Polymer Science U.S.S.R*. Volume 20, 1977, pp. 654-660.

8. Boukhili, R., F. X. de Charentenay and T. Vu-Khanh. *International Journal of Fatigue*. Volume 8, Issue 3, July 1986, pp. 127-134.

9. Bunn, C.W. and E.V. Garner. *Proc. Roy. Soc*. 47 (1947), A189.

10. Cottrell, A. H. Dislocations and Plastic Flow in Crystals. Clarendon Press, Oxford. 1953.

11. Coulomb, C. A. *Mem. Math. Phys*. 7, 343 (1773).

12. Dowling, N. E. Mechanical Behavior of Materials: Engineering Methods for Deformation, Fracture, and Fatigue, 2nd Edition. Prentice Hall. Upper Saddle River, New Jersey 1999.

13. Dowling, N.E. and Begley, J.A. *ASTM STP 590, American Society for Testing and Materials*. Philadelphia, 1976, pp. 82-103.

14. Drucker, D. C. and W. Prager. *Quart. Appl. Math*. 10:157, 1952.

15. Fujii, S. *JSAE Review*. Volume 24, Issue 4. October 2003. pp. 471-475.

16. Georgia Tech MSE Electron Microscopy Center. http://www.mse.gatech.edu/academics/facilities/EMC/EMC-Electron_Microscope/emc-electron_microscope.html.

17. Griffith, A. A. *M. Eng. (of the Royal Aircraft Establishment)*. February 1920, pp. 163-198.

18. Hattori, K. *Materials Science and Engineering: C*. Volume 17, Issues 1-2 , 1 November 2001. pp. 27-32.

19. Hearle, J. W. S. et al. Fibre Failure and Wear of Materials: An Atlas of Fracture, Fatigue and Durability. Ellis Horwood Limited. Chichester, West Sussex, England, 1989.

20. Hermans, J. J. et al. *Recl. Trav. Chim*. 65, 427. 1946.

21. Hertzberg, R. W., and J. A. Manson. Fatigue of Engineering Plastics. Academic Press, Inc. New York, NY, 1980.

22. Huevel, H. M., R. Huisman and K. C. J. B. Lind. *Journal of Polymer Science*. Polymer Phys. Edition 14, 921. 1976.

23. Hutchinson, J. W. *Journal of Mech. Phys. Solids*. Volume 16, 1968, pp. 13-31.

24. Inglis, C. E. *Trans. Inst. Naval Arch*. Volume 55, 1913, pp. 219-233.

25. Ishibashi, T., K. Aoki and T. Ishii. *Journal of Applied Polymer Science*. 14, 1597. (1970).

26. Ito, M., et al. *Polymer*. Volume 42, Issue 1, January 2001. pp. 241-248.

27. Kausch, H. H. Polymer Fracture, 2nd Edition. New York, Springer-Verlag, 1985, 456 p.

28. Kausch, H. H. Polymer Fracture. Springer-Verlag. Berlin, 1978.

29. Kausch, H. H., J. A. Hassell, and R. I. Jaffee. Deformation and Fracture of High Polymers. Plenum Press. New York, New York, 1973.

30. Khan, A. S. and S. Huang. Continuum Theory of Plasticity. John Wiley & Sons, Inc. New York, 1995.

31. Kim, B. H., C. R. Joe and D. M. Otterson. *Polymer Testing*. 8 (1989), pp. 119-130.

32. Krempl, E. and C. M. Bordonaro. *International Journal of Plasticity*. Volume 14, Issues 1-3. 1998, pp. 245-258.

33. Lim, J.G. et al. *Progress in Polymer Science*. Volume 14, Issue 6, 1989. pp. 763-809.

34. Michielsen, S. *Journal of Applied Polymer Science*. Volume 52, 1994, pp. 1081-1089.

35. Michielsen, Steve. *Fundamentals of High Modulus/High Tenacity Melt Spun Fibers*. NTC Project M01-GT01 Annual Report. November 2003.

36. Murase, S., et al. *Polymer*. Volume 38, Issue 18, September 1997. pp. 4577-4585.

37. Murthy, N. S., et al. *Polymer*. Volume 36, Issue 20, 1995. pp. 3863-3873.

38. Naskar, A. K., A. K. Mukherjee a, and R. Mukhopadhyay. *Polymer Degradation and Stability*. Volume 83, Issue 1 , January 2004. pp. 173-180.

39. Newell, J.A. and D.D. Edie. *Carbon*. Volume 34, Issue 5, 1996, pp. 551-560.

40. Northolt, M. G. and D. J. Sikkema. *Adv. Polymer Science*. (98) 115, 1990.

41. Northolt, M. G. and R. van der Hout. *Polymer*. (26) 230, 1985.

42. Northolt, M. G., A. Roos, and J. H. Kampschreur. *Journal of Polymer Science Physical Edition*. (27) 1107, 1989.

43. Northolt, M. G., J. J. M. Baltussen, and B. Schaffers-Korff. *Polymer*. Volume 36, Number 18, 1995, pp. 3485-3492.

44. NTC Proposal, GT. http://www.ptfe.gatech.edu/faculty/michielsen/michelsen-highmod.htm.

45. Paris, P.C. and Erdogan, F. *Journal of Basic Engineering*. Volume 85, 1960, pp. 528-534.

46. Paris, P.C., Gomez, M.P., and Anderson, W.P. *The Trend in Engineering*. Volume 14, 1961, pp. 9-14.

47. Penning, J. P., et al. *Polymer*. Volume 44, Issue 19, September 2003. pp. 5869-5876.

48. Prevorsek DC, Murthy NS, Kwon YD. *Rubber Chem. Technol*. 1987, 60(4):659–73.

49. Prevorsek, D.C., Y. D. Kwon, R. K. Sharma. *Journal of Applied Polymer Science*. 1980, 25:2063–104.

50. Rice, J. R. *Journal of Applied Mechanics*. June 1968, pp. 379-386.

51. *Standard Test Method for Determining J-R Curves of Plastic Materials*. D 6068-96. American Society of Testing and Materials. West Conshohocken, PA 19428, 1996.

52. Suzuki, A. and A. Endo. *Polymer*. Volume 38, Issue 12, 1997. pp. 3085-3089.

53. Suzuki, A., H. Murata, and T. Kunugi. *Polymer*. Volume 39, Issue 6-7, 1999. pp. 1351-1355.

54. Suzuki, A., Y. Chen, and T. Kunugi. *Polymer*. Volume 39, Issue 22, 1998. pp. 5335-5341.

55. Termonia, Y. and P. Smith. *Mat. Res. Soc. Symp. Proc*. Volume 79, 1987.

56. Timoshenko, S. and J. N. Goodier. *Theory of Elasticity, 3rd Ed*. McGraw-Hill. New York, 1970.

57. Tobolsky, A. V. and H. Mark. Polymer Science and Materials. Wiley-Interscience. New York, p. 236, 1971.

58. Ward, I. M. and D.W. Hadley. Mechanical Properties of Solid Polymers. J. Wiley & Sons. Chichester, New York, 1993.

59. Ward, I. M. Mechanical Properties of Solid Polymers. Wiley-Interscience. New York, 1971.

60. Warner, Steven B. Fiber Science. Prentice Hall. Upper Saddle River, NJ 07458, 1995.

61. Zhurkov, S.N., V. S. Kuksenko and A. I. Slutsker. *Proceedings of the Second International Conference on Fracture*. Brighton, 1969, p. 531.

62. Ziabicki, A. and K. Kedzierska. *Journal of Applied Polymer Science*. 2, 14. (1959).

63. Ziabicki, A. and K. Kedzierska. *Journal of Applied Polymer Science*. 6, 111. (1962).

64. Zinck, P., J. F. Gérard and H. D. Wagner. *Engineering Fracture Mechanics*. Volume 69. Issue 9, June 2002, pp. 1049-1055.

65. Shigemitsu, M. et al. *Polymer*. Volume 38. Number 18, November 1997, pp. 4577-4585.

66. Cook, J. and J. E. Gordon. *Proc. Roy. Soc*. A282, 508. (1964).

67. Cherry, B. W. and Hang, P. T. *Proceedings of the Australian Fracture Group*. Melbourne: Monash University, 1974, pp. 41-50.

68. Michielsen, S. *Journal of Materials Science Letters*. 11, (1992), pp. 982-984.

69. ASTM E 1820-01. *Standard Test Method for Measurement of Fracture Toughness*. ASTM International, West Conshohocken, PA, 2001.

70. Huang, D. D. *Polymer Engineering and Science*. Volume 36. Number 18, September 1996, pp. 2270-2274.

71. Huang, D. D., B. Wood, and E. A. Flexman. *Advanced Materials*. Volume 10. Number 15, 1998, pp. 1207-1211.

72. Valanis, K. E. *Arch. Mech*. 1971, 23:517.

73. Valanis, K. C. *Arch. Mech*. 1980, 32:171.

74. Bernal, C. R., A. N. Cassanelli, and P. M. Frontini. *Polymer Testing*. Volume 14. Issue 1, 1995, pp. 85-96.

75. Irwin, G. R. *Sagamore Research Conference Proceedings*. Volume 2. 1956, pp. 289-305.

76. Enduratec Corporation. http://www.enduratec.com/product.cfm.

77. Adams, G. C. et al. *Polymer Engineering Science*. 30 (1990) 241.

78. ASTM D 6068-96. *Standard Test Method for Determining J-R Curves of Plastic Materials*. ASTM International, West Conshohocken, PA, 1996.

79. Hadley, D. W. et al. *Journal of Material Science*. 4 (1969) 152.